DESIGN AND APPLICATION OF FLUX CORRECTED TRANSPORT FOR REACTIVE SOLUTE TRANSPORT MODELING

BY

GUOYIN WANG

THESIS

Submitted in partial fulfillment of the requirements
for the degree of Master of Science in Civil Engineering
in the Graduate College of the
University of Illinois at Urbana-Champaign, 2013

Urbana, Illinois

Adviser:

Professor Albert J. Valocchi

ABSTRACT

Understanding reactive solute transport, which couples flow , transport, and chemical/ biological reaction in porous media, is important in areas such as aquifer remediation, groundwater contamination and geochemical reaction modeling. Due to the large time scales involved, lack of accessibility to the subsurface and heterogeneous physical and chemical parameters, numerical simulation models are important and widely used in most of these studies. Conventional numerical methods to solve solute transport can produce non-physical values (negative concentrations) even for some simple cases when considering full tensor dispersion. Particularly when considering heterogeneous flow fields, irregular grids, nonlinear reactions and large time scales, the non-physical values can spread out to the whole domain and cause numerical convergence problems for reactive transport cases. Conventional finite element and finite difference methods to discretize full tensor dispersion may lead to non-physical solutions independent of the grid size; therefore, this problem cannot be ignored. The well-known Flux Corrected Transport (FCT) technique can be used to solve this problem. This methodology can produce a high-order, physical solution by combining a high-order solution (high accuracy, but non-physical) and a low-order solution (low accuracy, but positive) with a nonlinear flux limiter. The nonlinear flux limiter is an anti-diffusion component, which can diminish the artificial-dispersion from low-order method and hence improve the accuracy without producing a non-physical solution. In this study, the accuracy of Flux Corrected Transport is tested for different cases with complex flow fields and chemical reactions. We consider cases where accurate modeling of full tensor dispersion is required to simulate mixing-induced nonlinear reaction. The results indicate that FCT is a simple, flexible and accurate method to obtain positive solution for solute transport modeling but may take a lot of CPU time.

To my parents, for their love and support.

ACKNOWLEDGMENTS

I would like to give special thanks to my advisor, Dr. Albert J. Valocchi, for his continuous support on my work, extensive help building up my knowledge system and his advice towards my academic development.

I would like to thank to my colleague, Mr. Oscar J. Garcia-Cabrejo, for providing the Flux-Corrected Transport code, that was used as the basis for the reactive transport model, and helping me learning numerical methods to build up reactive transport model.

I am grateful to the Department of Energy, grant DOE DEFC02-07ER64323 for financial support.

TABLE OF CONTENTS

LIST OF TABLES

LIST OF FIGURES

CHAPTER 1

INTRODUCTION

The transport of contaminants in aquifers is usually represented by the advection-dispersion-reaction equation. The numerical solution of the advection-dispersion equation has been widely researched for many years within and outside the groundwater modeling community [2]. However, the past and on-going research in this area reflects difficulties in solving advection-dispersion equation by numerical methods [3].The difficulties have been summarized as follows [4]:

1. While advection and dispersion are simultaneous processes, their effect on mass transport are different: advection is hyperbolic, so the sharp fronts of concentration plume propagate along the characteristic lines. On the contrary, dispersion is parabolic, so the sharp gradients tend to smoothed out.

2. Mathematically, the need to treat simultaneously hyperbolic term (advection) and parabolic term (dispersion) has not been fully overcome by any numerical method.

Most numerical methods for solving the advection-dispersion equation are classified as Eulerian, Lagrangian and mixed Eulerian-Lagrangian [5]. Eulerian methods work well in flow simulation and are commonly used in solute transport modeling. In Eulerian methods, the transport equation is solved on a fixed spatial grid. The advantages of Eulerian methods are: they are easy to program and implement, generally mass conservative and accurate, and efficient in solving dispersion-dominated problems [2]. The most common Eulerian methods are finite-difference, finite-volume and finite-element. However, for advection-dominated problems, an Eulerian method is susceptible to excessive numerical dispersion or artificial oscillation [6]. Oscillations are normally caused by advection term with large Peclet number,and this can

lead to negative concentrations. This can be controlled by using a smaller grid space. But when there is full tensor dispersion, with arbitrary grids, we can get negatives which cannot be eliminated by decreasing grid size(dx)or time scale (dt).

To improve the numerical methods, several goals need to be considered for numerically solving the advection-dispersion equation [6]:

1. avoiding the spurious oscillations which can affect the stability and convergence of solution for reactive transport;

2. minimizing numerical dispersion for advection-domain transport, especially for the case with sharp front concentration;

3. preserving the mass conservation property of the advection and dispersion equation;

There are several novel numerical schemes to preserve positivity of concentration, including Total Variation Diminishing (TVD) approach [7],Flux limiter[8], Flux Corrected Transport (FCT) [9], Multi-Point Flux Approximation (MPFA) [10], Local Extreme diminishing (LED) [11], nonlinear monotone finite volume method [12] and numerical conditional optimization [13]. However, algorithms like TVD, are usually for explicit methods. Kuzmin stated that by 2004 no other implicit high-resolution finite-element schemes were available for arbitrary time stepping except FEM-FCT methology [14]. Even though explicit methods are typically more accurate than implicit ones, the stability limitation makes them inefficient for problems with large time scales and strongly varying velocities [14]. As a result, the small time step will lead a large computational cost.

FCT algorithm, as predictor-corrector algorithm, can be classified as diffusion-antidiffusion (DAD) method [15], which has the following basic ideas [16]:

1. Produce advanced low-order scheme to give enough diffusion and good phase error which suppresses undershoots and overshoots.

2. Correct the solution using anti-diffusive limiter to keep the "steepness" of the concentration.

The pioneering work of FCT has established the basic concept and principles for applying FCT, which is essentially using a low-order method in regions with steep gradients [14]. However, the original FCT algorithm named

SHASTA was a specialized one-dimensional finite-difference scheme. Then it was dramatically improved by a genuinely multidimensional flux limiter and a combination of high-order and low-order discretization [9]. Recently, an extension of FCT to Finite Element Modeling (FEM), multidimensional cases and fully implicit time stepping has been developed [14]. The conservative flux decomposition procedure has been proposed for both convective and diffusive terms, the mathematical properties of positivity-preserving schemes has been proved and a multidimensional limiter has been employed for different FEM schemes [17].

The negative concentration from numerical solution of advection-dispersion equation can be a big problem for reactive transport. Most reactive transport codes are based on the advection-dispersion-reaction equations, but the method by which transport codes incorporate the chemistry varies [18]. Generally, the chemistry system can be modeled using the following assumptions: kinetic, local equilibrium or mixed kinetic-equilibrium. Depending on the time scale of reaction and time scale of the problems, reactions could be models as equalibrium or kinetic: aqueous reaction are fast and are usually treated as equalibrium, water-rock reaction, such as precipitation, dissolution and adsorption, are relatively slow and are usually treated as kinetic [19] [20] [21].

Because of the chemical aspects, such as speciation, the reactive transport are more complex. By considering both equilibrium-controlled and kinetically-controlled reactions, the reactive transport model leads to a differential algebraic system of equations (DAE) [21] which is computationally expensive to solve. There has been considerable focus on numerical techniques to solve this problem which couples both reaction part and transport part. Steefel and MacQuarrie [22] have provided a summary of these methods, which can be divided into three categories: operator splitting (OS), global implicit approaches (GIA), and sequential iterative and sequential non-iterative approaches (SIA/SNIA). Each technique has its advantage and disadvantage. The GIA is most computational expensive, but quite stable. The SIA can deal with specific problem with heavy restriction. The OS is most straightforward to apply, but may gain large splitting error [22] [23]. In this thesis, we will focus on GIA and SIA. The negative concentration problem is easilly handled by OS, since the negative concentration can be filtered away before applying reaction module. However, the negative concentration

can be a big problem for implicit approach,

The purpose of this thesis is to confirm the performance of FCT method in solute transport modeling, to explore the effert of cross-dispersion term in reactive transport model and to apply FCT method to reactive transport model which consider full tensor dispersion and different types of reactions.

In this thesis, based on the pioneering work of FCT, I will present the design of multidimensional FCT schemes with fully implicit time stepping and finite volume method to obtain a positive solution for advection and dispersion equation with full-tensor dispersion coefficient. I will also present the design of GIA and SIA approaches to produce the numerical solution for reactive transport. By providing several tests, I will demonstrate the convergence rate of FCT method as compared to high and low order solutions, show the influence of full-tensor dispersion and extend the implementation of FCT method to reactive transport model. Specifically, in Chapter 2, I will present the governing equations for advection and dispersion, and the tensor components of the dispersion coefficient; the analytical and semi-analytical solution for the advection-dispersion equation will be presented for some special cases. In Chapter 3, I will present the numerical methods to solve the advection-dispersion equations, especially the design of the FCT algorithm; the h-convergence test of FCT compared with low and high order solutions will be presented to demonstrate the order of FCT algorithm. In Chapter 4, I will present the governing equation for chemical reaction and the advection-dispersion-reaction system; the solution strategy to numerically solve the mixed-equilibrium-kinetic transport problem; and the procedure to apply FCT methodology solving approach of the reactive transport equations. In Chapter 5, I will present reactive transport examples which shows the influence of full-tensor dispersion and FCT methodology.

In this thesis, I demonstrate that the fully implicit multidimensional FCT scheme can gangrene the positivity and the high-order accuracy of the solution for transport problem. The mixing-controlled reaction tests and nonlinear reactions show that the cross-dispersion term can generate great changes to the solution of reactive transport problem. These results also proves that applying FCT method to free-ion approach can solve the negative value and convergence problems by considering the cross-dispersion term. More reactive tests need to be added in the future, such as more complex chemical system and different type of reactions like ion-exchange, precipitation/dissolution.

Future work also need to be done to apply FCT method to total component approach, to apply global implicit approach to nonlinear reaction tests and to apply parallel computing technique to FCT method, which can decrease the CPU time of applying FCT to reactive transport problem.

CHAPTER 2

TRANSPORT MODEL

In this section, an introduction of the governing equation for transport model is provided with the emphasis on the structure of dispersion tensor, and the methods to get analytical or semi-analytical solutions for the transport model are also discussed to provide a benchmark solution.

2.1 Governing Equation

The reactive transport of contaminants, considering advection, dispersion, fluid sink/sources and equilibrium-controlled adsorption is shown in the following form:

$$\underbrace{\theta R\frac{\partial c}{\partial t}}_{\text{storage term}} = \underbrace{\frac{\partial}{\partial x_i}\left(\theta D_{ij}\frac{\partial c}{\partial x_j}\right)}_{\text{advection term}} - \underbrace{\frac{\partial}{\partial x_i}\left(q_i c\right)}_{\text{dispersion term}} + \underbrace{R_k}_{\text{source term}} \tag{2.1}$$

The term on the left side of equation (2.1) represents the temporal variation of the storage term, where c is the aqueous concentration [$\mathrm{M/L^3}$]. The first two terms on the right hand-side represent the net flux due to the advection and dispersion (spatial variation of fluxes). R_k stands for the source/sink term due to the chemical reaction [$\mathrm{ML^3/T}$]. $D_{ij}$are the components of the hydrodynamic dispersion tensor, $\mathbf{D}$[$\mathrm{L^2/T}$], q_i is the Darcy velocity [$\mathrm{L/T}$], R is the retardation factor which is caused by equilibrium absorption, θ is the porosity, x_i are spatial coordinates [L], and t is the time [T] [6].

Here, we ignore the source term which will be discussed later as the reaction term and assume constant porosity, then equation (2.1) can be simplified:

$$\frac{\partial c}{\partial t} = \frac{\partial}{\partial x_i}\left(D_{ij}\frac{\partial c}{\partial x_j}\right) - \frac{\partial}{\partial x_i}\left(v_i c\right) \tag{2.2}$$

v_i are the components of the water velocity vector [$\mathrm{L/T}$] . The two/three-

dimensional dispersion tensor $\mathbf{D}$ is defined by the standard form:

$$D_{ij} = \left(\alpha_T |v| + D^{mol}\right) \delta_{ij} + (\alpha_L - \alpha_T) \frac{v_i v_j}{|v|} \tag{2.3}$$

the dispersion tensor components are related with the velocity components, the longitudinal dispersivity α_L, and transverse dispersivity α_T, and the molecular diffusivity D_{mol} [24]. Usually the molecular diffusivity is much smaller than the dispersion coefficient and longitudinal dispersivity is about ten times of transverse dispersivity. The expression shows that even for uniform flow field, if the flow is not parallel to the dispersion Cartesian axes of grid, the cross-dispersion term is required. The former research shows that full-tensor dispersion improves the accuracy and reduces the grid orientation error of numerical solution [25]. The equation (2.3) can be written in a specific two-dimension form:

$$D_{xx} = \alpha_L \frac{v_x v_x}{|v|} + \alpha_T \frac{v_y v_y}{|v|} \tag{2.4a}$$

$$D_{xy} = D_{yx} = \alpha_L \frac{v_x v_y}{|v|} - \alpha_T \frac{v_y v_x}{|v|} = (\alpha_L - \alpha_T) \frac{v_x v_y}{|v|} \tag{2.4b}$$

$$D_{yy} = \alpha_L \frac{v_y v_y}{|v|} + \alpha_T \frac{v_x v_x}{|v|} \tag{2.4c}$$

For the case with horizontal flow in x direction, velocity in y direction is zero, so the equation (2.4b) is equal to zero. For the case with diagonal flow, velocities in x and y direction are not zero, so the equation (2.4b) is not equal to zero. For the case with longitudinal dispersivity equal to transverse dispersivity, the equation (2.4b) is always equal to zero for arbitrary flow field. The non-zero cross-dispersion term will cause negative concentration in numerical solution, which is the focus of this thesis and will be discussed below.

2.2 Analytical Solution and Semi-analytical Solution

2.2.1 General analytical solution

To evaluate the accuracy of FCT scheme, we need to get the analytical solution of advection-dispersion equation. For most practical cases, it is not possible to find an analytical solution, but for a benchmark problem with instantaneous "pulse" concentration distribution with uniform one-direction flow field and without cross-dispersion term, the analytical/semi-analytical solution can be obtained [26]. This chemical spilling problem is belonging to the class of initial value problems, in which the initial concentration is specified and the analytical solution can be specified through time and space.

Consider the case with a uniform flow field in x-direction, uniform scalar dispersion coefficient and no retardation, then equation (2.1) can be written in a new form:

$$\frac{\partial c}{\partial t} = D_{ii}\frac{\partial^2 c}{\partial x_{ii}^2} - v\frac{\partial c}{\partial x_1} \tag{2.5}$$

where v is the velocity [L/T], D_{ii} is the component of dispersion coefficient $\mathbf{D}$ [L^2/T]. The analytical solution of equation (2.5) is based on Fourier Analysis in terms of waves of various frequencies and wave number as the following form:

$$c \sim Ae^{i\left(\tilde{k}\cdot\tilde{x}-\omega t\right)} \tag{2.6a}$$

$$\omega = k_x v + i\lambda + i\left(D_{xx}k_x^2 + D_{yy}k_y^2\right) \tag{2.6b}$$

where A is the wave amplitude, $\tilde{k}$ is the wave number vector (k_x and k_y are its components) and ω is the wave frequency. By combining equation (2.6a) and (2.6b), the physical meaning relationship can be obtained:

$$c \sim Ae^{i[k_x(x-vt)+k_y y]} \cdot e^{-\left[D_{xx}k_x^2 + D_{yy}k_y^2\right]} \tag{2.7}$$

In equation (2.7), the first component stands for advection, which does not change the magnitude, just generate a translation in space; while the second component stands for dispersion, which produces a decay of concentration with larger k (shorter wavelengths) dissipating first. By using Fourier Inversion Theorem, we can get the analytical solution for a infinite domain in the

following form:

$$c\left(x,y,t\right)=\int\int_{\Omega}c\left(\xi,\eta,0\right)G_{x}G_{y}d\xi d\eta \tag{2.8a}$$

$$G_{x}\left(x,t|\xi,0\right)=\frac{1}{\sqrt{4\pi D_{xx}t}}exp\left(-\frac{\left(x-\xi-vt\right)^{2}}{4\pi D_{xx}t}\right) \tag{2.8b}$$

$$G_{y}\left(y,t|\eta,0\right)=\frac{1}{\sqrt{4\pi D_{yy}t}}exp\left(-\frac{\left(y-\eta\right)^{2}}{4\pi D_{yy}t}\right) \tag{2.8c}$$

In the equation (2.8a), Ω is the 'pulse' zone in the domain with non-zero initial concentration, ξ and η are initial mass point position, and G_x and G_y are Green's Function in x and y direction which gives the contribution to the solution at point (x, y, t) due to the initial unit condition.

2.2.2 Analytical Solution of Rectangular Source Model

A simple realization of equation (2.8a) is rectangular source. At time zero, the source zone is in shape of rectangular and well mixed, and the background initial concentration is zero. The initial mass condition is as follows:

$$M=c_{0}LW \tag{2.9}$$

where M is the initial mass of rectangular source region with length L in x direction, width W in y direction and initial concentration c_0, as shown in Figure 2.1.

Under this initial condition, the analytical solution can be obtained[27]:

$$c\left(x,y,t\right)=c_{0}\int_{-L/2}^{L/2}G_{x}d\xi\int_{-W/2}^{W/2}G_{y}d\xi\eta \tag{2.10}$$

$$=\frac{c_{0}}{4}\left\{erf\left(\frac{x-vt+L/2}{\sqrt{4\pi D_{xx}t}}\right)-erf\left(\frac{x-vt-L/2}{\sqrt{4\pi D_{xx}t}}\right)\right\} \tag{2.11}$$

$$\cdot\left\{erf\left(\frac{y+W/2}{\sqrt{4\pi D_{yy}t}}\right)-erf\left(\frac{y-W/2}{\sqrt{4\pi D_{yy}t}}\right)\right\}$$

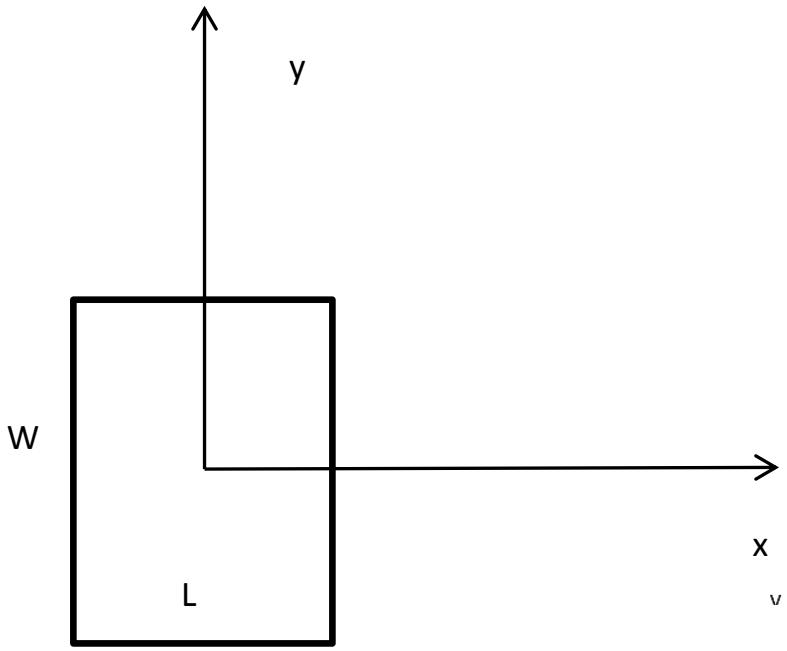

Figure 2.1: Initial Condition for a rectangular source model. L is the length in x direction, W is the width in y direction.

2.2.3 Semi-analytical Solution of Rectangular Source Model (with cross-dispersion term)

When considering uniform flow at an angle and cross-dispersion term, the advection-dispersion equation cannot be simplified as equation (2.5), since the axis coordinates are not parallel or normal to the dispersion component (in other words, it is anisotropic). So we need to transfer full-tensor dispersion into its main direction:

$$\begin{bmatrix} D_{xx} & D_{xy} \\ D_{yx} & Dyy \end{bmatrix} \rightarrow \begin{bmatrix} D_L & 0 \\ 0 & D_T \end{bmatrix} \tag{2.12}$$

It means that D_L and D_T are in orthogonal direction again (in other words, in principal direction) and the transformation need to be orthogonal transformation to rotate but not change length of the dispersion tensor $\mathbf{D}$ [28]. The process is accomplished by getting the eigenvalue of the matrix, which is in the following form:

$$\begin{bmatrix} D_{xx} - \lambda & D_{xy} \\ D_{yx} & D_{yy} - \lambda \end{bmatrix} = 0 \tag{2.13}$$

where λ is the eigenvalue of the matrix, so the root of λ is the principle component of dispersion tensor. The larger root is D_L and the smaller root is the D_T.

For the Cartesian coordinate system (x, y), we need to introduce new coordinate (x^*, y^*) such that its axises are parallel and orthogonal to the flow direction as shown in Figure 2.2.

According the Figure 2.2, the relationship between two coordinate system is[29]:

$$x = x^* \cos\alpha - y^* \sin\alpha \tag{2.14}$$

By applying Fick's law to the (x^*, y^*) coordinate system, the flux of dispersion in principal direction, F_x^* and F_y^* can be obtained:

$$F_x^* = -D_L \frac{\partial c}{\partial x^*} \tag{2.15a}$$

$$F_y^* = -D_T \frac{\partial c}{\partial y^*} \tag{2.15b}$$

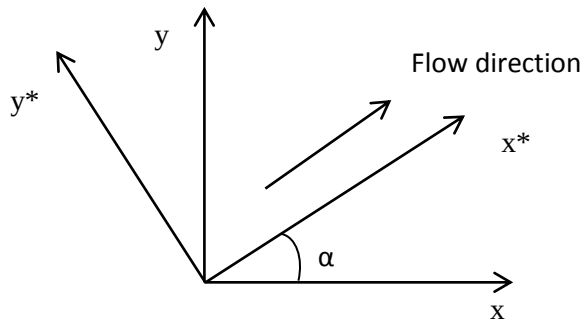

Figure 2.2: Anisotropic dispersion coefficient, x and y are original coordinate system, $x^*$and y^* are coordinate system which is parallel and orthogonal to flow direction, α is the angle between two systems.

The flux in terms of the (x, y) coordinate system can be express similar to equation (2.14):

$$F_x = F_x^* \cos\alpha - F_y^* \sin\alpha \tag{2.16a}$$

$$F_y = F_y^* \cos\alpha + F_x^* \sin\alpha \tag{2.16b}$$

By combining equation (2.15) and (2.16), we can obtain:

$$F_x = -D_L \frac{\partial c}{\partial x^*} \cos\alpha + D_T \frac{\partial c}{\partial y^*} \sin\alpha \tag{2.17}$$

By applying the chain rule, we can get[30]:

$$\frac{\partial c}{\partial x^*} = \frac{\partial c}{\partial x}\frac{\partial x}{\partial x^*} + \frac{\partial c}{\partial y}\frac{\partial y}{\partial x^*} = \frac{\partial c}{\partial x}\cos\alpha + \frac{\partial c}{\partial y}\sin\alpha \tag{2.18a}$$

$$\frac{\partial c}{\partial y^*} = \frac{\partial c}{\partial x}\frac{\partial x}{\partial y^*} + \frac{\partial c}{\partial y}\frac{\partial y}{\partial y^*} = \frac{\partial c}{\partial y}\cos\alpha - \frac{\partial c}{\partial x}\sin\alpha \tag{2.18b}$$

We can rewrite equation (2.17) in the (x, y) coordinate system:

$$F_x = -D_{xx} \frac{\partial c}{\partial x} \cos\alpha - D_{xy} \frac{\partial c}{\partial y} \sin\alpha \tag{2.19a}$$

$$F_y = -D_{yx} \frac{\partial c}{\partial x} \cos\alpha - D_{yy} \frac{\partial c}{\partial y} \sin\alpha \tag{2.19b}$$

By conbaining equation (2.17) and (2.19), the following relationship between

dispersion coefficient component can be obtained:

$$D_{xx} = D_L \cos^2 \alpha + D_T \sin^2 \alpha \tag{2.20a}$$

$$D_{xy} = D_{yx} = (D_L - D_T) \sin \alpha \cos \alpha \tag{2.20b}$$

$$D_{yy} = D_T \cos^2 \alpha + D_L \sin^2 \alpha \tag{2.20c}$$

In this way, we can confirm the principal direction component of dispersion coefficient obtained from equation (2.13) (however, using this equation only, it is hard to get the principle component of dispersion tensor).

By changing the Cartesian coordinate system, we can simplify the governing equation to the form of equation (2.5), so the analytical solution can also be expressed using equation (2.8a). However, by the changing the Cartesian coordinate system, the source region Ω changes from rectangular to diamond for diagonal flow condition as shown below:

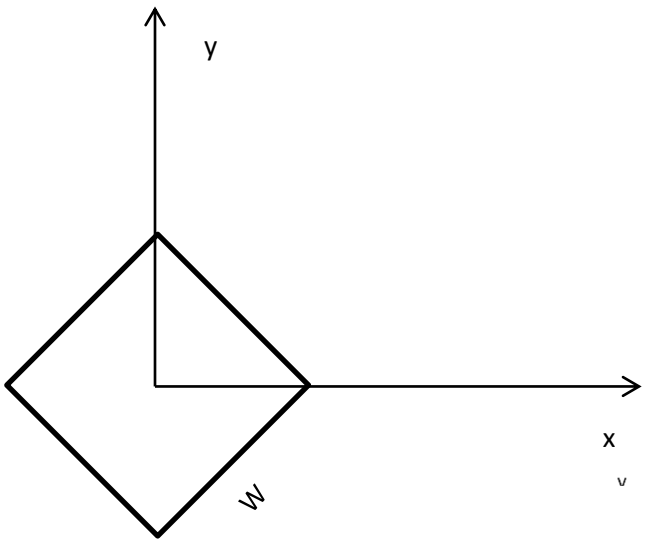

Figure 2.3: Initial condition for a diamond source model. W is the width of the diamond source.

The integration equation (2.8a) cannot be split into equation (2.11). To

get the accurate integration value, we need to use high-precision numerical quadrature methology. For one dimensional integration, Newton-Cotes method can only integrate exactly a polynomial of the degree $n-1$, with n nodes and n weights; while Gaussian Quadrature has accuracy for polynomial degree of $2n-1$, with n optimally chosen nodes and n weights. Since the one dimensional numerical quadrature is in the following moment equation form:

$$I(f) = \int_a^b f(x)\,dx \approx Q_n(f) = \sum_{i=1}^{n} \omega_i f(x_i) \tag{2.21}$$

which has $2n$ free parameters, so Gaussian quadrature has the highest possible accuracy for same number of nodes by optimally choosing nodes and weights[28]. The nodes of Gaussian quadrature can be obtained by using orthogonal Legendre polynomial P_n (the zero roots of P_n is the nodes). The Legendre product rules also guarantee that the quadrature will be exact with n points if $2nth$ derivative of integrand is zero [31]. It is also proved that the weights are always positive for any n, so that the Gaussian quadrature rules are always stable and the approximate value will converge to the exact integral as n increases [28].Considering the large amount of computing work, CPU time, the stability and the high-accuracy solution demand, Gaussian-Legendre quadrature is the optimal way to obtain the integration of the Green function in equation (2.8a).

The source zone can be divided into four triangle elements. The total integration is the sum of each element. Dunavant has developed high-degree efficient symmetrical Gaussian rules (up to degree 20) and produce the weights and nodes position for the standard triangle in coordinate system, as shown in Figure 2.4 [1][32].

For any function in the standard triangle in coordinate system, the Gaussian quadrature rule can be performed using the following equation:

$$\int_A f(\alpha,\beta)\,dA = A\sum_{i=1}^{ng} \omega_i f(\alpha_i,\beta_i) \tag{2.22}$$

where for the ith Gaussian point, the location is (α_i, β_i), and the corresponding Gaussian weight is ω_i. For polynomial function with highest order p, ng is the sufficient number of nodes to guarantee the quadrature error to be zero. To get the number of nodes, node positions and weights, the moment equa-

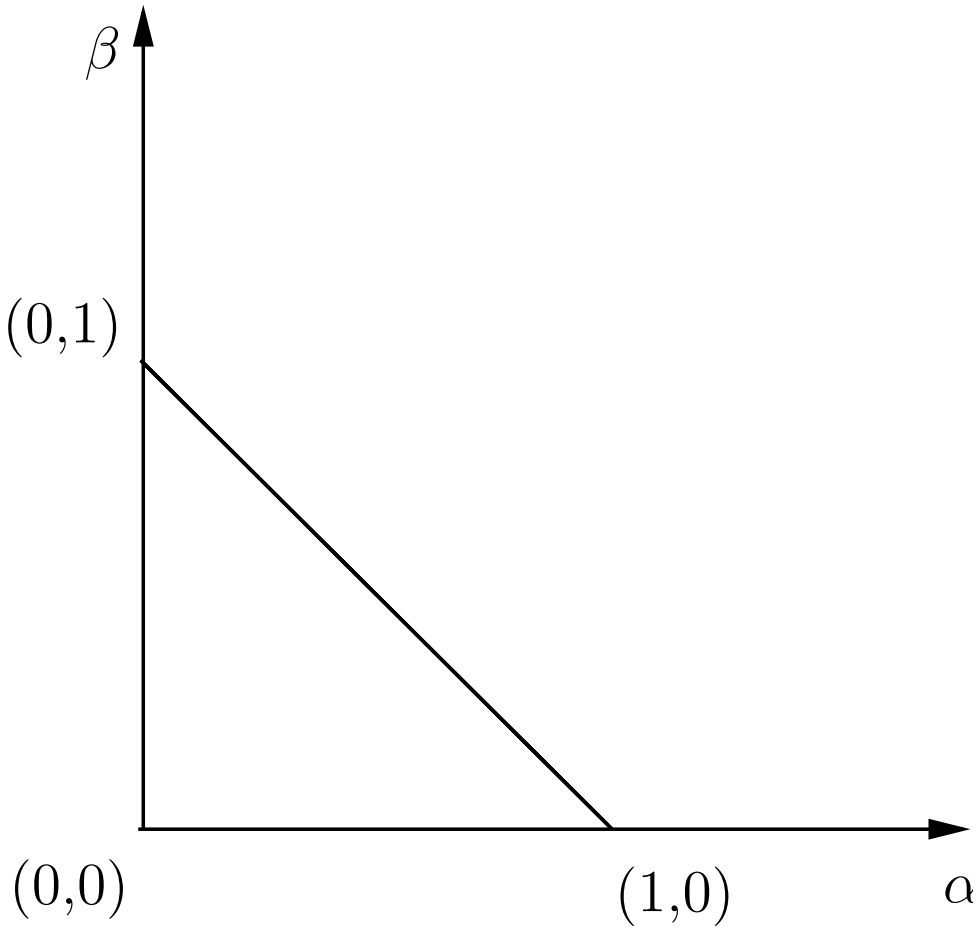

Figure 2.4: Natural coordinate standard triangle[1]. (x, y) is the natural coordinate and the vertex of the standard triangle is $(0, 0)$, $(0, 1)$, and $(1, 0)$

tion need to be set up and solved [33]. For an arbitrary order p polynomial, it has np terms as the part of system of moment equations:

$$\int_A f_1(x,y)\,dA - A\sum_{i=1}^{ng}\omega_i f_1(x_i,y_i) = 0 \tag{2.23a}$$

$$\cdots$$

$$\int_A f_{np}(x,y)\,dA - A\sum_{i=1}^{ng}\omega_i f_{np}(x_i,y_i) = 0$$

$$np = \frac{(p+1)(p+2)}{2} \tag{2.23b}$$

Sylvester proved that for the triangle, Newton-Cotes rules requires $n(n+1)/2$ nodes to be accurate for polynomial of degree n [34]. For Gaussian quadrature, the number nodes can be much less, since this system of nonlinear equations is highly dependent and be reduced. The system of moment equations can be solved by deMoivre's theorem in polar coordinates [32]. The number of nodes for Gaussian quadrature is shown in the table 2.1.

Table 2.1: Degree and nodes' number of Gaussian quadrature [1]

Degree of polynomial n	number of nodes ng (orders)
1	1
2	3
3	4
5	7
6	12
7	13
8	16
9	19
10	25
11	27
12	33
13	37
14	42
15	48
16	52
17	61
18	70
19	73
20	79

The nodes' positions for degree 1,5,10 and 20 for unit triangle by using Dunvant MATLAB library are shown in Figure 2.5.

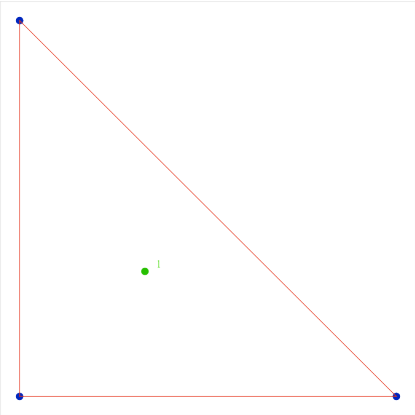

(a) Nodes position of degree 1

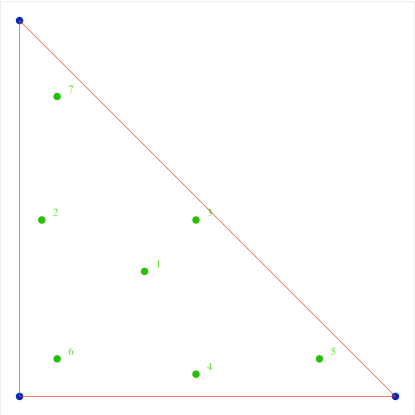

(b) Nodes position of degree 5

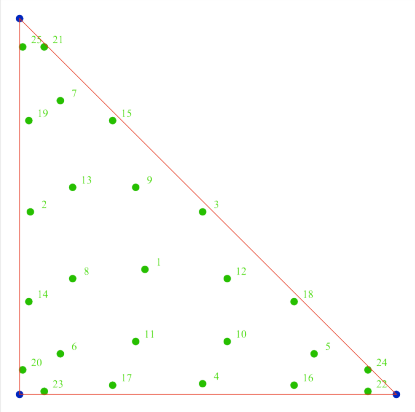

(c) Nodes position of degree 10

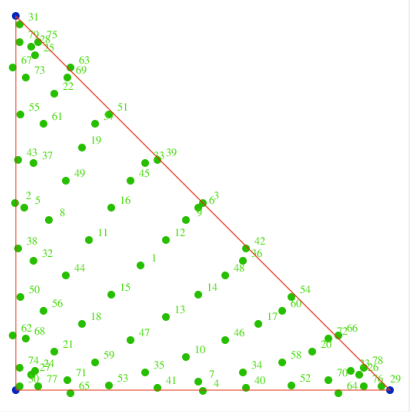

(d) Nodes position of degree 20

Figure 2.5: Nodes position of degree 1,5,10,20, red line is the edge of unit triangle, blue points are the vertex of the unit triangle, green points are the nodes for Gaussian quadrature

The Gaussian quadrature in unit triangle can be transformed to any arbitrary physical triangle by using the affine transformation as the following equation:

$$\begin{aligned} x_i &= t(1,1)(1-\alpha_i-\beta_i) + t(1,2)\alpha_i + t(1,3)\beta_i \\ y_i &= t(2,1)(1-\alpha_i-\beta_i) + t(2,2)\alpha_i + t(1,3)\beta_i \\ & i = 1,2,\ldots,n \end{aligned} \tag{2.24}$$

where $t\,(p,q)$ is the component of $T\,(2,3)$, which is the coordinate of physical triangle vetices, $(\alpha_i,\beta_i)^T$ are the coordinates of Gaussian quadrature nodes

in unit triangle (reference space), $(x_i, y_i)^T$ are the coordinates of Gaussian quadrature nodes in physical triangle (physical space).

So by transferring coordinate system to the flow direction, transferring dispersion coefficient and using Gaussian quadrature rules, we can get the semi-analytical solution of the case with two dimensional flow and full dispersion tensor.

One examples can be made to produce the semi analytical solution: the domain is 100×100, with initial pulse in the middle of the domain as 10×10. The velocity is diagonal flow, so by changing the coordinate, the semi-analytical solution at the early time (time $= 1$) is shown in Figure 2.6.

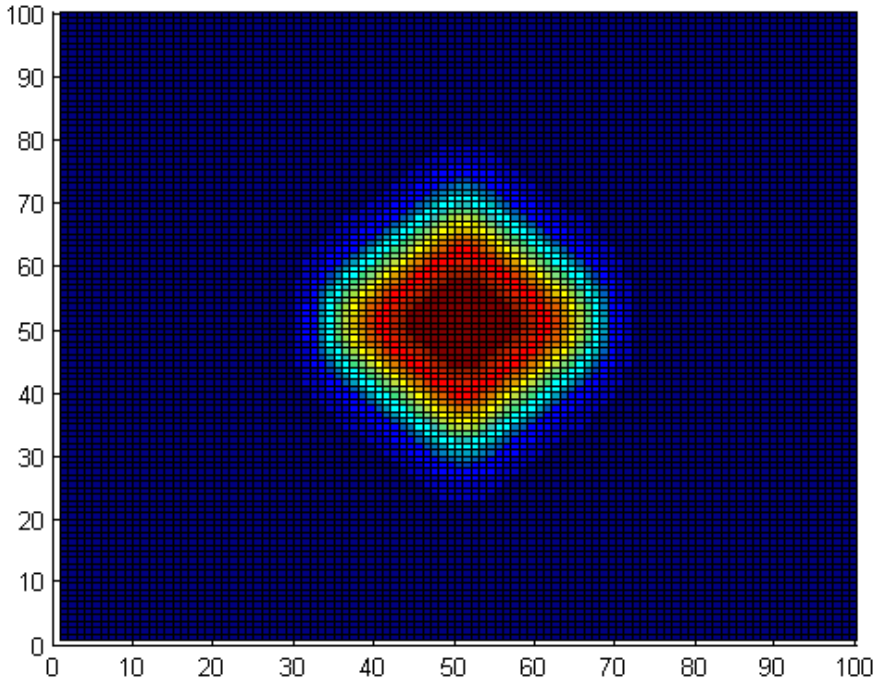

Figure 2.6: semi-analytical solution at early time (time $= 1$, $D_x = 0.5$, $D_y = 0.2$)

The semi-analytical solution cannot be obtained at initial condition since the equation has to be divided by zero time. At later time (time=100), the pulse diffuse away and the analytical solution is shown in Figure 2.7.

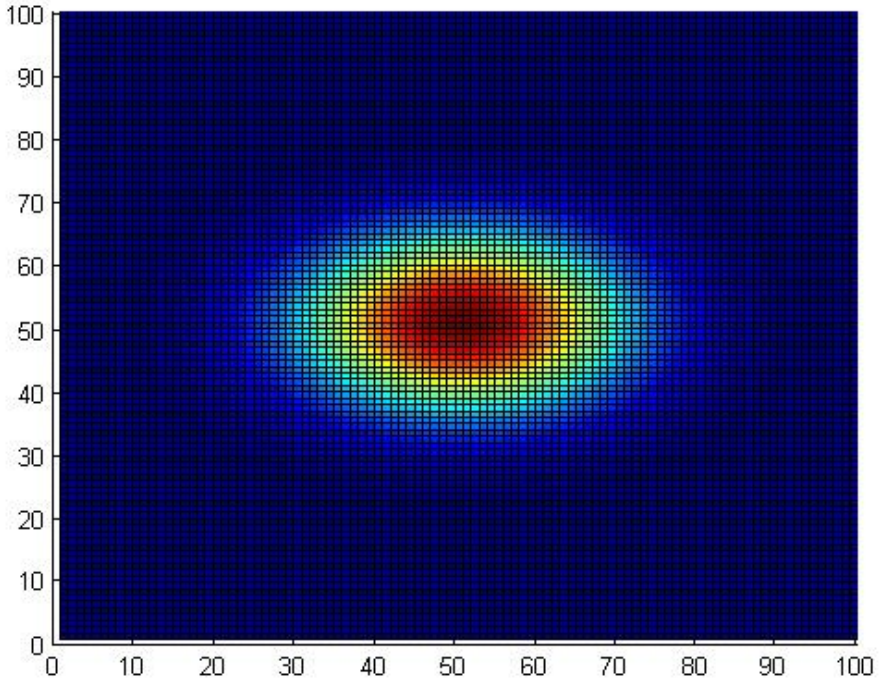

Figure 2.7: semi-analytical solution at later time (time=100, $D_x = 0.5$, $D_y = 0.2$)

2.3 Summary

In this section, I have presented the governing equation of the transport model and the component of the dispersion tensor. The effect of cross-dispersion in numerical model will be disscussed in the Chapter 3. I have also presented efficient methods to obtain the analytical/semi-analytical solution for the transport model with some specific initial condition. The semi-analytical solution will be used in benckmark problems in Chapter 3 to test the convergence rate of the FCT method.

CHAPTER 3

FLUX CORRECTED TRANSPORT ALGORITHM AND NUMERICAL SIMULATION

3.1 Flux Corrected Transport Algorithm

Considering the generic simple form for equation 2.1 (only one component, without reaction term and retardation factor):

$$\frac{\partial c}{\partial t} + \nabla \cdot (vc) = \nabla \cdot (\mathbf{D} \nabla c) \tag{3.1}$$

for the two dimensional system, the general discretization, such as finite volume mesh, can be expressed by the numerical flux at the edge of the cell as shown in figure 3.1.

$$c^{n+1} = c^n + \Delta t \left\{ \frac{1}{\triangle x} \left[F_W - F_E \right] + \frac{1}{\triangle y} \left[F_S - F_N \right] \right\} \tag{3.2}$$

F_W and F_E are fluxes in x direction; F_S and F_N are fluxes in y direction. The flux is the combination of transport, which is the product of velocity and concentration, and of dispersion, which is the product of the concentration gradient and the dispersion coefficient as shown in the following equation:

$$F_w = v_x c|_w - D_{xx} \frac{\partial c}{\partial x}|_w - D_{xy} \frac{\partial c}{\partial y}|_w \tag{3.3}$$

The procedure of applying FCT algorithm is as follows [35]:

1. Compute F^L, the "low order fluxes" which guaranteed the positive solution. As shown in Figure 3.1, low order fluxes F^L are the inlet and outlet fluxes of one cell which based on low order spatial discretization, such as upwind method and ignoring cross-dispersion term discussed below.

2. Compute F^H,the "high order fluxes" which produce the "accurate"

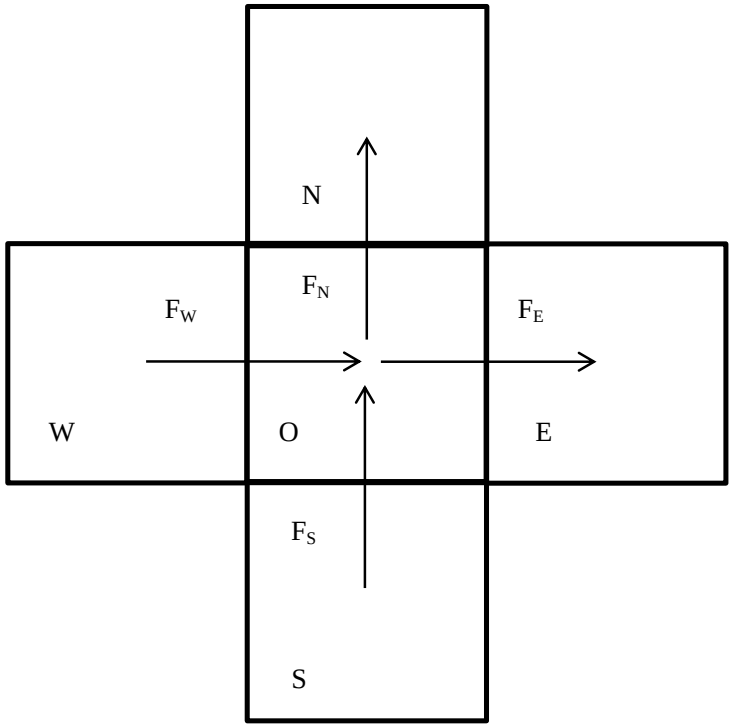

Figure 3.1: Numerical flux between one cell and its neighbor cells for two dimensional system. The arrows are the flux, which is positive if the flux direction same as the arrow direction.

solution with less artificial dispersion. As shown in Figure 3.1, high order fluxes F^H are the inlet and outlet fluxes of one cell which based on high order spatial discretization, such as central difference method discussed below.

3. Define the anti-diffusion flux [36] as equation 3.4below:

$$A_p = F_p^H - F_p^L \quad p = W, E, S, N \tag{3.4}$$

4. Compute the low order solution c^L for the next time step first, by using equation 3.5. The flux can be calculated either from current time step (explicit) or from next time step (implicit).

$$c^L = c^n + \triangle t \left\{ \frac{1}{\triangle x} \left[F_W^L - F_E^L \right] + \frac{1}{\triangle y} \left[F_S^L - F_N^L \right] \right\} \tag{3.5}$$

5. Using flux limiter to produce "corrected flux" A_p^C, which can guarantee the positive solution, based on anti-diffusion flux using equation 3.6.

$$A_p^C = C A_p \quad p = W, E, S, N \tag{3.6}$$

6. Apply the limited anti-diffusive fluxes back, using equation 3.7

$$c^{n+1} = c^L + \triangle t \left\{ \frac{1}{\triangle x} \left[A_W^C - A_E^C \right] + \frac{1}{\triangle y} \left[A_S^C - A_N^C \right] \right\} \tag{3.7}$$

3.2 Discretization

3.2.1 Temporal discretization

Kuzmin has proved that after applying FCT algorithm, the numerical diffusion linearly depends on the size of time steps, either for the backward Euler method, which is first-order accurate, or for Crank-Nicolson method, which second-order accurate [14]. Most past work on FCT is explicit. Considering the stability and the cost of computing, fully implicit method (which is unconditionally stable) is applied in this thesis. The special process to apply FCT using implicit method will be discussed below.

3.2.2 Spatial discretization

The finite volume spatial discretization is usually second-order accurate for dispersion using central-difference approximation and second-order accurate for transport using central-difference approximation, or first-order accurate for transport using up-wind approximation. Figure 3.2 shows the schematic to discretize the dispersion part with cross-dispersion term.

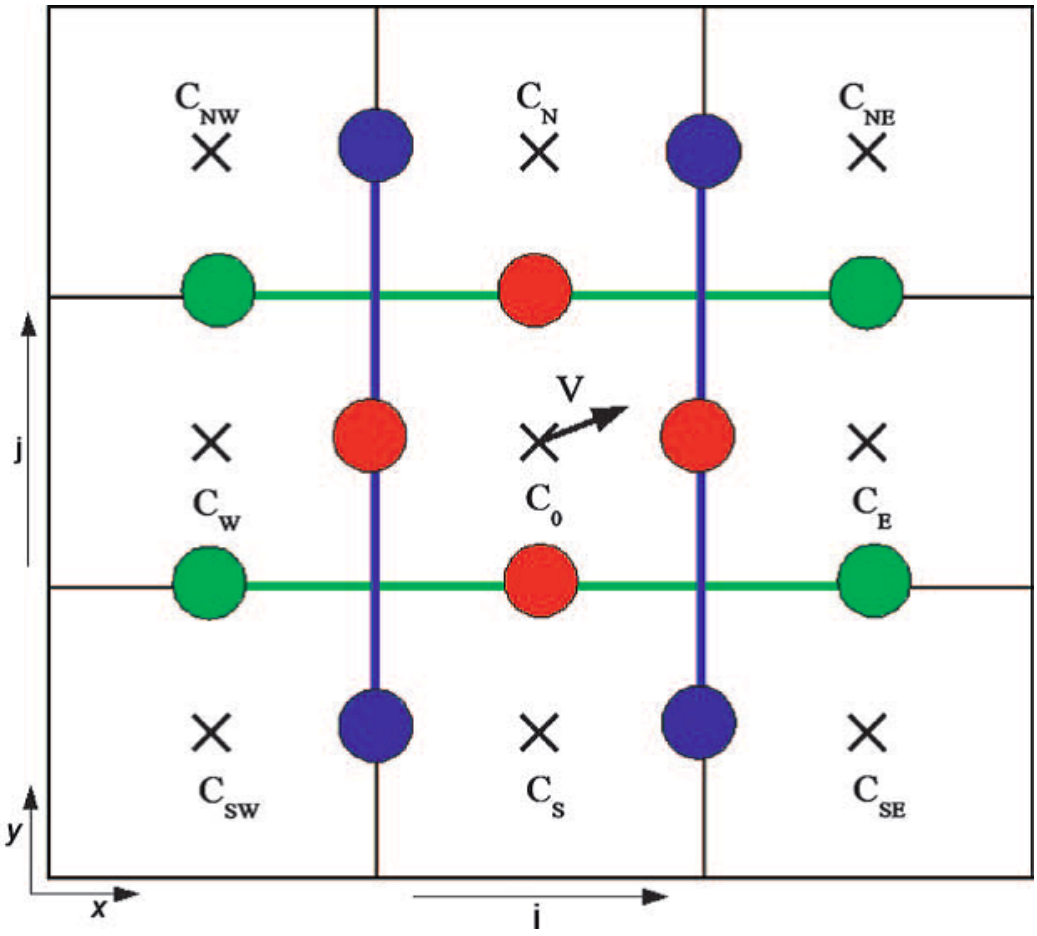

Figure 3.2: Grid used for centered-difference approximation of full-tensor dispersion. Red circles are the positions where gradient can be directly computed. Green (x direction) and blue circles (y direction) are the positions where concentration is approximated as the average of the adjunct nodes to compute the gradient [6].

For simple case, the velocity, dispersion coefficient and the grid are uniform. As shown in Figure 3.1, for normal-dispersion term, the approximation in x

direction is in the following form:

$$\frac{\partial}{\partial x}\left(D_{xx}\frac{\partial c}{\partial x}\right)=\frac{1}{(\triangle x)^2}\left[D_{xx}\left(c_E-c_0\right)-D_{xx}\left(c_0-c_W\right)\right] \tag{3.8}$$

For cross-dispersion term, the approximation in x direction is in the following form:

$$\frac{\partial}{\partial x}\left(D_{xy}\frac{\partial c}{\partial y}\right)=\frac{1}{4\triangle x\triangle y}\left[D_{xy}\left(c_{ES}+c_S-c_{NE}-c_N\right)-D_{xy}\left(c_S+c_{WS}-c_N-c_{NW}\right)\right] \tag{3.9}$$

For the transport term, the approximation in x direction is in the following form:

$$\frac{\partial}{\partial x}\left(v_x c\right)=\frac{1}{\triangle x}\left\{v_x\left[\left(1-\beta\right)c_0+\beta c_E\right]-v_x\left[\left(1-\beta\right)c_W+\beta c_0\right]\right\} \tag{3.10}$$

For center-difference approximation, $\beta=0.5$ and for up-wind approximation, $\beta=1$ when velocity is positive. So the fully-implicit dispersion approximation is given as the following [6]:

$$\begin{aligned} C_0^n=\alpha_0 C_0^{n+1}+\alpha_N C_N^{n+1}+\alpha_S C_S^{n+1}+\alpha_E C_E^{n+1}+\alpha_W C_W^{n+1} \\ +\alpha_{SW} C_{SW}^{n+1}+\alpha_{SE} C_{SE}^{n+1}+\alpha_{NW} C_{NW}^{n+1}+\alpha_{NE} C_{NE}^{n+1} \end{aligned} \tag{3.11}$$

where the coefficient $\alpha_i$are given by the following form:

$$\begin{aligned} \alpha_0 &= 1+2\triangle t\left(\frac{D_{xx}}{\triangle x^2}+\frac{D_{yy}}{\triangle y^2}\right)-\frac{\triangle t v_x}{\triangle x^2}\left(1-2\beta\right)-\frac{\triangle t v_y}{\triangle y^2}\left(1-2\beta\right) \\ \alpha_E &= \frac{-D_{xx}}{\triangle x^2}\triangle t-\frac{\triangle t v_x}{\triangle x^2}\beta \\ \alpha_W &= \frac{-D_{xx}}{\triangle x^2}\triangle t+\frac{\triangle t v_x}{\triangle x^2}\left(1-\beta\right) \\ \alpha_N &= \frac{-D_{yy}}{\triangle y^2}\triangle t-\frac{\triangle t v_y}{\triangle y^2}\beta \\ \alpha_S &= \frac{-D_{yy}}{\triangle y^2}\triangle t+\frac{\triangle t v_y}{\triangle y^2}\left(1-\beta\right) \\ \alpha_{SW} &= \alpha_{NE}=\frac{-D_{xy}}{2\triangle x\triangle y}\triangle t \\ \alpha_{SE} &= \alpha_{NW}=\frac{D_{xy}}{2\triangle x\triangle y}\triangle t \end{aligned} \tag{3.12}$$

so the the linear system 3.13 is obtained:

$$\mathbf{L}\left[c^{n+1}\right] = \mathbf{R}\left[c^{n}\right] \tag{3.13}$$

for fully-implicit approximation, $\mathbf{L}$ is a nine-diagonal matrix, $\mathbf{R}$ is the identity matrix. Two sufficient positivity theorems have been proposed [37]:

1. A local extreme diminishing scheme discretized in time by the backward Euler method is unconditionally positive. Other time stepping schemes preserve positivity under an appropriate CFL-like condition.

2. A sufficient condition for the scheme 3.13 to preserve positivity is that:

   (a) $\mathbf{L}$ must be a M-Matrix, that is $L_{ii} > 0$ and $L_{ij} < 0$, for $i \neq j$

   (b) All the entries in $\mathbf{R}$ must be positive , $R_{ij} > 0$

Using standard finite volume discretization of full dispersion tensor on a structured grid does not satisfy the condition 2(a) and leads to the occurrence of negative concentration [38]. In the following part, I will concentrate on the full dispersion and omit the advective transport part.

3.3 Application of FCT

In this section, I will follow the procedure of Kuzimin [37] [39] [14] [35] [17] [16] to to show the robust application procedure of FCT.

3.3.1 High-order scheme

Let's write the dispersion equation in semi-discrete high-order form using coefficient shown above:

$$\frac{dC}{dt} = -D\nabla C = K^{H}\nabla C \tag{3.14}$$

where K^H denotes the discrete transport operator for high order spatial method. K^H is a nine-diagonal matrix. For each node p, Eqn. (3.14) has coefficients which are similar to equation (3.11), as shown in the following:

$$
\begin{aligned}
k_0^H &= -2\triangle t\left(\frac{D_{xx}}{\triangle x^2}+\frac{D_{yy}}{\triangle y^2}\right)\\
k_E^H &= \frac{D_{xx}}{\triangle x^2}\triangle t\\
k_W^H &= \frac{D_{xx}}{\triangle x^2}\triangle t\\
k_N^H &= \frac{D_{yy}}{\triangle y^2}\triangle t\\
k_S^H &= \frac{D_{yy}}{\triangle y^2}\triangle t\\
k_{SW}^H = k_{NE}^H &= \frac{D_{xy}}{2\triangle x\triangle y}\triangle t\\
k_{SE}^H = k_{NW}^H &= \frac{-D_{xy}}{2\triangle x\triangle y}\triangle t
\end{aligned}
\tag{3.15}
$$

So for each node p , this equation can be written as fluxes format:

$$
\frac{dc_p}{dt}=\sum_{s\neq p}k_{ps}^H\left(c_s-c_p\right) \tag{3.16}
$$

The numerical solutions show that using high order equation scheme will result in negative concentrations. Since K^H matrix is not an M-matrix as discussed above, it cannot guarantee the positive solution anymore.

3.3.2 Low-order scheme

Kuzmin demonstrates that it is possible to obtain low-order matrix K^L from the high-order matrix K^H: K^L is a M-matrix and leads to a monotonic and non-negative solution. K^H is modified by adding a proper amount of artificial diffusion to eliminate all negative off-diagonal entries:

$$
K^L = K^H + D \tag{3.17}
$$

$$
\begin{aligned}
d_{pp} &= -\sum_{k\neq p}d_{pk}\\
d_{ps} = d_{sp} &= max\left\{0,-k_{ps}^H,-k_{sp}^H\right\}
\end{aligned}
\tag{3.18}
$$

From equation (3.11), it is clear that most entries in D are zero, except when it shows up in the diagonals resulting from the discretization of cross-

dispersion (k^H_{SE} and k^H_{NW}) or it shows up in the main diagonal. So the non-zero entries are shown below:

$$\begin{aligned} d_{SE} = d_{NW} = -k^H_{SE} = \frac{D_{xy}}{2\triangle x \triangle y}\triangle t \\ d_0 = \frac{-2D_{xy}}{2\triangle x \triangle y}\triangle t \end{aligned} \tag{3.19}$$

It is clear that D is a tridiagonal matrix, follows the form of a discrete equation (the flux is proportional to the difference between central node and neighborhood node in diagonal direction), and it still keeps the mass conservation properties. For dispersive transport, the procedure above separates the dispersion into different directions, which can be viewed as a special kind of "operator-splitting". The above procedure can also be applied to the advection part. For advective transport, the procedure above makes the second-order central-difference coefficient matrix earn the same order of accuracy as the first-order up-wind scheme. Also, the form of the matrix is also the same as the up-wind coefficient matrix after admitting the decomposition into fluxes [17]. It can be understood as a weighted averaging procedure where the weight depends on the grid and time step and the value of D [6]. We use notation of Kuzmin and let c^H represent the solution of high-order method at the new time level $n+1$, C^n represent the solution at the old time level n. Using fully implicit (backward Euler) time discretization, the Equation 3.14 changes to the following:

$$\left(\frac{1}{\triangle t}I - K^L\right)C^H = \frac{1}{\triangle t}C^n - DC^H \tag{3.20}$$

The equation can be split into two parts, the left-hand side part can be solved first to produce low-order solution :

$$\left(\frac{1}{\triangle t}I - K^L\right)C^L = \frac{1}{\triangle t}C^n \tag{3.21}$$

Also write the discrete equation for an arbitrary grid point p , then the equation (3.16) changes to:

$$\frac{dc_p}{dt} = \sum_p k^H_{sp}c_p + \sum_{p\neq s} d_{sp}\left(c_p - c_s\right) = \sum_p k^L_{sp}c_p \tag{3.22a}$$

$$\frac{1}{\triangle t}c_p^H - \sum_s k_{ps}^L c_s^H = \frac{1}{\triangle t}c_p^n - \sum_{s\neq p} d_{sp}\left(c_s^H - c_p^H\right) \tag{3.22b}$$

3.3.3 Limiting strategy

We can also think the last term above to represent fluxes between nodes p and s. That is:

$$\sum_{s\neq p} d_{sp}\left(c_s^H - c_p^H\right) = \sum_{s\neq p} f_{ps}^* \qquad f_{sp}^* = -f_{ps}^* \tag{3.23}$$

These fluxes are omitted in low-order scheme because of causing negative concentration. These "high-order" fluxes are overestimated or underestimated because of discretization or rough average of physical variables, such as concentration, velocity and dispersion coefficient. In order to get results of high accuracy, we need to add the "limited"fluxes back, which avoid negative solution by limiting flux and hence guarantee non-negative concentration [17]. The flux limiting strategy is the key element of FCT method as shown below:

$$\frac{1}{\triangle t}c_p^H - \sum_s k_{ps}^L c_s^H = \frac{1}{\triangle t}c_p^n + \sum_{s\neq p} \alpha_{ps} f_{sp}^* \tag{3.24}$$

The correction factors α_{sp} vary between 0 and 1: when $\alpha_{sp} = 1$, the equation is the exact high-order solution; when $\alpha_{sp} = 0$, the equation can be viewed as a kind of "low-order " method (by changing the coefficient matrix into K^L, the second-order gradient for cross-dispersion is destroyed); when $\alpha_{sp} \in (0, 1)$, the possible solution in between. Here we apply Zalesak's limiter to select the limiter can be readily extended to implicit time discretizations[14].The ins and outs of flux correction process are elucidated below.

3.3.4 Prelimiting step

The prelimitting step is an easy but important beginning step. This step is to keep the steep front of the concentration by canceling the anti-diffusive flux which is opposite to the direction of the concentration gradient. The pre-

limitting step to cancel the anti-diffusive fluxes directed down the gradient of c is shown below:

$$f_{sp} = 0 \qquad \text{if} \quad f_{sp}\,(c_s - c_p) < 0 \tag{3.25}$$

In Kuzmin's experience, it is benefit for explicit scheme and also remains relevant for the implicit schemes. The purpose of prelimiting step is to ensure that the limited flux does not smooth the low-order solution and thus do not introduce new diffusion into the solution [14]. It is also proved that the pre-limiter will preserve the monotonicity of the concentration [40].

3.3.5 Zalesak's limiter

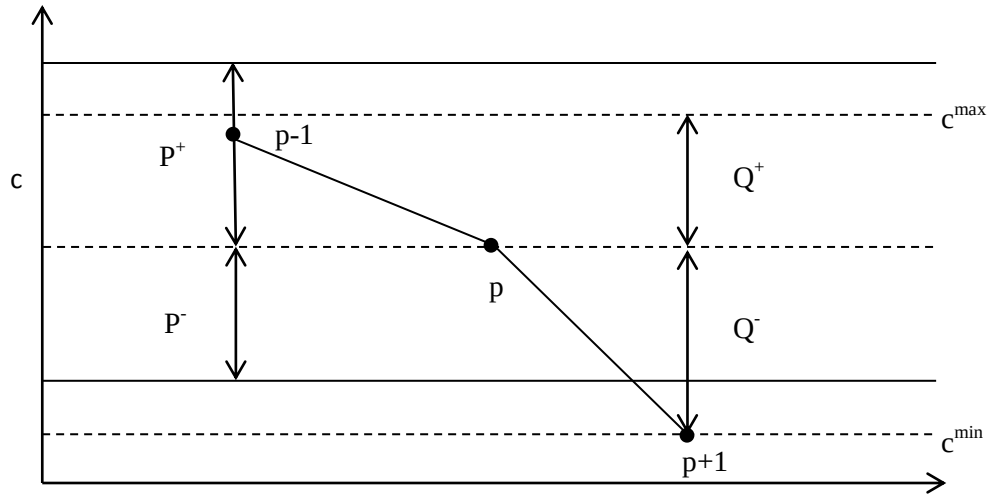

Figure 3.3: Zalesak's limiter in one dimension

Let c_p^{max} and c_p^{min} denote the maximum and minimum concentration in node p and its nearest neighbors (stencil S_p):

$$c_p^{max/min} =_{min}^{max} c_s \qquad \text{if} \quad s \in S_p \tag{3.26}$$

The straightforward estimate of local maximum and minimum is shown below:

$$c_p^{max} = max\left(c_W,\, c_E,\, c_{N,},\, c_S,\, c_{SW},\, c_{SE},\, c_{NW},\, c_{NE},\, c_p\right) \tag{3.27a}$$

$$c_p^{min} = min\left(c_W,\, c_E,\, c_{N,},\, c_S,\, c_{SW},\, c_{SE},\, c_{NW},\, c_{NE},\, c_p\right) \tag{3.27b}$$

These quantities represent the upper and lower bounds for the nodal values of the final solution. The task of the limiter is to guarantee the anti-diffusive fluxes cannot create new extrema [14].

The solution value at node p is affected by incoming anti-diffusive fluxes from neighboring nodes. The worst situation is that all the fluxes have the same sign and enhance a local extreme. So we give the denotation of all positive/negative contributions to node p based on the possible extreme of the inlet/outlet fluxes to give the upper bound and lower bound of the concentration:

$$P_p^+ = \frac{1}{m_p} \sum_{s \neq p} \left\{max\left(0, f_{sp}\right)\right\} \tag{3.28a}$$

$$P_p^- = \frac{1}{m_p} \sum_{s \neq p} \left\{min\left(0, f_{sp}\right)\right\} \tag{3.28b}$$

m_p is the amplification coefficient of matrix due to the temporal and spatial discretization, which guarantees the unit of P_p^+ and P_p^- is same as concentration [$^{\mathrm{M}}/_{\mathrm{L}^3}$] (in this thesis, $m_p = \Delta t$). The physical potential of concentration is the difference between local maximum/minimum concentration and concentration of node p. So the maximum/ minimum increment which node p is allowed to accept is given as:

$$Q_p^+ = c_p^{max} - c_p \tag{3.29a}$$

$$Q_p^- = c_p^{min} - c_p \tag{3.29b}$$

For the traditional numerical methods, the oscillation occurs because the unlimited fluxes are beyond the physically admissible range and make the unphysical decrease/increase in concentration. So the upper/lower bound should be based on the minimum of net fluxes and physical-permitted increment/decrement. Based on this principle, the maximum percentage of a flux

into/out of node p can be given as below:

$$R_p^+ = \begin{cases} min\left\{1, Q_p^+/P_p^+\right\} & P_p^+ > 0 \\ 0 & P_p^+ = 0 \end{cases} \tag{3.30a}$$

$$R_p^- = \begin{cases} min\left\{1, Q_p^-/P_p^-\right\} & P_p^- < 0 \\ 0 & P_p^+ = 0 \end{cases} \tag{3.30b}$$

Considering the connecting two grids have same flux with opposite sign, we can give the bonds for each nodes bounds by giving the minimum of correction factor:

$$\alpha_{ps} = \begin{cases} min\left\{R_p^+, R_s^-\right\} & f_{ps} \geq 0 \\ min\left\{R_s^+, R_P^-\right\} & f_{ps} < 0 \end{cases} \tag{3.31}$$

3.3.6 Positivity-preserving Proof

The purpose here is to introduce FCT scheme to avoid rising to non-physical phenomena. So the positivity-preserving property of FCT scheme needs to be confirmed. A widely-used sufficient positivity criterion is based on the concept of an $M - matrix$ which is mentioned in section 3.2.2 as shown below [39]:

Definition. A symmetric positive definite matrix with positive entries and non-positive off-diagonal entries is called an $M - matrix$

If cross-dispersion terms are not considered, all coefficient k_{ps}^H in equation (3.13) are non-negative, which means the scheme is stable and hold the property called local extreme diminishing (LED) [39]. The LED property means that for one node and its neighbor nodes, the local maximum cannot increase and the local minimum cannot decrease and hence the global minimum cannot decrease. This criterion implies positivity and prevents the non-physical osculations [41]. When taking cross-dispersion terms into consideration, it is not guaranteed that the right hand side entries are non-negative, since the coefficient k_{ps}^H is negative for cross-dispersion term.

However, by applying the limiting strategy with Zalesak's limiter, the LED property is guaranteed [16]:

$$c_p^{min} = c_p + Q_p^- \leqslant \bar{c_p} \leqslant c_p + Q_p^+ = c_p^{max} \tag{3.32}$$

So for equation (3.22b), the RHS entries are all non-negative and hence match the positivity suffcient condition. This proof implies that the FCT scheme possess the positivity and LED properties.

3.3.7 h-convergence analysis of FCT

In this part, I will study the spatial convergence of the FCT methods when solving the dispersion equation with full-tensor dispersion. I will use test problems considering either horizontal flow or diagonal flow, compare the error between numerical solutions and semi-analytical solution and make regression of errors to get the actual order of FCT algorithm in different cases. The error is measured as the root mean square error of concentration (RMSE) as shown below:

$$RMSE = \sqrt{\frac{1}{N}\sum (c_N - c_A)^2} \tag{3.33}$$

where N is the total numbers of nodes in the whole domain, c_N is the numerical solution which is obtained from high-order method or FCT method, and c_A is the analytical/semi-analytical solution which is obtained from analytical method discussed in Chapter 2.

For each case, I will first decrease the error of temporal discretization by shortening the time step until the temporal error is relatively small enough compared to the total error, so that the influence of time step can be omitted. Then for each case, I will apply a series of tests with different grid space to provide the relationship between grid space and spatial error, in other words, the h-convergence rate.

Three different cases are tested with parameters in Table 3.1:

1. test A is diagonal flow test with normal dispersion coefficient tensor;
2. test B is diagonal flow test without cross-dispersion term;
3. test C is horizontal flow test with normal disperssion coefficient tensor.

For case A, the relationship between RMSE and grid space for high-order method is shown in Figure 3.4. In case A, the RMSE results from FCT and

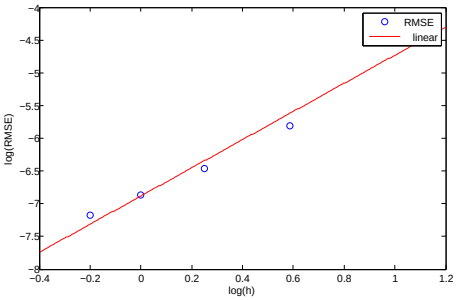

(a) RMSE result for case A (high-order)

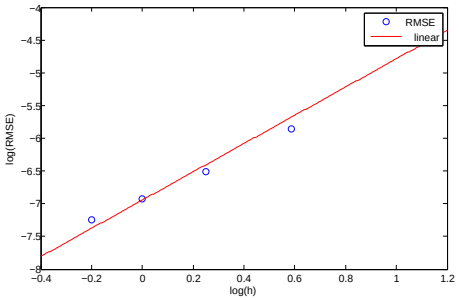

(b) RMSE result for case A (FCT)

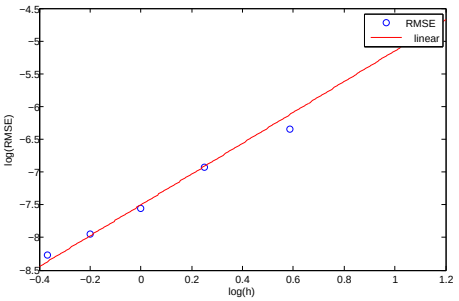

(c) RMSE result for case B

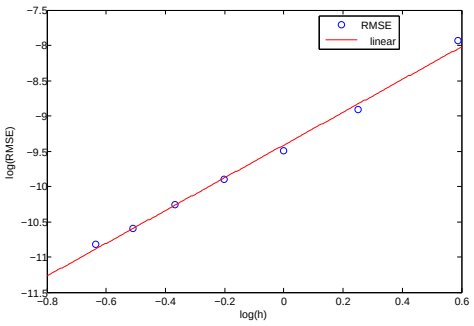

(d) RMSE result for case C

Figure 3.4: Relationship between RMSE and grid space for case A, B and C, the blue grid is the RMSE value (log value) for high-order or FCT method for each space, the red line is the linear fitting line with the slope $k \approx 2$

Table 3.1: Parameters for h-convergence tests

Parameter		Value
V_x		2
V_y	test A	2
	test B	2
	test C	0
α_L		0.1
α_T	test A	0.01
	test B	0.1
	test C	0.01
c_{pulse}		1
$c_{background}$		0
total time		18
final time step		0.01875
grid space	test A	0.69-3
	test B	0.69-3
	test C	0.53-1.8
grid number	test A	729-13689
	test B	729-13689
	test C	2025-23409

high-order solution are slightly different, but it is clear that FCT method is second-order accurate as the high-order solution. In case B and C, the cross-dispersion terms are zero since $\alpha_L = \alpha_T$ or $V_x = V_y$. So the FCT and high-order method solution are same as shown in Figure 3.4c and 3.4d. So it is obvious to see that for these situation, FCT method is same as the high-order solution, which is second-order accurate.

3.4 Summary

In this chapter, I present the common numerical method to solve the advection-dispersion equation and the negative-concentration problem caused by cross-dispersion term. To solve the negative-concentration problem, I present the procedure of applying the FCT method, prove the positivity-guaranteed property of FCT, and test the h-convergence rate of FCT method. The work in this chapter shows that the FCT method is sufficient and accurate enough to solve the advection-dispersion equation and to avoid the negative-

concentration problem.

CHAPTER 4

REACTIVE TRANSPORT MODEL

This section presents a general overview of the governing equations for reactive transport in porous media and the iterative solution technique for reactive transport. We will consider the case of "fully coupled" or "global implicit" formulation in which the transport (advection and dispersion) is solved simultaneously with nonlinear reaction. Two alternative numerical solution strategies (Total Component Approach and Free-Ion Approach) are presented.

4.1 Governing Equations-Chemical Reactions

We consider the case where there are multiple dissolved chemicals that can undergo reactions to form dissolved complexes, according to the following:

$$\sum_{i=1}^{N_c} v_{ji}\hat{c}_i = \hat{x}_j \quad j = 1, 2, \ldots, N_x \tag{4.1}$$

where $\hat{c}_i$ represents the chemical formula for component i, $\hat{x}_j$ represents the chemical formula for aqueous complex j, N_x is the number of aqueous complexes, and N_c is the number of components which can be shown to equal the total number of species N minus the number of linearly independent reactions [42]. The stoichiometric coefficient Eq.(4.1),v_{ji}, is the number of moles of component i in complex j. We furthermore consider the case where all aqueous-phase speciation reactions are at equilibrium, which is usually reasonable since these are fast reactions. Since the reactions (4.1) are at equilibrium, the mass action law can be used to write the concentration of each complex, x_j, as a function of the concentration of the components, c_i [42].

$$x_j = K_j \prod_{i=1}^{N_c} c_i^{v_{ji}} \tag{4.2}$$

where K_j is the equilibrium constant for the reaction given by (4.1). We can define the total dissolved concentration of the component as

$$\Psi_i = c_i + \sum_{i=1}^{N_c} v_{ji} x_i = c_i + \sum_{i=1}^{N_c} v_{ji} K_j \prod_{i=1}^{N_c} c_i^{v_{ji}} \tag{4.3}$$

Equation (4.3) shows how the equilibrium relationship partitions the total dissolved concentration (or mass) of species i among the 'free ion' c_i and the complexes x_j. it can be considered a nonlinear relation between the Ψ_i and c_k:

$$\Psi_i = g_i \left(c_1, c_2, \ldots, c_{N_c} \right) \tag{4.4}$$

If we consider the total dissolved concentration Ψ_i as a known quantity, then solution of the linear system (4.4) will yield the free ion concentration c_i. This is sometimes denoted the "speciation" calculation.

While the free ion concentration c_i is always positive, it is possible for the total component concentration Ψ_i to be negative, since the stoichiometric coefficients can be positive and negative. One example is hydrogen- at high pH, Ψ_{H^+} can be negative. Hence, to keep the total component concentration to be positive, the components need to be chosen carefully.

The chemical species also undergo reactions with the solid phase. Some examples are adsorption, precipitation and dissolution, etc. These reactions are usually slow and hence are described mathematically by a nonlinear kinetic rate expression. In general, the reaction rate will depend upon the concentration of the free ion and complex species. We can write the nonlinear reaction symbolically as:

$$R_i(c_1, c_2, \ldots, c_{N_c}) \tag{4.5}$$

Note that for simplicity we neglect the dependence of reaction rate upon any immobile-phase concentration.

The chemical source/sink reactions (4.5) can lead to an increase or decrease in the dissolved species concentration. There can also be a variety of kinetic reactions that occurs in the dissolved phase (e.g. radionuclide decay); these

reactions can also be expressed generically as in eqn (4.5). Concentration profiles for the free ion may not always be monotonic (though they are always positive); in fact it is quite impossible for profiles to exhibit multiple peaks and valleys.

4.2 Governing Equations–Advection-Dispersion-Reaction

The overall mass balance for the total dissolved component is the familiar advection-dispersion-reaction equation.

$$\frac{\partial \Psi_i}{\partial t} + L(\Psi_i) = R_i \qquad i = 1, 2, \ldots, N_c \tag{4.6}$$

where $L()$ is the advection-dispersion operator given by

$$L(\Psi_i) = \nabla \cdot (v\Psi_i - D_H \nabla \Psi_i) \tag{4.7}$$

where v is the velocity vector and D_H is the hydrodynamics dispersion tensor. Note that the advection-dispersion-reaction equation (4.6) for each chemical i are coupled together through the nonlinear source/sink term R_i. However, the reaction term R_i is a function of the free ion concentrations c_i, not the total component concentration Ψ_i. If Ψ_i is given, then the free ion concentration can be obtained by solving the speciation reaction (4.4). Therefore, the complete set of governing equations actually consists of the partial differential system (4.6) plus nonlinear algebraic system (4.4).

4.3 Solution Strategy

4.3.1 Operator Splitting

Operator splitting strategy is a non-iterative strategy, which does not fully couple the advection-dispersion and reaction parts. There is an extensive body of literature in the field of geoscience and environmental engineering regarding numerical solution of the system (4.6)[22][21][43]. Operator split-

ting strategy is the most simple and straightforward approach to calculate reaction in one time step, which entails the following steps over one time step:

1. Solve the nonreactive form of (4.6) with $R_i = 0$ over the time step.

2. Solve a system of coupled nonlinear ordinary differential equations for the reactions over the time step, using the result of step 1 as the initial condition. This step requires solution of the differential-algebraic-system (DAE) consisting of reaction ordinary differential equations with R_i on the right-hand-side, plus the nonlinear algebraic system (4.4).

This is a really simple approach and it can work well under some conditions with slow reactions and small time steps [44][23]. Another advantage of OS approach is to avoid non-physical concentration problem before reaction step. Since the transport term and reaction term are decoupled, it is easier to eliminate non-physical concentration by using high-resolution spatial schemes in transport step, such as TVD and FCT scheme. However, it has been found that for heterogeneous porous media, FCT scheme may not work as well as TVD for some cases in OS approach [45] [46].

4.3.2 Fully Coupled, Total Component Approach

To consider long time scales (tens to hundreds of years), implicit time discretization needs to be used due to stability and convergence problem. To apply backward Euler discretization to PDEs (4.6):

$$\frac{\Psi_i^{n+1,m+1} - \Psi_i^n}{\Delta t} + L(\Psi_i^{n+1,m+1}) = R_i^{n+1,m+1} \qquad i = 1, 2, \ldots, N_c \tag{4.8}$$

where superscript n refers to the time level and superscript m refers to the iteration count. Next we use a first-order Taylor's Series to expand the reaction term about known values at iteration n:

$$R_i^{n+1,m+1} = R_i^{n+1,m} + \sum_{k=1}^{N_c} \frac{\partial R_i}{\partial \Psi_k} (\Psi_k^{m+1} - \Psi_k^m) \tag{4.9}$$

The derivatives in eqn (4.9) requires some attention to compute because the reactions rate expressions are typically given in terms of the free ion concentration c_i not the total dissolved component concentration Ψ_i. So $\frac{\partial R_i}{\partial \Psi_k}$ is a function of the free ion concentration; hence computation of the derivatives at old iteration requires speciation—That is the nonlinear system (4.4) is solved for c_i^m given values for Ψ_i^m.

The approach above leads to a Newton-Raphson solution of the nonlinear coupled PDEs (4.6). Let us consider a particular spatial discretization of the advection -dispersion operator in (4.8). Assume the discrete equation for chemical species i at spatial grid point p can be expressed as follows:

$$f_{i,p}^{m+1} = \sum_s a_{p,s} \Psi_{i,s}^{n+1,m+1} - R_{i,p}^{n+1,m+1} - \frac{\Psi_{i,p}^n}{\Delta t} = 0 \tag{4.10}$$

where $f_{i,p}^{m+1}$ refers to the advection-dispersion-reaction equation for node p (it does not stand for flux). The summation above is over all spatial grid points s that are connected to grid point p; this connectivity and coefficients $a_{p,s}$ depend upon the particular numerical method. Note that the coefficients $a_{p,s}$ come from discretization of the non-reactive advection-dispersion equation (3.11). Letting the vector $\mathbf{\Psi}$ denote the values of all the chemical components at all the grid points (i.e., $\mathbf{\Psi}$ has the length $N_c \times N$ where N_c is the number of dissolved chemical components and N is the number of spatial points). We also define:

$$\delta \mathbf{\Psi}^{m+1} = \mathbf{\Psi}^{n+1,m+1} - \mathbf{\Psi}^{n+1,m} \tag{4.11}$$

Then we have the following Newton iteration scheme to advance the solution over one time step:

$$\mathbf{J}^m \delta \mathbf{\Psi}^{m+1} = -\mathbf{f}^m \tag{4.12}$$

The entries of residual vector $\mathbf{f}^m$ are shown in eqn (4.10). The entries of vector $\mathbf{\Psi^m}$ are shown as follows:

$$\mathbf{\Psi^m} = \begin{pmatrix} \mathbf{\Psi}_1 \\ \mathbf{\Psi}_2 \\ \vdots \\ \mathbf{\Psi}_N \end{pmatrix} \qquad with \qquad \mathbf{\Psi}_p = \begin{pmatrix} \Psi_{1,p} \\ \Psi_{2,p} \\ \vdots \\ \Psi_{N_c,p} \end{pmatrix} \tag{4.13}$$

where N stands for the total number of nodes, N_c is the number of com-

ponents. The entries show that we number all the components at each nodes. The coefficients of the Jacobian matrix are defined in the usual way as $J_{\alpha,\beta} = \frac{\partial f_\alpha}{\partial \Psi_\beta}$. In particular we have:

$$\begin{array}{lll} s \neq p & \dfrac{\partial f_{i,p}}{\partial \Psi_{i,s}} = a_{p,s} & \dfrac{\partial f_{i,p}}{\partial \Psi_{j,s}} = 0 \\ s = p & \dfrac{\partial f_{i,p}}{\partial \Psi_{i,p}} = a_{p,p} - \dfrac{\partial R_{i,p}}{\partial \Psi_{i,p}} & \dfrac{\partial f_{i,p}}{\partial \Psi_{j,p}} = -\dfrac{\partial R_{i,p}}{\partial \Psi_{j,p}} \end{array} \tag{4.14}$$

Note that in each iteration (4.12), we need to solve the nonlinear speciation problem (4.4) at every grid block in order to compute the free ion concentration which is required to evaluate the reaction rate and the derivatives appearing in the Jacobian (4.14), which can be expressed by using the chain rule:

$$\frac{\partial R_{i,p}}{\partial \Psi_{j,s}} = \sum_{k=1}^{N_c} \frac{\partial R_{i,p}}{\partial c_{k,s}} \frac{\partial c_{k,s}}{\partial \Psi_{j,s}} \tag{4.15}$$

The Jacobian in (4.12) equals the coefficient matrix from discretization of the advection-dispersion operator, plus additional terms along diagonal blocks from the kinetic reaction source-sink term.

Therefore we can write the Jacobian as follows:

$$\mathbf{J^m} = \mathbf{A} + \mathbf{J}^{R,m} \tag{4.16}$$

where

$$\mathbf{A} = \begin{pmatrix} A_{11} & A_{12} & \dots & A_{1N} \\ A_{21} & A_{22} & \dots & A_{2N} \\ \vdots & \vdots & \ddots & \vdots \\ A_{N1} & A_{N2} & \dots & A_{NN} \end{pmatrix} \quad with \quad \mathbf{A}_{p,s} = a_{p,s} \begin{pmatrix} 1 & 0 & \dots & 0 \\ 0 & 1 & \dots & 0 \\ \vdots & \vdots & \ddots & \vdots \\ 0 & 0 & \dots & 1 \end{pmatrix}_{N_c \times N_c}$$

$$\mathbf{J}^R = \begin{pmatrix} \mathbf{J}^R_{22} & 0 & \dots & 0 \\ 0 & \mathbf{J}^R_{22} & \dots & 0 \\ \vdots & \vdots & \ddots & \dots \\ 0 & 0 & \dots & \mathbf{J}^R_{NN} \end{pmatrix} \quad with \quad \mathbf{J}^R_{p,p} = - \begin{pmatrix} \frac{\partial R_{1,p}}{\partial \Psi_{1,p}} & \frac{\partial R_{1,p}}{\partial \Psi_{2,p}} & \dots & \frac{\partial R_{1,p}}{\partial \Psi_{N_c,p}} \\ \frac{\partial R_{2,p}}{\partial \Psi_{1,p}} & \frac{\partial R_{2,p}}{\partial \Psi_{2,p}} & \dots & \frac{\partial R_{2,p}}{\partial \Psi_{N_c,p}} \\ \vdots & \vdots & \ddots & \vdots \\ \frac{\partial R_{N_c,p}}{\partial \Psi_{1,p}} & \frac{\partial R_{N_c,p}}{\partial \Psi_{2,p}} & \dots & \frac{\partial R_{N_c,p}}{\partial \Psi_{N_c,p}} \end{pmatrix} \tag{4.17}$$

In each Newton-Raphson iteration, the final step is to get the free ion c_i from total component Ψ_i by solving the nonlinear equations (4.3) or (4.4).

4.3.3 Fully Coupled, Free-Ion Approach

This approach has some advantages in complex problems where the free-ion values can vary over many orders of magnitude. The basic idea is to solve for the free ion concentration c_i instead of the total dissolved component Ψ_i. Therefore, we re-write the Newton-Raphson iteration as follows:

$$\mathbf{J}^m \delta \mathbf{c}^{m+1} = -\mathbf{f}^m \tag{4.18}$$

where $\delta \mathbf{c}^{m+1} = \mathbf{c}^{n+1,m+1} - \mathbf{c}^{n+1,m}$ and the vector $\mathbf{c}$ represents all the free-ion species at all the node points (i.e., just like $\mathbf{\Psi}$ above, $\mathbf{c}$ has length $N_c \times N$ where N_c is the number of dissolved chemical components and N is the number of spatial grid points). The coefficients of the Jacobian matrix are defined as $J_{\alpha,\beta} = \frac{\partial f_\alpha}{\partial c_\beta}$. In this case, we can use the chain rule to evaluate these derivatives, since as shown in eqn (4.10) f_i is a function of Ψ_i and from the speciation equations (4.4) Ψ_i is a function of $c_1, c_2, \ldots, c_{N_c}$. To make the notation more concise, we will define the components of the Jacobian used to solve the nonlinear speciation problem (4.4) as follows:

$$J^{\Psi}_{i,j} = \frac{\partial g_i}{\partial c_j} \tag{4.19}$$

Then the coefficients of Jacobian in equation (4.18) are

$$\begin{array}{lll} & s \neq p & \dfrac{\partial f_{i,p}}{\partial c_{i,s}} = a_{p,s} \left(J^{\Psi}_{i,i}\right)_s \qquad \dfrac{\partial f_{i,p}}{\partial c_{j,s}} = a_{p,s} \left(J^{\Psi}_{i,j}\right)_s \\ s = p & \dfrac{\partial f_{i,p}}{\partial c_{i,p}} = a_{p,p} \left(J^{\Psi}_{i,i}\right)_p - \dfrac{\partial R_{i,p}}{\partial c_{i,p}} & \dfrac{\partial f_{i,p}}{\partial c_{j,p}} = a_{p,p} \left(J^{\Psi}_{i,j}\right)_p - \dfrac{\partial R_{i,p}}{\partial c_{j,p}} \end{array} \tag{4.20}$$

Comparing the above with the total component formulation (4.14), we can see that the free ion formulation has a some what more dense Jacobian matrix. But unlike the total component formulation, we do not need to solve the nonlinear speciation problem after each iteration since speciation is already built into the Jacobian matrix. Now we can rewrite the Jacobian matrix in this case similar to (4.17), that is:

$$\mathbf{J^m} = \mathbf{A}^m + \mathbf{J}^{R,m} \tag{4.21}$$

with the difference of sub matrix:

$$\mathbf{A} = \begin{pmatrix} A_{11} & A_{12} & \dots & A_{1N} \\ A_{21} & A_{22} & \dots & A_{2N} \\ \vdots & \vdots & \ddots & \vdots \\ A_{N1} & A_{N2} & \dots & A_{NN} \end{pmatrix} \quad with \quad \mathbf{A}^m_{p,s} = a_{p,s} \begin{pmatrix} J^{\Psi}_{1,1} & J^{\Psi}_{1,2} & \dots & J^{\Psi}_{1,N_c} \\ J^{\Psi}_{2,1} & J^{\Psi}_{2,2} & \dots & J^{\Psi}_{2,N_c} \\ \vdots & \vdots & \ddots & \vdots \\ J^{\Psi}_{N_c,1} & J^{\Psi}_{N_c,2} & \dots & J^{\Psi}_{N_c,N_c} \end{pmatrix}$$

$$\mathbf{J}^R = \begin{pmatrix} \mathbf{J}^R_{22} & 0 & \dots & 0 \\ 0 & \mathbf{J}^R_{22} & \dots & 0 \\ \vdots & \vdots & \ddots & \dots \\ 0 & 0 & \dots & \mathbf{J}^R_{NN} \end{pmatrix} \quad with \quad \mathbf{J}^R_{p,p} = - \begin{pmatrix} \frac{\partial R_{1,p}}{\partial c_{1,p}} & \frac{\partial R_{1,p}}{\partial c_{2,p}} & \dots & \frac{\partial R_{1,p}}{\partial c_{N_c,p}} \\ \frac{\partial R_{2,p}}{\partial c_{1,p}} & \frac{\partial R_{2,p}}{\partial c_{2,p}} & \dots & \frac{\partial R_{2,p}}{\partial c_{N_c,p}} \\ \vdots & \vdots & \ddots & \vdots \\ \frac{\partial R_{N_c,p}}{\partial c_{1,p}} & \frac{\partial R_{N_c,p}}{\partial c_{2,p}} & \dots & \frac{\partial R_{N_c,p}}{\partial c_{N_c,p}} \end{pmatrix} \tag{4.22}$$

4.3.4 Log Formulation

The approach is sometimes advantageous for problems when the solution varies over several orders of magnitude. The idea is to solve each iteration for $\delta \ln \mathbf{c}$ instead of $\delta \mathbf{c}$ as follows:

$$\mathbf{J}^m \delta \ln \mathbf{c}^{m+1} = -\mathbf{f}^m \tag{4.23}$$

The coefficients of Jacobian matrix can be derived from the free-ion approach by using the chain rule:

$$J_{\alpha,\beta} = \frac{\partial f_\alpha}{\partial \ln c_\beta} = \frac{\partial f_\alpha}{\partial c_\beta} \times \frac{\partial c_\beta}{\partial \ln c_\beta} = \frac{\partial f_\alpha}{\partial c_\beta} \times c_\beta \tag{4.24}$$

Then the coefficients of the Jacobian in equation (4.23) are:

$$\begin{array}{lll} s \neq p & \dfrac{\partial f_{i,p}}{\partial \ln c_{i,s}} = a_{p,s} \left(J^{\Psi}_{i,i}\right)_s c_{i,s} & \dfrac{\partial f_{i,p}}{\partial \ln c_{j,s}} = a_{p,s} \left(J^{\Psi}_{i,j}\right)_s c_{j,s} \\ s = p & \dfrac{\partial f_{i,p}}{\partial \ln c_{i,p}} = a_{p,p} \left(J^{\Psi}_{i,i}\right)_p c_{i,p} - \dfrac{\partial R_{i,p}}{\partial c_{i,p}} c_{i,p} & \dfrac{\partial f_{i,p}}{\partial \ln c_{j,p}} = a_{p,p} \left(J^{\Psi}_{i,j}\right)_p c_{j,p} - \dfrac{\partial R_{i,p}}{\partial c_{j,p}} c_{j,p} \end{array} \tag{4.25}$$

So the Jacobian in this case similar to the free ion approach, that is:

$$\mathbf{J^m} = \mathbf{A}^m + \mathbf{J}^{R,m} \tag{4.26}$$

with the difference in terms of each sub matrix:

$$\mathbf{A} = \begin{pmatrix} A_{11} & A_{12} & \dots & A_{1N} \\ A_{21} & A_{22} & \dots & A_{2N} \\ \vdots & \vdots & \ddots & \vdots \\ A_{N1} & A_{N2} & \dots & A_{NN} \end{pmatrix}$$

$$\text{with} \quad \mathbf{A}^m_{p,s} = a_{p,s} \begin{pmatrix} J^{\Psi}_{1,1}c_{1,1} & J^{\Psi}_{1,2}c_{1,2} & \dots & J^{\Psi}_{1,N_c}c_{1,N_c} \\ J^{\Psi}_{2,1}c_{2,1} & J^{\Psi}_{2,2}c_{2,2} & \dots & J^{\Psi}_{2,N_c}c_{2,N_c} \\ \vdots & \vdots & \ddots & \vdots \\ J^{\Psi}_{N_c,1}c_{N_c,1} & J^{\Psi}_{N_c,2}c_{N_c,2} & \dots & J^{\Psi}_{N_c,N_c}c_{N_c,N_c} \end{pmatrix}$$

$$\mathbf{J}^R = \begin{pmatrix} \mathbf{J}^R_{22} & 0 & \dots & 0 \\ 0 & \mathbf{J}^R_{22} & \dots & 0 \\ \vdots & \vdots & \ddots & \dots \\ 0 & 0 & \dots & \mathbf{J}^R_{NN} \end{pmatrix} \tag{4.27}$$

$$\text{with} \quad \mathbf{J}^R_{p,p} = - \begin{pmatrix} \frac{\partial R_{1,p}}{\partial c_{1,p}}c_{1,p} & \frac{\partial R_{1,p}}{\partial c_{2,p}}c_{2,p} & \dots & \frac{\partial R_{1,p}}{\partial c_{N_c,p}}c_{N_c,p} \\ \frac{\partial R_{2,p}}{\partial c_{1,p}}c_{1,p} & \frac{\partial R_{2,p}}{\partial c_{2,p}}c_{2,p} & \dots & \frac{\partial R_{2,p}}{\partial c_{N_c,p}}c_{N_c,p} \\ \vdots & \vdots & \ddots & \vdots \\ \frac{\partial R_{N_c,p}}{\partial c_{1,p}}c_{1,p} & \frac{\partial R_{N_c,p}}{\partial c_{2,p}}c_{2,p} & \dots & \frac{\partial R_{N_c,p}}{\partial c_{N_c,p}}c_{N_c,p} \end{pmatrix}$$

The update of c^{m+1} need to be done carefully, since the result of Newton-Raphson approach is $\delta \ln c^{m+1}$ instead of δc^{m+1}. So the update of c^{m+1} is like this:

$$\begin{aligned} \ln c^{m+1} &= \ln c^m \delta \ln c^{m+1} \\ c^{m+1} &= c^m \exp(\delta \ln c_{i,p}) \end{aligned} \tag{4.28}$$

4.3.5 Sequential Iteration Approach

The chemical species can be divided into two classes: mobiles (dissolved) and immobile (adsorbed chemicals,precipitated chemicals or attached microorganisms). Let's assume that there are N_c mobile species/components as above and there are $\bar{N}_c$ immobile species. Then the system of governing equations need to be modified [44] [47]. The system of equations with mobile species are PDEs (the advection-dispersion-reaction equation discussed above), on the contrary, the system of equations with immobile species, such as adsorption, precipitation and dissolution, etc are ODEs which are coupled

with mobiles' equations by N_R reaction terms as follows [21]:

$$\begin{aligned} \frac{\partial \Psi_i}{\partial t} + L(\Psi_i) &= \sum_{r=1}^{N_R} v_{ir} R_r \qquad i = 1, 2, \ldots, N_c \\ \frac{\partial \bar{c}_i}{\partial t} &= \sum_{r=1}^{N_R} \bar{v}_{ir} R_r \qquad i = 1, 2, \ldots, \bar{N}_c \end{aligned} \tag{4.29}$$

where Ψ_i stands for the total component of mobile phase, $\bar{c}_i$ stands for the immobile species' concentrations, R_r stands for the reaction term such as adsorption, precipitation and dissolution, v_{ir} and $\bar{v}_{ir}$ are stoichiometric coefficients for the moles of mobile and immobile species. If any mobile component does not react with immobile species, the total aqueous concentration Ψ_i is conserved and governed by the linear advection-dispersion reaction. Otherwise, the mass balance equation will have nonlinear reaction terms on the right-hand side [48]. These reaction can be described either as a kinetic reaction or equilibrium reaction, depending on the reaction speed. The reaction term usually has a nonlinear expression which depends upon the concentration of free ion, complex species and immobile-phase concentration. Global implicit method is conceptually straightforward to solve this system of equations, but requires most computing resources per time step and has some trouble in the calculation: since the reaction term is complex and depends on immobile species as well, it can be hard to get straight forward analytical expression for reactive part of Jacobian matrix, $\mathbf{J}_R$, for fully implicit approach. On the other hand, a much larger Jacobian matrix need to be built up to solve the concentration of mobile and immobile species at same time during each iteration in Newton-Raphson approach.

In order to make efficient computation, the large differential algebraic system of equations (DAE) need to be reformulated to reduced form of equations (compared to the original formulation). To make the reduction, several methods have been proposed: one method is systematically transform the governing equations to a reduction form of GIA [21] [49] [22] [43]; another method is sequential iteration approach (SIA), which is to decouple the mobile and immobile species, and to solve each mass balance equations separately in sequence (this step requires an extra iteration part in Newton-Raphson iteration) [22]. Sequential iteration approach (SIA) has been proved as a method which avoid the construction of the large matrices and corrects the error in

classic operator splitting approach[50][19][51][52].

The basic idea of SIA is to arrive at a fully coupled solution at $m+1$ iteration by using the reaction term from m iteration. In this way, rather than solving for the entire system, the reaction term is assumed constant during each iteration step as follows:

$$\frac{\Psi_i^{n+1,m+1} - \Psi_i^n}{\Delta t} + L(\Psi_i^{n+1,m+1}) = \sum_{r=1}^{N_R} v_{ir} R_r^{n+1,m} \qquad i = 1, 2, \ldots, N_c \quad (4.30)$$

where $L()$ is the advection-dispersion operator. Then the Newton-Raphson iteration can be applied to solve this system of equations. It is straight forward to see that the reaction part of Jacobian matrix, $\mathbf{J}^R$ becomes the zero matrix. So the residual equation (4.10) can be simplified into:

$$f_{i,p}^{m+1} = \sum_s a_{p,s} \Psi_{i,s}^{n+1,m+1} - R_{i,p}^{n+1,m} - \frac{\Psi_{i,p}^n}{\Delta t} = 0 \qquad (4.31)$$

and Jacobian matrix can be also simplified as:

$$\mathbf{J}^m = \mathbf{A} \qquad (4.32)$$

where $\mathbf{A}$ depends on which fully-implicit approach is used(total component or free ion approach).

The next step is to update the immobile species by using the relationship between mobile species and immobile species (e.g. adsorption isothermal):

$$\bar{c}_i^{n+1,m+1} = h_i(c_1^{n+1,m+1}, c_2^{n+1,m+1}, \ldots, c_{N_c}^{n+1,m+1}) \qquad i = 1, 2, \ldots, \bar{N}_c \quad (4.33)$$

where $h_i()$ is the nonlinear relationship between mobile species and immobile species. Then, the reaction term is updated by using concentration at $m+1$ iteration step:

$$\sum_{r=1}^{N_R} \bar{v}_{ir} R_r^{n+1,m+1} = \frac{\bar{c}_i^{n+1,m+1} - \bar{c}_i^n}{\Delta t} \qquad i = 1, 2, \ldots, \bar{N}_c \qquad (4.34)$$

The SIA approach is attractive since it can decrease the complexity of Jacobian matrix and avoid the operator splitting error. At the same time, SIA approach has two main problems:

1. The solution of the numerical problem may oscillate and make the iteration hard to converge [51]. When considering large time step for fully implicit method, the solution may stick to some nearby solution and only converge to low-precision solution.

2. SIA may decrease the convergence rate of Newton-Rapson approach. Since by estimating the immobile-phase reaction, the solving strategy actually change from Newton-Raphson approach, which is second-order method, to fix-point-like approach, which is first-order method. From Taylor Series expansion, it can be obtained that SIA approach approximates the reaction term by only using the first-order derivatives of the aqueous species. If the reaction term only relies on aqueous species, Newton's method is obtained; otherwise, the convergence rate will decrease and may have convergence problem [53].

CHAPTER 5

APPLICATION

In most past researches, the cross-dispersion term is usually ignored for reactive transport model due to non-physical value and convergence problem. However, the effect of cross-dispersion term may be significant for result of reactive transport model with heterogeneous flow field. The influence of cross-dispersion term in reactive transport, either equilibrium or kinetic, is still not clear for numerical model when the grid is not parallel or perpendicular to the flow direction.

Flux-corrected transport (FCT) method and total variation diminishing (TVD) method have been proved given excellent non-negative results when applied to non-reactive solute transport by using OS approach to decouple transport term (explicit) and reaction term [45] [54] [46]. But there are still problems for these two method: TVD method is usually explicit and hence cannot be applied in global implicit approach; for nonlinear reactions,FCT method, can produce low level oscillations which can give spurious results [45]. It is still unclear whether FCT method will work well in global implicit approach or sequential approach.

In order to answer these two questions, continuous input and initial pulse reactive transport problems in two-dimension with different kinds of reactions are set up. Each problem consider horizontal flow field, which does not need to consider cross-dispersion term and can be used as the benchmark example; diagonal flow field, in which scalar dispersion and full tensor dispersion results are compared; and heterogeneous flow field, which is for real flow field test. Different types of reactions, such as equilibrium/kinetic aqueous reaction, adsorption, and bio-chemical reaction. FCT method is applied in the tests (specifically, diagonal flow field and heterogeneous flow field tests), in which non-physical concentration exits due to the full tensor dispersion. The effect of FCT method is shown by comparing original results and FCT results.

5.1 Mixing-controlled Reactive Transport

Many contaminants can act as electron donor and carbon source, and be degraded by microorganism (electron acceptor) by mixing. When the contaminant is continuously introduced into groundwater by advection, a source zone, where electron acceptors are readily consumed, is formed a source zone and a plume evolves [48], as shown in Figure 5.1.

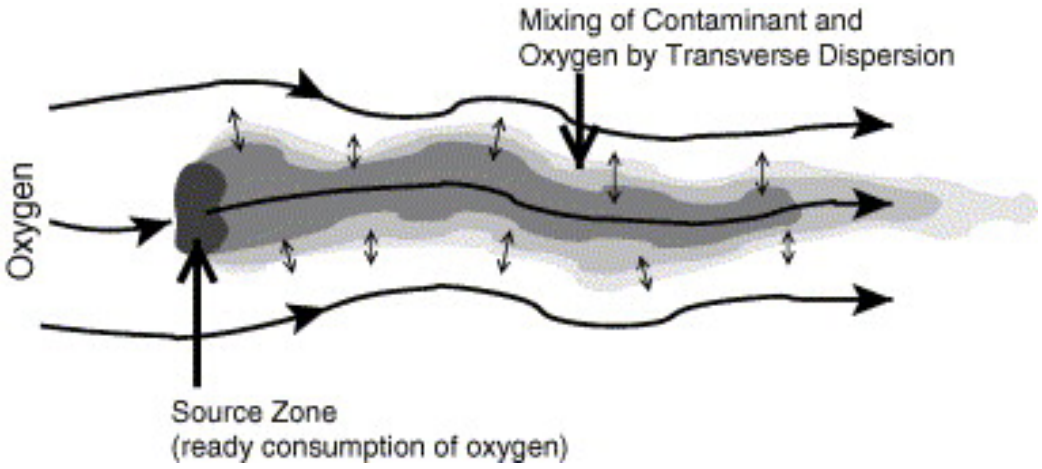

Figure 5.1: Situation of the plume from a continuously emitting source [55]

For horizontal flow field, in steady state, it has proved that the only mixing mechanism is the transverse dispersion and the corresponding plume length is controlled by transverse dispersion [56] [57] [58] [59] [60]. While for diagonal flow field, in steady state, as explained above, the mixing mechanism is both longitude and transverse dispersion (which is the transverse dispersion for diagonal direction shown in Chapter 2). It means that for steady state simulation, ignoring the cross-dispersion term may lead to bad results.

Cirpka and Valocchi have given the analytical solution to a simplified model with different types of reactions [55] [61]. The assumptions for the simplified model are: the domain is semi-infinite along the downstream of the source zone; the velocity field is horizontal; the contaminant concentration is uniform introduced into the domain via an inflow face; and the contaminant concentration is zero outside the plume, while the electron acceptor concentration is zero in the plume [48]. It has also been proved that for the horizontal flow field, the steady state plume length depends on the ratio of the concentration entering the domain, which depends on the type of the reaction (weighted by the stoichiometric coefficient), the lateral extension of

the source zone, the velocity and the transverse dispersion coefficient [48].

The tests are based on the simplified model. But the source zone is a rectangular zone inside the domain, instead of existing on the boundary, as shown in Figure 5.1:

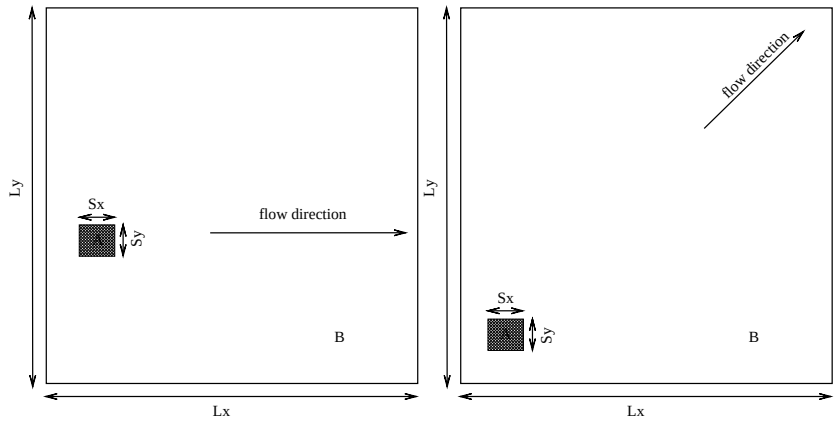

(a) Initial condition for horizontal flow field

(b) Initial condition for diagnol flow field

Figure 5.2: Initial condition for horizontal flow field. The colored zone is the source zone with the contaminant A, the background of the domain is filled with electron acceptor B, and the arrow is the flow direction. There is a constant concentration of B specified along the boundaries

where A is the contaminant introduced to the source zone, B is the electron acceptor which initially exists in the background, and the arrows show the direction of flow field for the test. The initial concentration of A, B and the product C is shown in the Table 5.1:

Table 5.1: Initial condition for continuously introduced contaminant

	source zone	background
c_A	1	10^{-15}
c_B	10^{-15}	2
c_C	10^{-15}	10^{-15}

The domain is square with width $L_x = L_y = 81$ and the source zone is also square with width $S_x = S_y = 5$. The grid space is $dx = dy = 1$. The time step for the simulation is 1000. The longitude dispersivity α_L is 1 and the transverse dispersivity α_T is 0.1. The velocity for horizontal flow field is $v_x = 5 \times 10^{-4}$, $v_y = 0$; and the velocity for diagonal flow field is

$v_x = v_y = {}^{5}/\sqrt{2} \times 10^{-4}$ (so the total velocity is $v_{total} = 5 \times 10^{-4}$ for either test). Under this condition, the longitudinal grid Peclet number and the transverse grid Peclet number are smaller than 2, so the oscillation caused by the advection is ignored, the only possible reason to get non-physical value is dispersion [62]. The boundary condition is constant concentration condition (same as background concentration).

5.1.1 Simple kinetic reaction

To consider the reaction between the electron donor and acceptor, the reaction rate must depends on the concentration of both reactants [48]. The simplest way to present the reaction is one-way irreversible kinetic reaction:

$$\alpha_A \mathrm{A} + \alpha_B \mathrm{B} \rightarrow \alpha_C \mathrm{C} \tag{5.1}$$

where α_i is stoichiometric coefficient of compound i. The simplest kinetic model is bilinear as follows [48]:

$$r = -\frac{1}{\alpha_A}\left.\frac{\partial c_A}{\partial t}\right|_{reac} = -\frac{1}{\alpha_B}\left.\frac{\partial c_B}{\partial t}\right|_{reac} = \frac{1}{\alpha_C}\left.\frac{\partial c_C}{\partial t}\right|_{reac} = k c_A c_B \tag{5.2}$$

where k is bilinear reaction rate coefficient. So the mixing-controlled setup is happening either the concentration of A is low and concentration of B is high, or the concentration of A is high and the concentration of B is low. For the well-mixed zone, the reaction rate will be high. The reaction terms for A, B, C in equation (4.6) are shown as following:

$$\begin{aligned} R_{\mathrm{A}} &= -\alpha_{\mathrm{A}} r \\ R_{\mathrm{B}} &= -\alpha_{\mathrm{B}} r \\ R_{\mathrm{C}} &= \alpha_{\mathrm{C}} r \end{aligned} \tag{5.3}$$

In this thesis, we simplify all the stoichiometric coefficients to be 1. In the first comparison, we consider four cases with different dispersion tensor and flow condition:

- Case 1: diagonal flow with full-tensor dispersion using usual Finite Volume method as shown in Figure 5.2a;

- Case 2: diagonal flow without cross-dispersion term using usual Finite Volume method as shown in Figure 5.2a;
- Case 3: diagonal flow with full-tensor dispersion using FCT method as shown in Figure 5.2a;
- Case 4: horizontal flow with full-tensor dispersion using usual Finite Volume method as shown in Figure 5.2b.

where we assume the simplest one-way irreversible kinetic reaction with same reaction rate $k = 10^{-3}$. For all the cases, the boundary condition and initial condition for concentration in pulse and background region are same. The convergence criterion is also the same for all cases (10^{-15}). The total simulation time is 100 time steps.

Figure 5.3, Figure 5.4 and Figure 5.5 show the distribution of concentrations of each components for four cases introduced above. Figure 5.3d, Figure 5.4d and Figure 5.5d show the horizontal flow case results, in which the cross-dispersion term is equal to zero and hence these can viewed as benchmark results. The results of Case 1, 2, 3 should be similar to the results of case 4 (rotated to diagonal direction). It is clear that the shape of plumes in case 1 and case 3 is similar to the plume in case 4. The plume in case 2 is different because of ignoring the cross-dispersion term (underestimate the dispersion in diagonal direction and overestimate dispersion off the diagonal direction). The shape of the plume shows that ignoring cross-dispersion term can make the plume shape change and the reaction can amplify the difference.

For case 1, Figure 5.3a, Figure 5.4a and Figure 5.5a show that in the mixing-controlled reactive transport model, the negative concentration of A, which is caused by cross-dispersion term in transport, widely exists in the background of the domain. Because of the mixing-controlled reaction, the negative concentration also affects B and C. However, the negative concentration region is different for each component: for A, the negative concentration region is on the background besides the plume; for B the negative concentration region is along the center of the plume; and for C the negative concentration region is the largest, on both the background besides the plume and the center of the plume.

For case 2, Figure 5.3a shows that the plume of A is much shorter than other cases. Figure 5.4a and Figure 5.5a show that the plume of B and C are

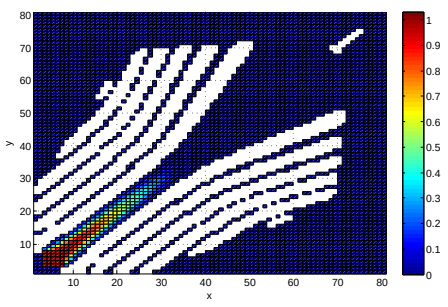

(a) Diagonal flow with full-tensor dispersion

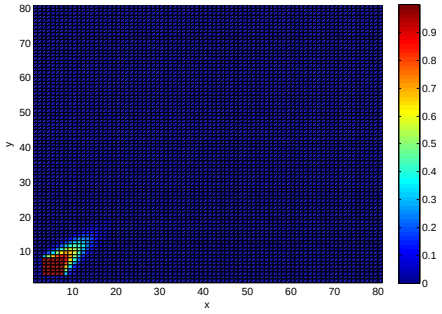

(b) Diagonal flow without cross-dispersion

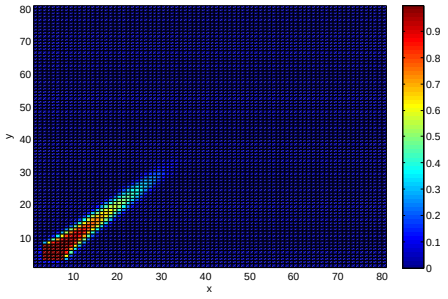

(c) Diagonal flow with full-tensor dispersion using FCT

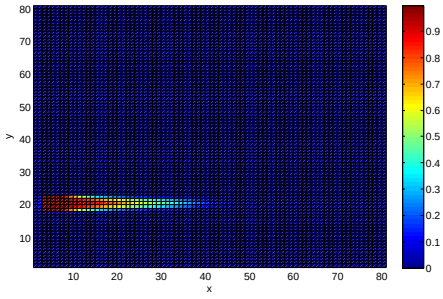

(d) Horizontal flow with full-tensor dispersion

Figure 5.3: Two-dimensional distribution of concentration of A for four kinetic mixing reaction test cases, the color shows the concentration of A and white region is the negative concentration zone

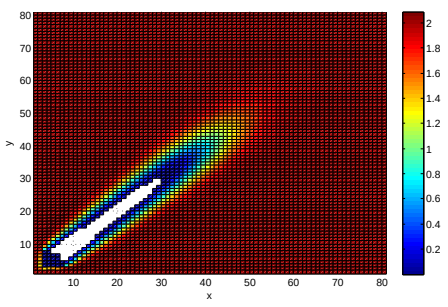

(a) Diagonal flow with full-tensor dispersion

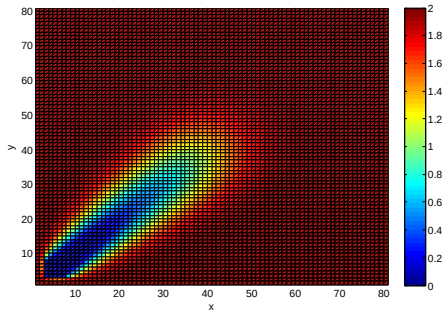

(b) Diagonal flow without cross-dispersion

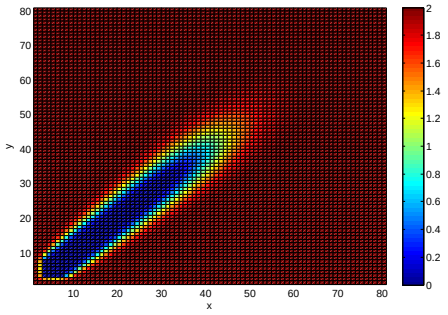

(c) Diagonal flow with full-tensor dispersion using FCT

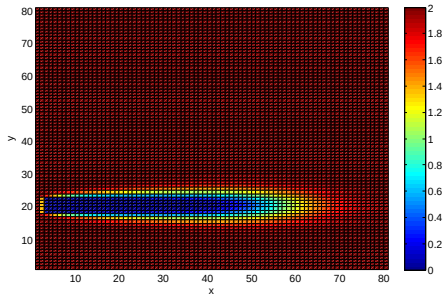

(d) Horizontal flow with full-tensor dispersion

Figure 5.4: Two-dimensional distribution of concentration of B for four kinetic mixing reaction test cases, the color shows the concentration of B and white region is the negative concentration zone

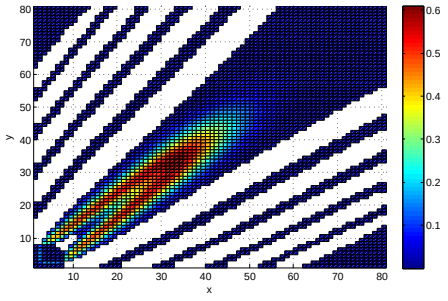

(a) Diagonal flow with full-tensor dispersion

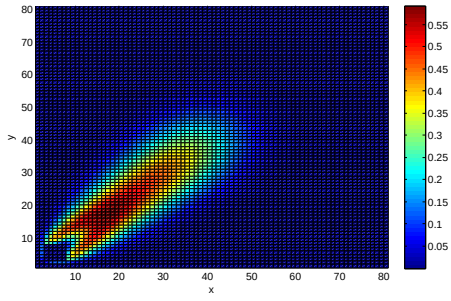

(b) Diagonal flow without cross-dispersion

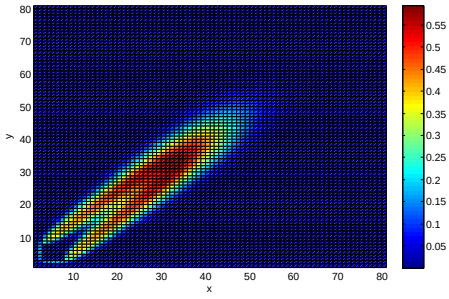

(c) Diagonal flow with full-tensor dispersion using FCT

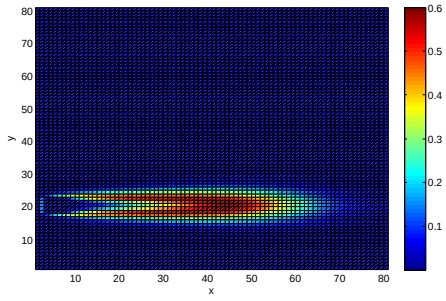

(d) Horizontal flow with full-tensor dispersion

Figure 5.5: Two-dimensional distribution of concentration of C for four kinetic mixing reaction test cases, the color shows the concentration of C and white region is the negative concentration zone

wider and shorter than the other cases, but not as short as the plume of A. By ignoring the cross-dispersion term, all the components disperse slower in the diagonal direction and faster in the transverse diagonal direction. So for case 2, A and B are better mixed. So by consuming by kinetic reaction, A can be blocked in a small region and have a quite short plume. And hence the distribution of the concentration of C is lagged. Since there is large amount of B in the background, the effect of mixing-controlled reaction is not that significant as A, so plume is not greatly changed.

For case 3, Figure 5.3c, Figure 5.4c and Figure 5.5c show that the plume is similar to the case 1 and 4, but does not have the negative region. So it can present the distribution of concentration of each component for the whole domain precisely.

Figure 5.6, Figure 5.7 and Figure 5.8 show the comparison of the concentration of each component along the center line of the flow direction. Figure 5.6 shows that in case 2, the gradient of A in the flow direction is much sharper than all the other cases. This result indicates that when considering the kinetic mixing-controlled reaction and diagonal flow field, ignoring cross-dispersion term can make significant change to the distribution of A. Figure 5.6 also shows that in the case 1 and case 3, the concentration of A has the similar distribution as case 4. It has been concluded that for the horizontal flow field, the criterion of the plume shape is transverse dispersion [63] [48]. So similarly, for diagonal flow field, cross-dispersion term must be another criterion. For case 1, besides the negative concentration problem, Figure 5.6 shows that it can also have the overshoot oscillation problem in the high-concentration region next to the source. And although by considering the cross-dispersion term, case 1 can have the similar shape of plume as case 4, the plume of A extends a little further than case 4. It is also shown that case 1 is less accurate than case 3. Figure 5.7 shows that the gradient of B in case 2 is less sharp than other cases. It is because in case 2, the dispersion of A is lagged by ignoring the cross-dispersion term and hence the mixing-controlled reaction is lagged. For case 1, since the negative concentration region of B is along the center of the plume, it is impossible to get the distribution of B along the central line. But for FCT solution, it still fit well to the benchmark results. Figure 5.8 shows the peak of the component C in the flow direction. The peak in case 2 is much nearer to the source zone and the shape of the concentration distribution in central is quite different from the other 3 cases.

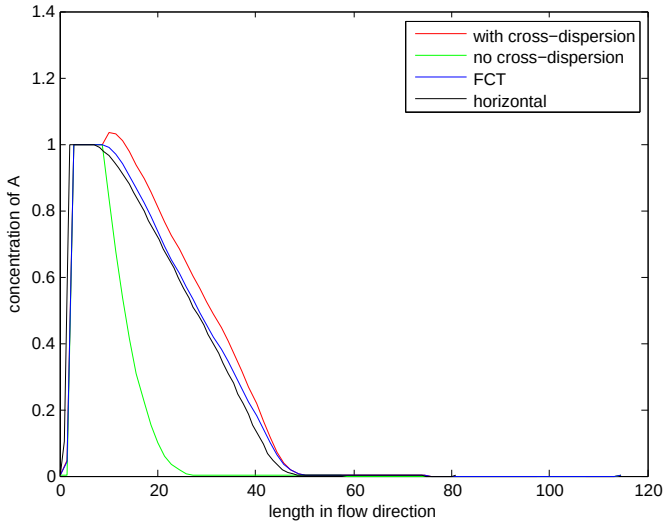

Figure 5.6: Comparison of concentration of A in flow direction, red line presents case 1 results, green line presents case 2 results, blue line presents case 3 results, black line presents case 4 results. For the region with negative concentration, the line is blank

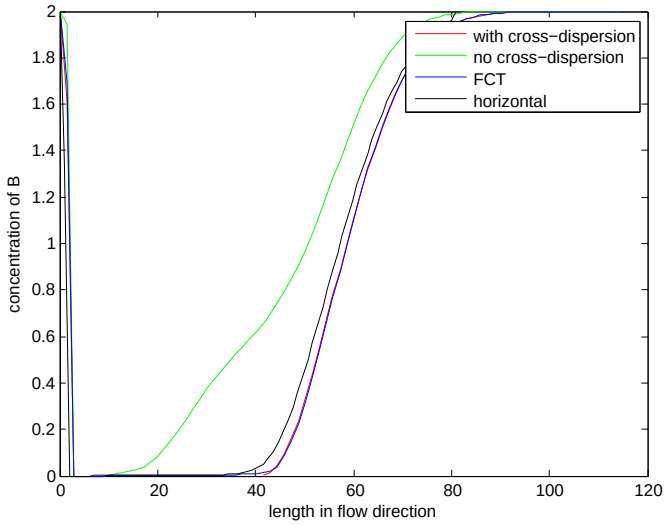

Figure 5.7: Comparison of concentration of B in flow direction, red line presents case 1 results, green line presents case 2 results, blue line presents case 3 results, black line presents case 4 results. For the region with negative concentration, the line is blank

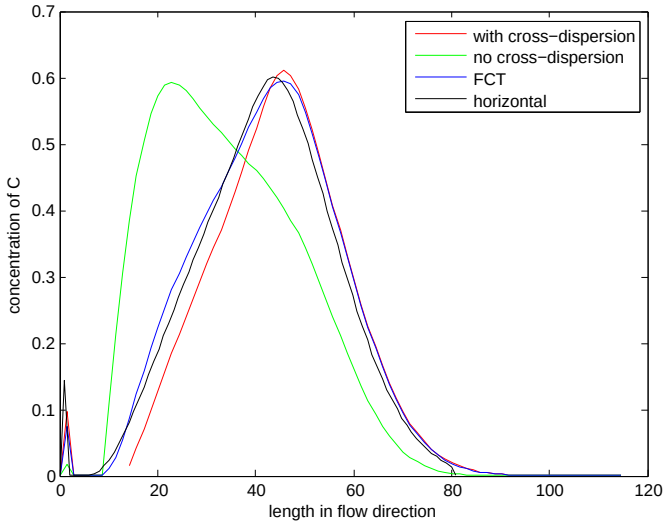

Figure 5.8: Comparison of concentration of C in flow direction, red line presents case 1 results, green line presents case 2 results, blue line presents case 3 results, black line presents case 4 results. For the region with negative concentration, the line is blank

The peak of case 1, 2 and 4 are almost in the same place. However, the peak values are slightly different: in case 1, the peak is higher, which may be caused by the oscillation of the concentration of A; and in case 3, the peak is lower, which may be caused by the "clipping" effect of FCT method [64]. Also same comments apply to Figure 5.6 and Figure 5.7, the solution of case 1 is less accurate than case 3 and has the negative concentration problems near the source zone.

Table 5.2: Minimum and maximum concentration for case 1

	min	max
A	-2.84E-002	1.03E+000
B	-7.82E-003	2.09E+000
C	-2.85E-002	6.10E-001

Table 5.3: Minimum and maximum concentration for case 2

	min	max
A	1.14E-040	1.00E+000
B	7.89E-046	2.00E+000
C	1.00E-015	5.93E-001

Table 5.4: Minimum and maximum concentration for case 3

	min	max
A	2.92E-033	1.00E+000
B	7.89E-046	2.00E+000
C	1.00E-015	5.95E-001

Table 5.2, Table 5.3, Table 5.4 and Table 5.5 show that maximum and minimum concentration of each component for four cases. Table 5.2 shows that the negative concentration of A is greatly amplified by the kinetic reaction. The magnitude of the negative concentration can reach 10^{-2}, which is a quite large amount. So it implies that the negative concentration cannot be ignored and can mess up the model. While on the other hand, Table 5.4 shows that FCT method can preserve the non-negative concentration well for each component. But FCT method has the "clipping" effect, which slightly decreases the maximum concentration of C as shown in Figure 5.8.

Table 5.5: Minimum and maximum concentration for case 4

	min	max
A	6.85E-046	1.00E+000
B	7.89E-046	2.00E+000
C	1.00E-015	6.01E-001

So it can be concluded that for simple kinetic mixing-controlled reaction modeling, cross-dispersion term is an important process, which can determines the shape of the plumes for each component. Without considering the cross-dispersion term, the length of the plume of A and the peak of C can be greatly lagged. However, when considering the full-tensor dispersion, the usual method will have the oscillation problem, which can overestimate the peak concentration and have the negative concentration problem, and the result is not quite accurate. However, the FCT method produces the accurate solution for each component and avoid the oscillation problem.

5.1.2 Simple kinetic reaction with speciation

Speciation can be added to the simple kinetic reaction tests as shown in equation (5.4):

$$\mathrm{B} + \mathrm{C} \rightleftharpoons \mathrm{BC} \tag{5.4}$$

The speciation means that C, the product of the reduction-oxidation reaction, can further react with B in a reversible reaction. So the total reaction is a two-step reaction.

The speciation gives the relationship between each species with the algebraic expression (law of mass action) as shown in equation (5.5) [48]:

$$K = \frac{\mathrm{BC}}{\mathrm{B} \times \mathrm{C}} \tag{5.5}$$

In this section, we set the equilibrium constant K as 10^{-3}. As shown in the simple kinetic reaction test, negative concentration can be obtained in case 1 for each component and the plume shape is different in case 2, so the complex BC concentration distribution may be influenced by these two problems.

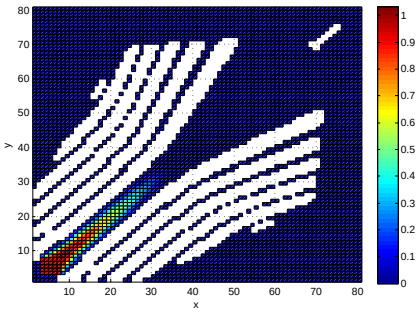

(a) Diagonal flow with full-tensor dispersion

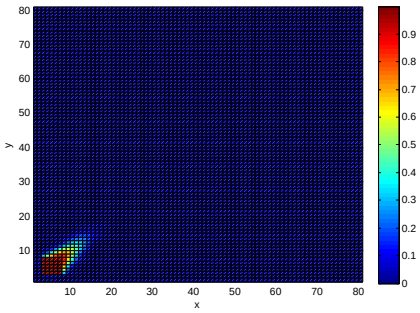

(b) Diagonal flow without cross-dispersion

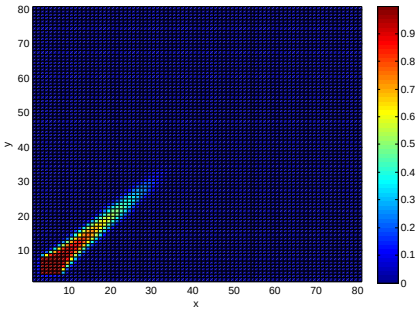

(c) Diagonal flow with full-tensor dispersion using FCT

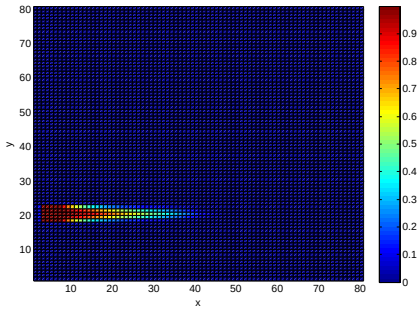

(d) Horizontal flow with full-tensor dispersion

Figure 5.9: Two-dimensional distribution of concentration of A for four kinetic mixing reaction test cases, the color shows the concentration of A and white region is the negative concentration zone

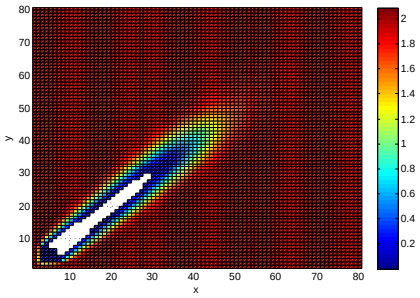

(a) Diagonal flow with full-tensor dispersion

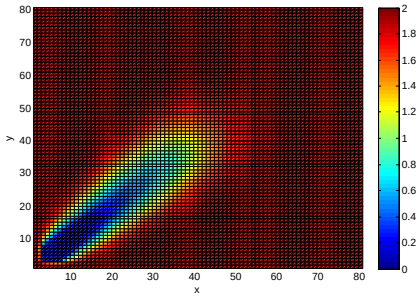

(b) Diagonal flow without cross-dispersion

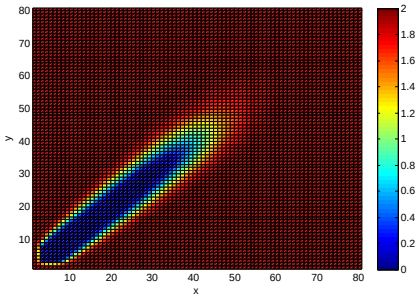

(c) Diagonal flow with full-tensor dispersion using FCT

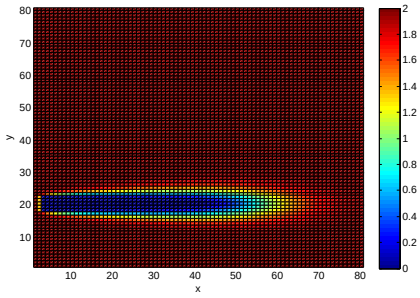

(d) Horizontal flow with full-tensor dispersion

Figure 5.10: Two-dimensional distribution of concentration of B for four kinetic mixing reaction test cases, the color shows the concentration of B and white region is the negative concentration zone

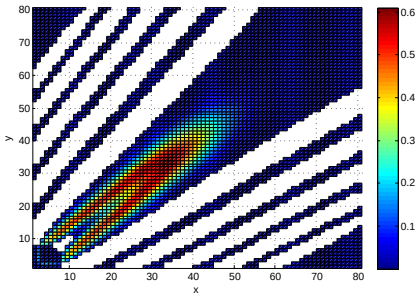

(a) Diagonal flow with full-tensor dispersion

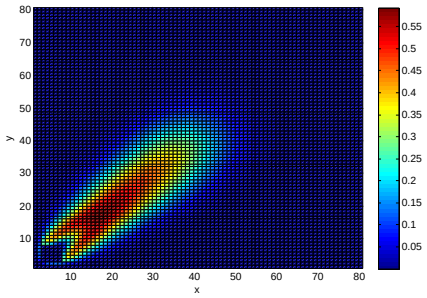

(b) Diagonal flow without cross-dispersion

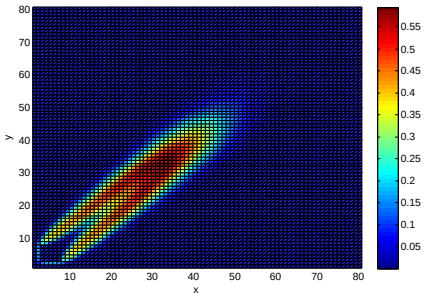

(c) Diagonal flow with full-tensor dispersion using FCT

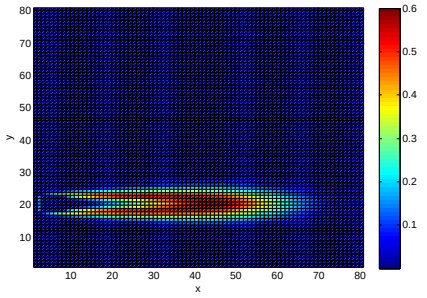

(d) Horizontal flow with full-tensor dispersion

Figure 5.11: Two-dimensional distribution of concentration of C for four kinetic mixing reaction test cases, the color shows the concentration of C and white region is the negative concentration zone

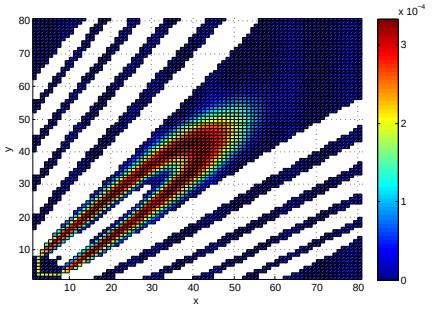

(a) Diagonal flow with full-tensor dispersion

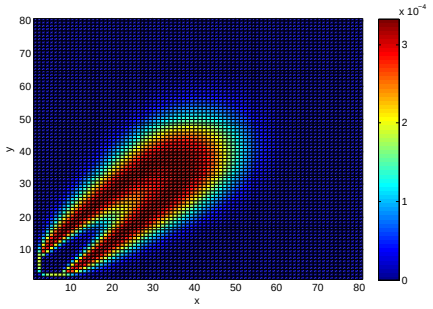

(b) Diagonal flow without cross-dispersion

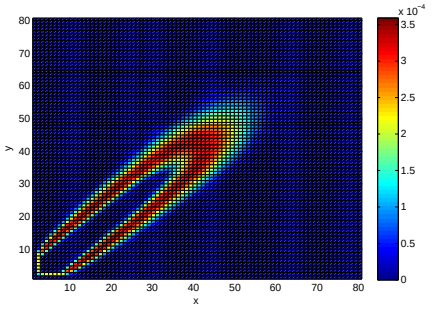

(c) Diagonal flow with full-tensor dispersion using FCT

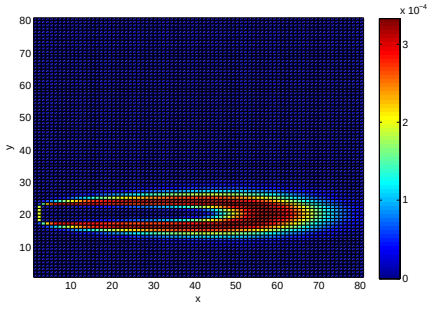

(d) Horizontal flow with full-tensor dispersion

Figure 5.12: Two-dimensional distribution of concentration of BC for four kinetic mixing reaction test cases, the color shows the concentration of C and white region is the negative concentration zone

Figure 5.9, Figure 5.10 and Figure 5.11 show the distribution of concentrations of each components for four cases introduced in the last section. The distributions of the concentration are similar as the simple kinetic reaction tests. Figure 5.12 shows the distribution of concentration of the complex BC for the four test cases. Figure 5.12a shows that for case 1, the negative concentration region for BC is larger than that for C, which can be viewed as the combination of the negative concentration region of both B and C. As shown in the law of action (5.5), if the concentration of B or C become negative, then, the concentration of BC become negative. Figure 5.12b shows that, by adding speciation, the overestimation of transverse dispersion for diagonal direction is amplified in the plume of BC for case 2. The plume of BC much wider than the other three cases.

Figure 5.13, Figure 5.14 and Figure 5.15 show the comparison of the concentration of each component along the center line of the flow direction. These plots are also similar to the simple kinetic reaction. Figure 5.16 shows the comparison of the concentration of BC along the center line of the flow direction. Case 1 and case 3 plot are similar to the benchmark solution. The fronts of the plume from case 1 and case 3 are quite accurate but the other sides of the plume are less accurate. Also at the front boundary of the plume, there are significant differences between cases 1, 3 and the benchmark solution: the benchmark solution does not diffuse as much as case 1 and 2 at the front. The shape of the plume is much wider for case 2, since the distribution of B and C are wider as shown in Figure 5.14 and Figure 5.15. However, the peak of BC is nearer to the benchmark solution. So it seems that ignoring the cross-dispersion term cannot present the position of the peak of C well, but maybe it can be used to present the peak of BC.

Table 5.6: Minimum and maximum concentration for case 1

	min	max
A	-2.84E-002	1.03E+000
B	-7.82E-003	2.09E+000
C	-2.85E-002	6.10E-001
BC	-5.94E-005	3.34E-004

Table 5.6, Table 5.7, Table 5.8 and Table 5.9 show the maximum and minimum concentration of each component and the complex for four cases.

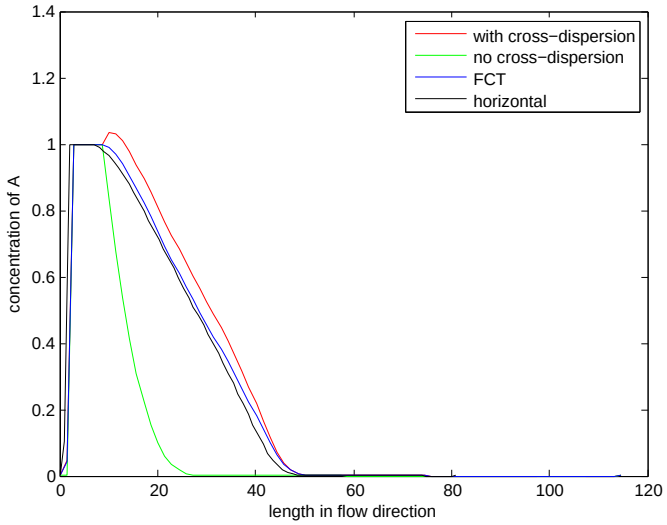

Figure 5.13: Comparison of concentration of A in flow direction, red line presents case 1 results, green line presents case 2 results, blue line presents case 3 results, black line presents case 4 results. For the region with negative concentration, the line is blank

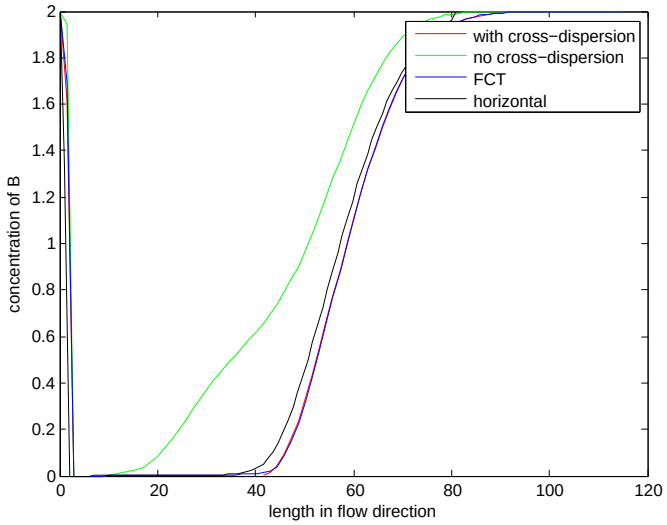

Figure 5.14: Comparison of concentration of B in flow direction, red line presents case 1 results, green line presents case 2 results, blue line presents case 3 results, black line presents case 4 results. For the region with negative concentration, the line is blank

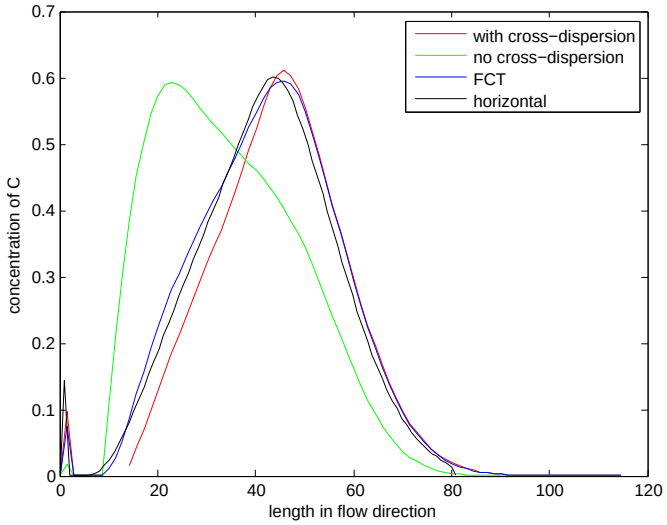

Figure 5.15: Comparison of concentration of C in flow direction, red line presents case 1 results, green line presents case 2 results, blue line presents case 3 results, black line presents case 4 results. For the region with negative concentration, the line is blank

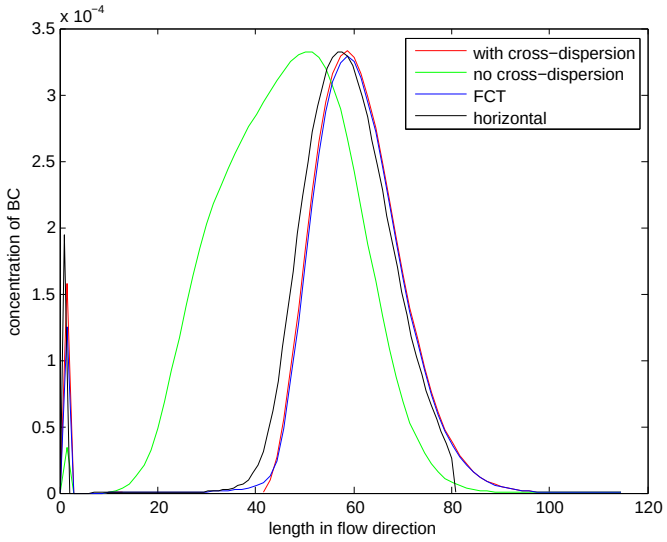

Figure 5.16: Comparison of concentration of C in flow direction, red line presents case 1 results, green line presents case 2 results, blue line presents case 3 results, black line presents case 4 results. For the region with negative concentration, the line is blank

Table 5.7: Minimum and maximum concentration for case 2

	min	max
A	1.15E-040	1.00E+000
B	7.89E-046	2.00E+000
C	1.00E-015	5.93E-001
BC	1.58E-063	3.33E-004

Table 5.8: Minimum and maximum concentration for case 3

	min	max
A	2.92E-033	1.00E+000
B	7.89E-046	2.00E+000
C	1.00E-015	5.95E-001
BC	1.58E-063	3.58E-004

Table 5.9: Minimum and maximum concentration for case 4

	min	max
A	6.85E-046	1.00E+000
B	7.89E-046	2.00E+000
C	1.00E-015	6.01E-001
BC	1.58E-063	3.33E-004

Table 5.6 shows that for case 1, the negative concentration is also relatively large for the complex BC and also the BC has the oscillation for the peak concentration. Table 5.8 shows that for the complex BC, FCT method can produce a higher peak value and this may be a problem for applying FCT method to the speciation test due to the "clipping" for component C.

So it can be concluded that for the simple mixing-controlled kinetic reaction with speciation, the cross-dispersion term is sill an important factor, the negative value problem can be larger for the complex, FCT method can still provide relative good result for the problem, but can be less accurate for the speciation problem.

5.1.3 Simple kinetic reaction in heterogeneous flow field

To further study the tests cases, we applied a heterogeneous flow field to the cases 1,2,3. The complicated flow field we use in this thesis is called multi-mode velocity field [13]. The velocity field is developed from a complicated stream function:

$$\psi(x,y) = x - y - \sum_{k=1}^{m} A_k \cos\left(n_{xk}\pi\frac{x}{L_x} - \frac{\pi}{2}\right)\sin\left(n_{yk}\pi\frac{y}{L_y}\right) \tag{5.6}$$

where $m = 3$, $(n_{x1}, n_{x2}, n_{x3}) = (4, 5, 10)$,$(n_{y1}, n_{y2}, n_{y3}) = (1, 5, 10)$, $(A_1, A_2, A_3) = (8, 2, 1)$, and $L_x = L_y = 81$. The stream function is shown in Figure 5.17. The corresponding components of the velocity are given by:

$$v_x = -\frac{\partial\psi}{\partial y} = 1 + \sum_{k=1}^{3} A_k \frac{n_{yk}\pi}{L_y}\cos\left(n_{xk}\pi\frac{x}{L_x} - \frac{\pi}{2}\right)\cos\left(n_{yk}\pi\frac{y}{L_y}\right) \tag{5.7a}$$

$$v_y = +\frac{\partial\psi}{\partial x} = 1 + \sum_{k=1}^{3} A_k \frac{n_{xk}\pi}{L_y}\sin\left(n_{xk}\pi\frac{x}{L_x} - \frac{\pi}{2}\right)\sin\left(n_{yk}\pi\frac{y}{L_y}\right) \tag{5.7b}$$

The initial concentration is different from other cases as shown in Table 5.10.

Figure 5.18, Figure 5.19 and Figure 5.20 show the distribution of concentrations of each components for three cases with heterogeneous flow field.

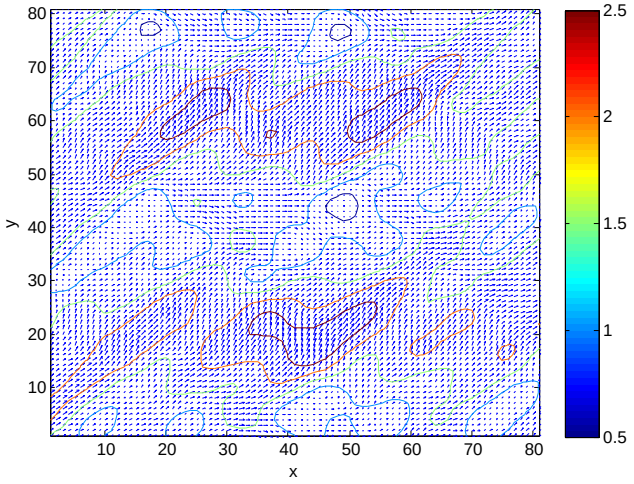

Figure 5.17: Stream function for multi-mode velocity, where the arrow shows the direction of velocity and the circle shows the contour of the velocity

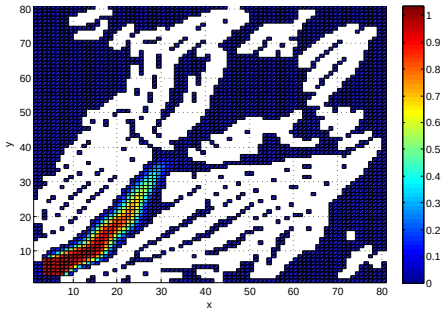

(a) Diagonal flow with full-tensor dispersion

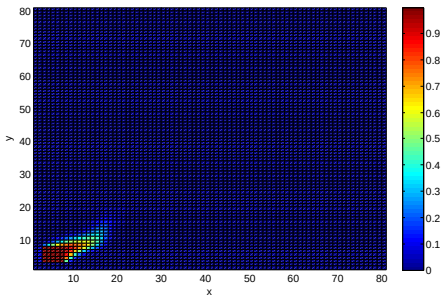

(b) Diagonal flow without cross-dispersion

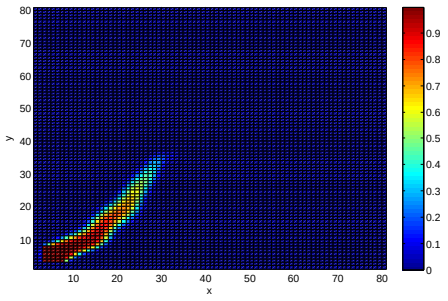

(c) Diagonal flow with full-tensor dispersion using FCT

Figure 5.18: Two-dimensional distribution of concentration of A for three kinetic mixing reaction test cases with heterogeneous flow field, the color shows the concentration of A and white region is the negative concentration zone

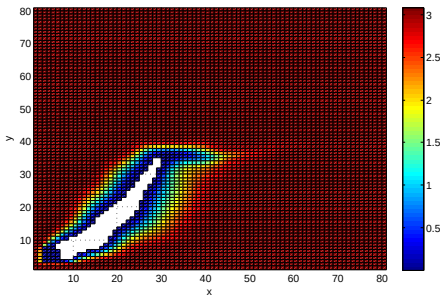

(a) Diagonal flow with full-tensor dispersion

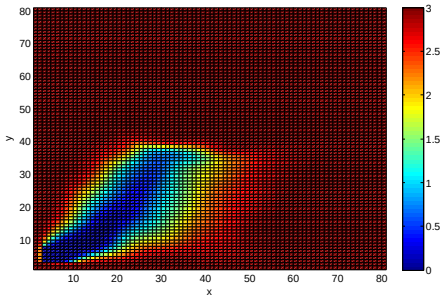

(b) Diagonal flow without cross-dispersion

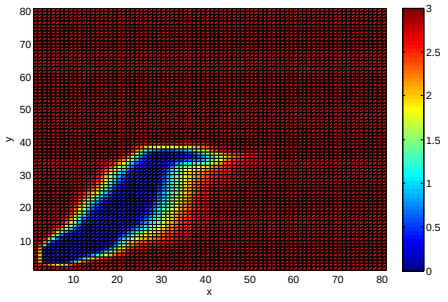

(c) Diagonal flow with full-tensor dispersion using FCT

Figure 5.19: Two-dimensional distribution of concentration of B for three kinetic mixing reaction test cases with heterogeneous flow field, the color shows the concentration of B and white region is the negative concentration zone

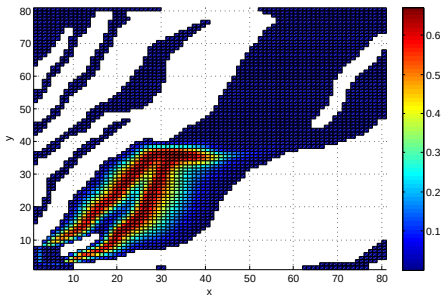

(a) Diagonal flow with full-tensor dispersion

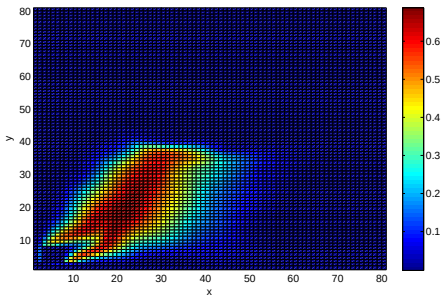

(b) Diagonal flow without cross-dispersion

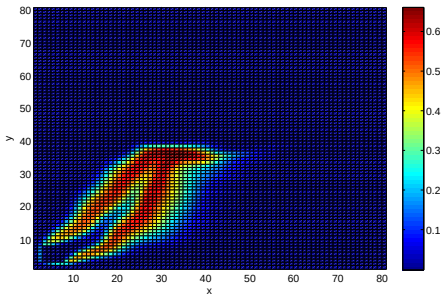

(c) Diagonal flow with full-tensor dispersion using FCT

Figure 5.20: Two-dimensional distribution of concentration of C for three kinetic mixing reaction test cases with heterogeneous flow field, the color shows the concentration of C and white region is the negative concentration zone

Table 5.10: Initial condition for continuously introduced contaminant in heterogeneous flow field

	source zone	background
c_A	1	10^{-15}
c_B	10^{-15}	3
c_C	10^{-15}	10^{-15}

Figure 5.18a and Figure 5.20a show that for case 1, the negative value of A and C show up almost everywhere in the domain around the plume. The heterogeneous flow field makes the negative concentration problem much worse than the diagonal flow field. Figure 5.18b shows that for case 2, the plume of A is strongly lagged by ignoring the cross-dispersion term. While Figure 5.19b and Figure 5.20b show that by ignoring the cross-dispersion term, the plume of B and C disperse further than the solution of case 1 and 3.

Figure 5.21, Figure 5.22 and Figure 5.23 show the comparison of the concentration of each component along the center line of the diagonal direction. Figure 5.21 shows that the distribution of A is similar for case 1 and 3, while for case 2, there is no peak in the plot since the plume is lagged. Figure 5.22 shows that for case 2, the plume of B is longer and diffuses the peak of the concentration away. Figure 5.23 shows that for case 2, there is no significant peak for the plume of C, since the plume of B and A are not well-mixed. In Figure 5.21, Figure 5.22 and Figure 5.23, the plots are similar for case 1 and 3. However, the solutions of case 1 vary more than the solutions of case 3. Based the conclusion of diagonal solution, maybe the difference is due to the oscillation of case 1.

Table 5.11: Minimum and maximum concentration for case 1

	min	max
A	-2.48E-002	1.04E+000
B	-1.32E-002	3.09E+000
C	-2.82E-002	6.71E-001

Table 5.11, Table 5.13 and Table 5.12 shows the maximum and minimum values of each components for each cases. Table 5.11 shows that for heterogeneous flow field, the negative value problem become worse especially for B. Table 5.12 shows that for the heterogeneous flow field, ignoring the

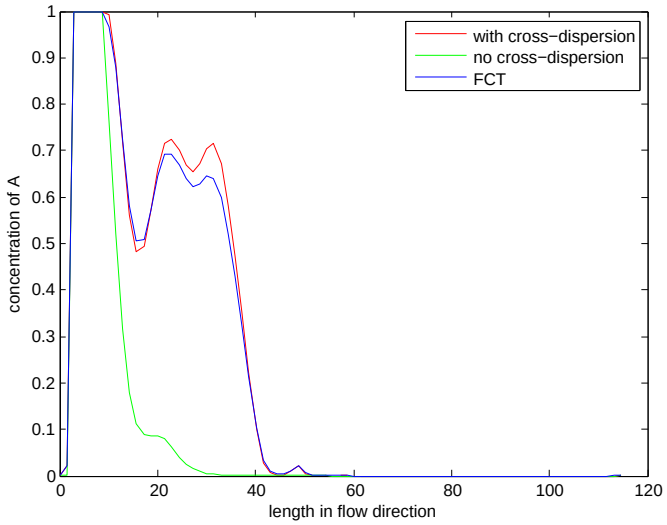

Figure 5.21: Comparison of concentration of A in diagonal direction, red line presents case 1 results, green line presents case 2 results, blue line presents case 3 results. For the region with negative concentration, the line is blank

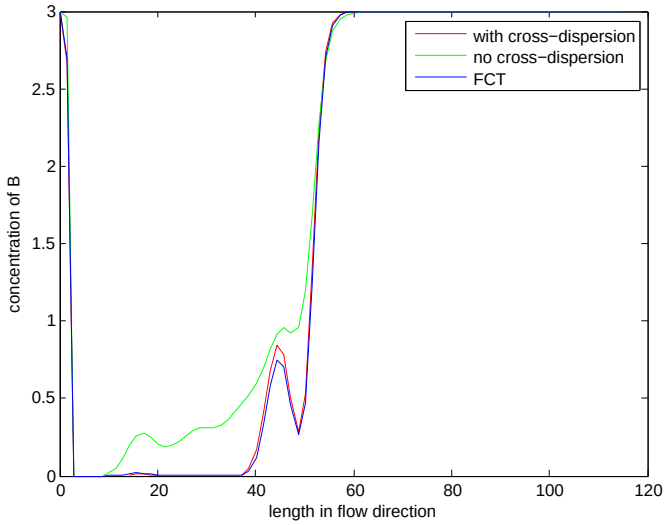

Figure 5.22: Comparison of concentration of B in diagonal direction, red line presents case 1 results, green line presents case 2 results, blue line presents case 3 results. For the region with negative concentration, the line is blank

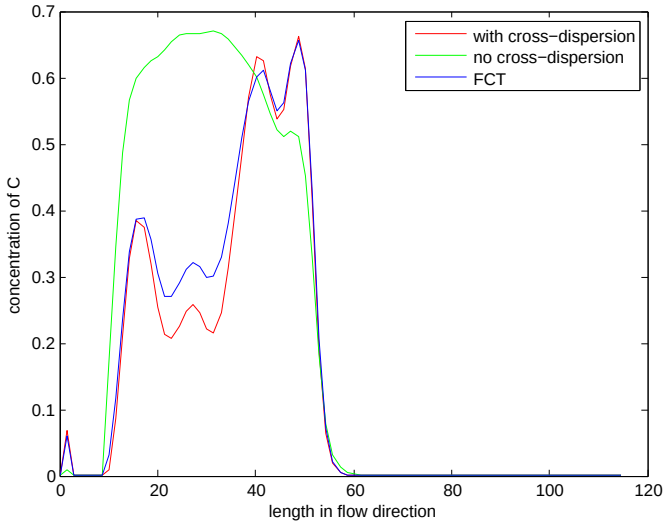

Figure 5.23: Comparison of concentration of C in diagonal direction, red line presents case 1 results, green line presents case 2 results, blue line presents case 3 results. For the region with negative concentration, the line is blank

Table 5.12: Minimum and maximum concentration for case 2

	min	max
A	7.95E-050	1.00E+000
B	7.89E-046	3.00E+000
C	1.00E-015	6.88E-001

Table 5.13: Minimum and maximum concentration for case 3

	min	max
A	1.20E-039	1.00E+000
B	7.89E-046	3.00E+000
C	1.00E-015	6.62E-001

cross-dispersion term can get the highest peak value of C, while at the same time, cases 2 has more dispersion than other cases. So the solutions of case 2 can not be quite trusted for the heterogeneous flow field.

The CPU time of case 1 is 1.1478×10^4 and the CPU time for case 3 is 1.5331×10^4. It shows that the flux-correction approach is time consuming and can be quite slow in the calculation since it calculates the fluxes for all the nodes in the domain. The results show that this approach can takes about 1/3 extra CPU time.

5.1.4 Equilibrium reaction

Another way to simulate the mixing-controlled reaction is to assume the chemical equilibrium reaction. So for the case of reversible reaction $\alpha_A \mathrm{A} + \alpha_B \mathrm{B} \rightleftharpoons \alpha_C \mathrm{C}$, the law of mass action is :

$$\mathrm{K}=\frac{C_C^{\alpha_C}}{C_A^{\alpha_A} \times {C_B}^{\alpha_B}} \tag{5.8}$$

where K is the equilibrium constant. Here we set K, α_i equals to 1.

So the linear concentration relationship between A, B and C are:

$$\begin{aligned} \Psi_A &= c_A + c_C \\ \Psi_B &= c_B + c_C \end{aligned} \tag{5.9}$$

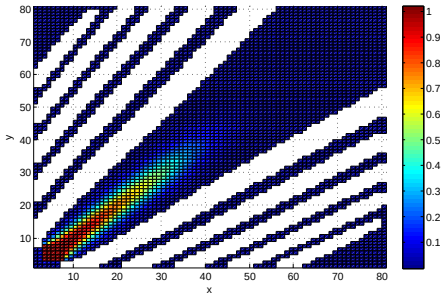

(a) Diagonal flow with full-tensor dispersion

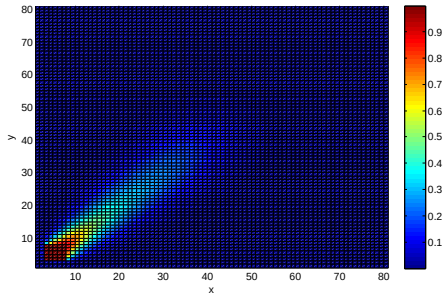

(b) Diagonal flow without cross-dispersion

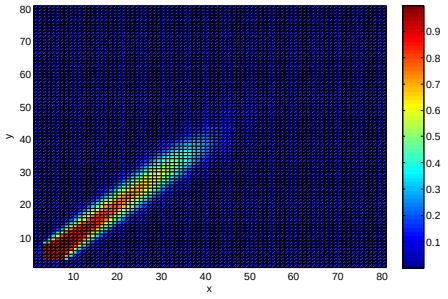

(c) Diagonal flow with full-tensor dispersion using FCT

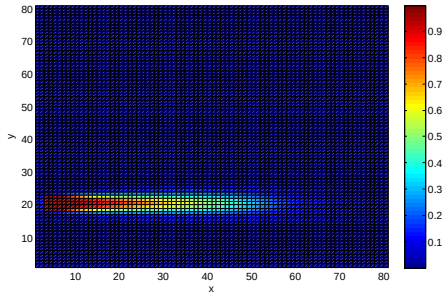

(d) Horizontal flow with full-tensor dispersion

Figure 5.24: Two-dimensional distribution of concentration of A for four kinetic mixing reaction test cases, the color shows the concentration of A and white region is the negative concentration zone

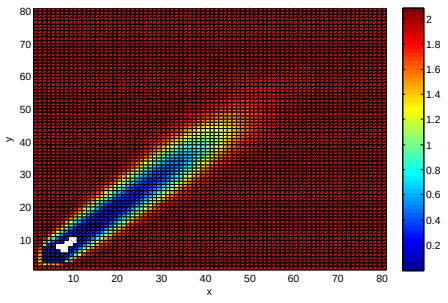

(a) Diagonal flow with full-tensor dispersion

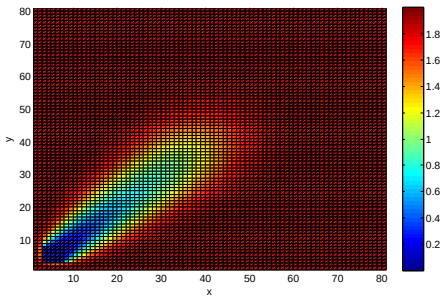

(b) Diagonal flow without cross-dispersion

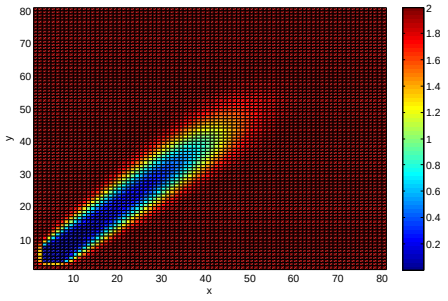

(c) Diagonal flow with full-tensor dispersion using FCT

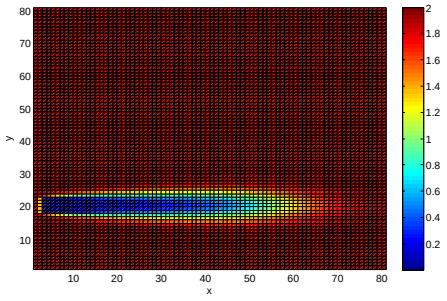

(d) Horizontal flow with full-tensor dispersion

Figure 5.25: Two-dimensional distribution of concentration of B for four kinetic mixing reaction test cases, the color shows the concentration of B and white region is the negative concentration zone

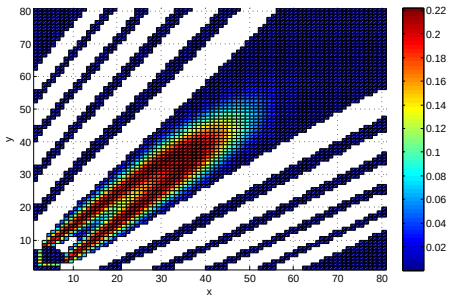

(a) Diagonal flow with full-tensor dispersion

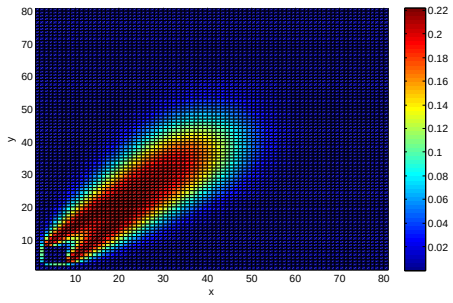

(b) Diagonal flow without cross-dispersion

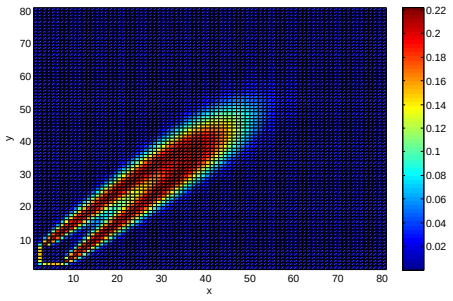

(c) Diagonal flow with full-tensor dispersion using FCT

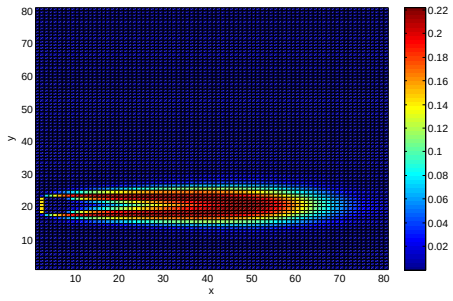

(d) Horizontal flow with full-tensor dispersion

Figure 5.26: Two-dimensional distribution of concentration of C for four kinetic mixing reaction test cases, the color shows the concentration of C and white region is the negative concentration zone

Figure 5.24, Figure 5.25 and Figure 5.26 show the distribution of concentration of each component for the equilibrium reaction cases. Figure 5.24a and Figure 5.3a show that for case 1, the negative concentration region for equilibrium reaction is in different shape and larger than the kinetic reaction test, since the negative concentration are only caused by cross-dispersion term and are amplified by the reaction term. Figure 5.24b shows the plume of A for case 2, which is not lagged by the irreversible reaction as Figure 5.24b. Figure 5.25a shows that for case 1, the negative region for B in the equilibrium reaction models also much smaller than the kinetic reaction.

Figure 5.27, Figure 5.28 and Figure 5.29 show the comparison of concentration along the flow direction of each component for the four cases. Figure 5.27 shows that for equilibrium reaction, the length of the plume for all the cases will be longer than the kinetic reaction solution, since the total concentration for component A and B is not persevered, so the extension of the plume does not slowed by the reaction. Similar to the kinetic reaction tests, the concentration distributions of case 1, 3 and 4 are similar, the distribution of concentration in case 2 is different but the length of the plume case 2 is similar to other cases, which is different from kinetic reaction tests. For case 1, the oscillation also exits, but for most part along the flow direction, case 1 is more accurate than case 3, which is also different from kinetic reaction tests. Figure 5.28 shows that for equilibrium reaction, B is not consumed totally near the source zone as the irreversible kinetic reaction and hence the breakthrough curve of B also starts from source zone. Figure 5.29 shows that for case 1, in the equilibrium reaction, the peak value for C is overestimated and the distribution of concentration of C is more accurate than case 3. For case 2, the distribution of concentration of C does not have a peak, instead case 2 produce a well-mixing zone for A and B and hence have a relatively large zone with high concentration of C.

Table 5.14: Minimum and maximum concentration for case 1

		min	max
A	total	-3.32E-002	1.01E+000
	free ion	-1.07E-002	1.02E+000
B	total	-2.27E-002	2.07E+000
	free ion	-1.12E-002	2.09E+000
C		-0.0224	0.22222117

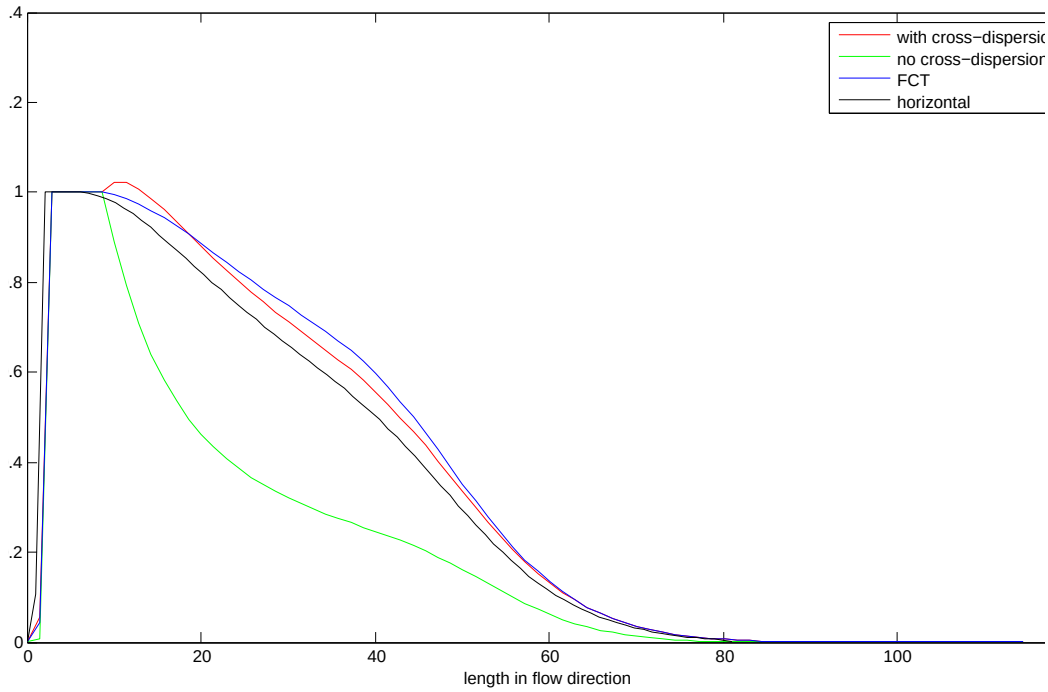

Figure 5.27: Comparison of concentration of A in flow direction,

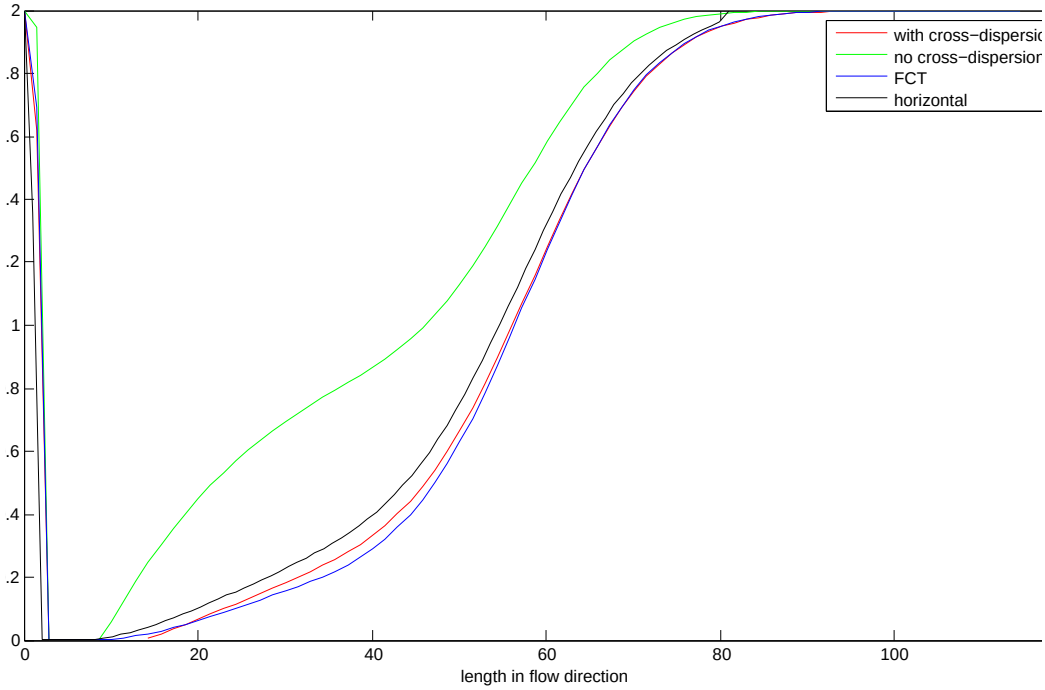

Figure 5.28: Comparison of concentration of B in flow direction

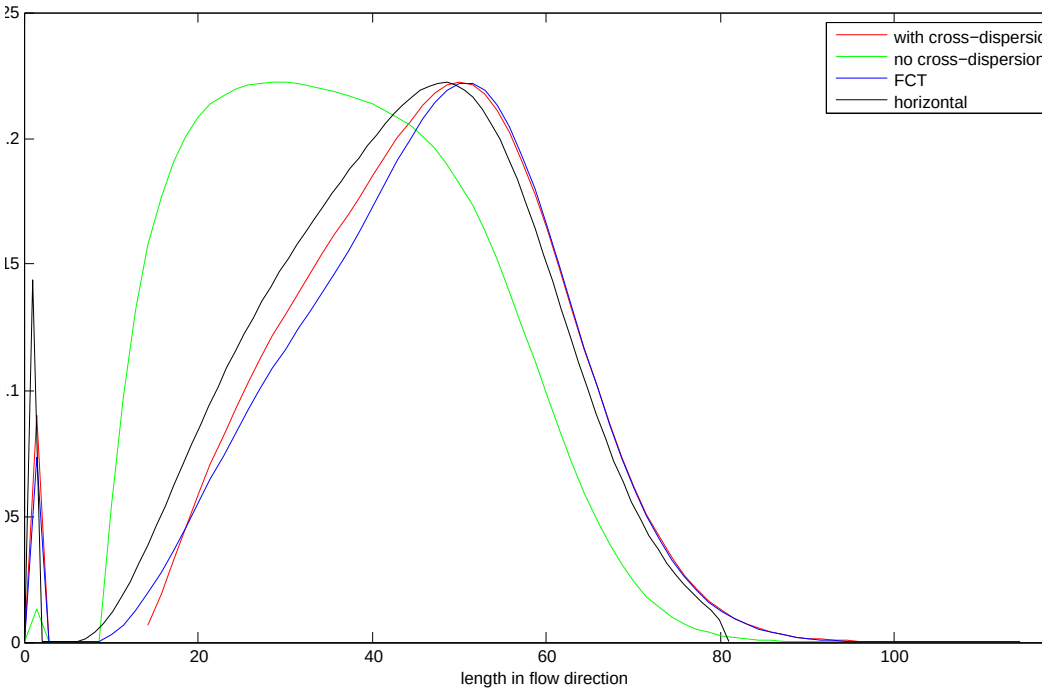

Figure 5.29: Comparison of concentration of C in flow direction

Table 5.15: Minimum and maximum concentration for case 2

		min	max
A	total	1.00E-015	1.00E+000
	free ion	3.33E-016	1.00E+000
B	total	1.00E-015	2.00E+000
	free ion	5.00E-016	2.00E+000
C		5.00E-016	0.22222126

Table 5.16: Minimum and maximum concentration for case 3

		min	max
A	total	1.00E-015	1.00E+000
	free ion	3.33E-016	1.00E+000
B	total	1.00E-015	2.00E+000
	free ion	5.00E-016	2.00E+000
C		5.00E-016	0.22221604

Table 5.17: Minimum and maximum concentration for case 4

		min	max
A	total	1.00E-015	1.00E+000
	free ion	3.33E-016	1.00E+000
B	total	1.00E-015	2.00E+000
	free ion	5.00E-016	2.00E+000
C		5.00E-016	0.22221365

Table 5.14, Table 5.15, Table 5.16 and Table 5.17 show the maximum and minimum value of each component (Ψ_A and Ψ_B)and each species (c_A, c_B and c_C). Table 5.14 shows that for equilibrium reaction tests, the maximum negative values for each species are smaller than the kinetic reaction tests, but the maximum negative value of the total components of A and B are amplified by the negative value from each specie. For the product C, it shows that equilibrium reaction produces less C than the irreversible kinetic reactions and hence the difference of the maximum concentration of C is smaller for equilibrium reactions.

In conclusion, for equilibrium reaction mixing-controlled reaction, ignoring the cross-dispersion term does not get lagged plume as kinetic reaction, but

can get much larger high concentration zone of the product. FCT method can produce the non-negative solution for the model but it is not as accurate as the kinetic mixing-controlled reaction model.

5.1.5 Biological reaction

For the kinetic reaction model, an extra catalyst may be needed, which controlled the reaction with its concentration. The most important and common catalyst in contaminant transport problem is biomass of active organisms [55]. Here we apply simple laws for enzyme kinetics, which is called double-Monod kinetics/ Michaelis-Menten terms [65] with immobile biomass:

$$r = -\frac{1}{\alpha_A}\left.\frac{\partial c_A}{\partial t}\right|_{reac} = -\frac{1}{\alpha_B}\left.\frac{\partial c_B}{\partial t}\right|_{reac} == \frac{1}{\alpha_C}\left.\frac{\partial c_C}{\partial t}\right|_{reac} \tag{5.10}$$

$$= \frac{r_{max}}{Y}\left(\frac{C_A}{K_A + c_A}\right)\left(\frac{C_B}{K_B + c_B}\right)c_{bio} \tag{5.11}$$

in which r_{max} is the maximum specific reaction rate, Y is the specific yield of reaction, K_A and K_B are the Monod half-rate coefficients, and c_{bio} is the biomass concentration. The growth rate of biomass is :

$$\frac{\partial c_{bio}}{\partial t} = r_{max}\left(\frac{C_A}{K_A + c_A}\right)\left(\frac{C_B}{K_B + c_B}\right)c_{bio} \tag{5.12}$$

In these testes, we neglect biomass decay and set $K_A = K_B = 1$, $r_{max} = 10^{-3}$, $Y = 0.1$, $r_{max} = 10^{-3}$, the initial concentration of biomass on the whole domain is 0.5.

Figure 5.30, Figure 5.31, Figure 5.32 and Figure 5.33 show the distributions of concentration of reactants A,B, product C, and the biomass. The distributions of concentration of reactants and the product are similar to the kinetic reaction. Figure 5.30 and Figure 5.33 show that the growth of biomass only happens on the boundary of the plume of A. Hence the length of the biomass growing region is similar as the length of the plume of A. It also shows that for case 1,2,3, the growing rates of biomass are all faster than case 4. Hence for biologic reaction, the solution for biomass is not well-estimated even considering cross-dispersion term and applying FCT method.

Figure 5.34, Figure 5.35, Figure 5.36 and Figure 5.37 show the comparison

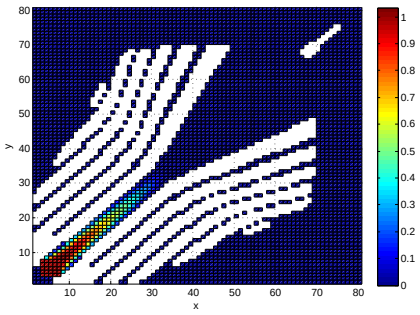

(a) Diagonal flow with full-tensor dispersion

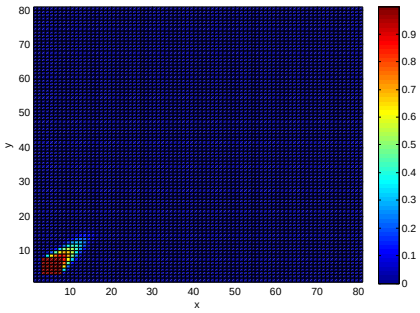

(b) Diagonal flow without cross-dispersion

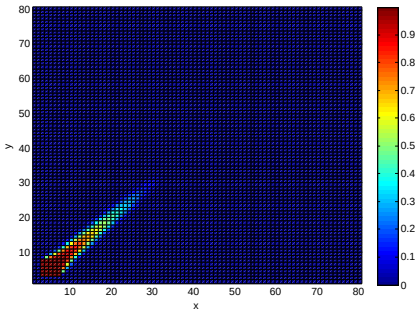

(c) Diagonal flow with full-tensor dispersion using FCT

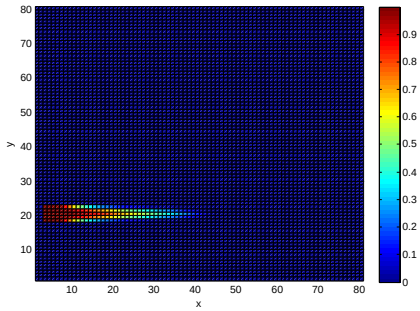

(d) Horizontal flow with full-tensor dispersion

Figure 5.30: Two-dimensional distribution of concentration of A for four biological mixing reaction test cases, the color shows the concentration of C and white region is the negative concentration zone

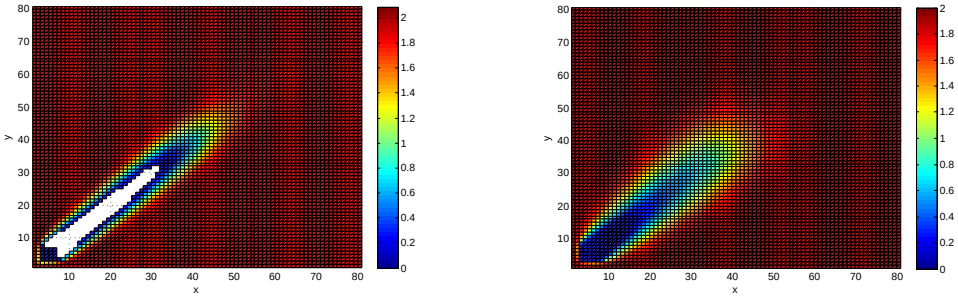

(a) Diagonal flow with full-tensor dispersion

(b) Diagonal flow without cross-dispersion

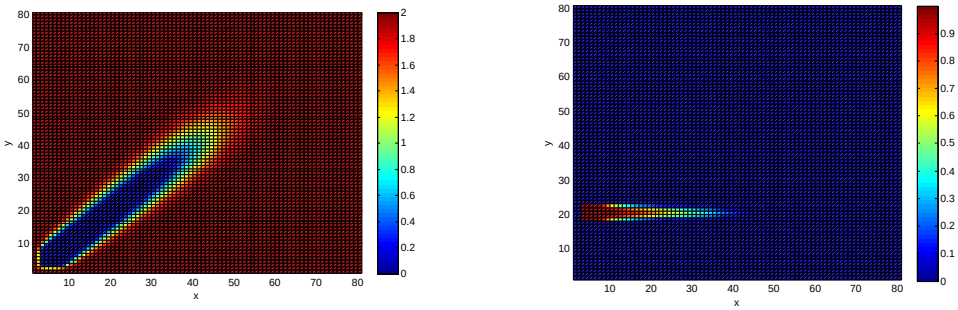

(c) Diagonal flow with full-tensor dispersion using FCT

(d) Horizontal flow with full-tensor dispersion

Figure 5.31: Two-dimensional distribution of concentration of B for four biological mixing reaction test cases, the color shows the concentration of B and white region is the negative concentration zone

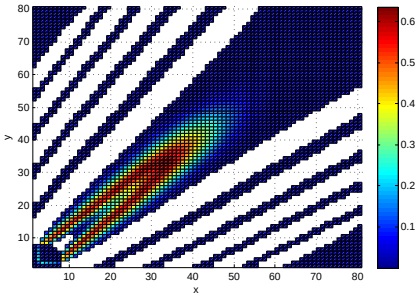

(a) Diagonal flow with full-tensor dispersion

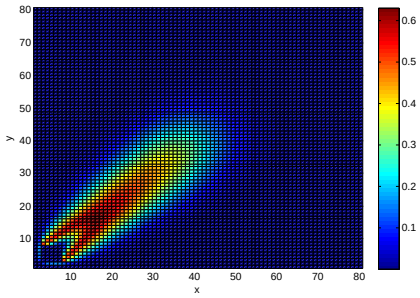

(b) Diagonal flow without cross-dispersion

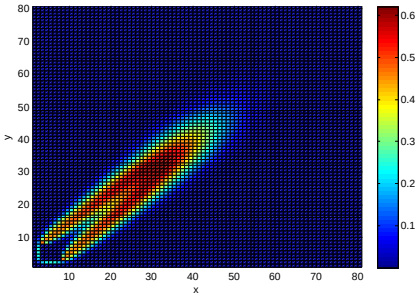

(c) Diagonal flow with full-tensor dispersion using FCT

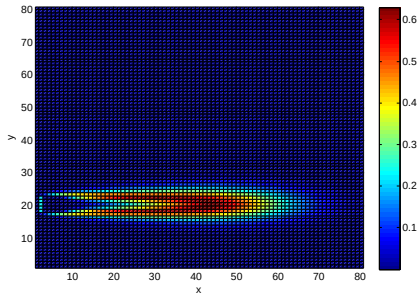

(d) Horizontal flow with full-tensor dispersion

Figure 5.32: Two-dimensional distribution of concentration of C for four biological mixing reaction test cases, the color shows the concentration of C and white region is the negative concentration zone

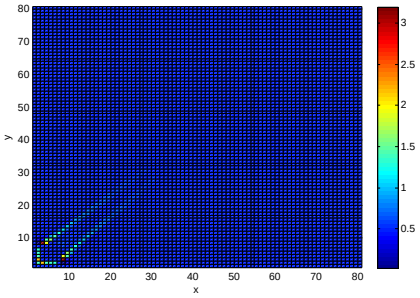

(a) Diagonal flow with full-tensor dispersion

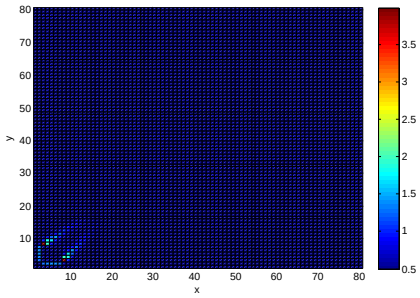

(b) Diagonal flow without cross-dispersion

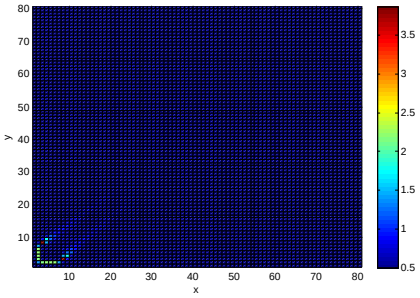

(c) Diagonal flow with full-tensor dispersion using FCT

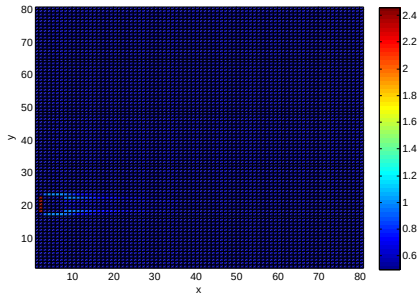

(d) Horizontal flow with full-tensor dispersion

Figure 5.33: Two-dimensional distribution of concentration of biomass for four biological mixing reaction test cases, the color shows the concentration of biomass and white region is the negative concentration zone

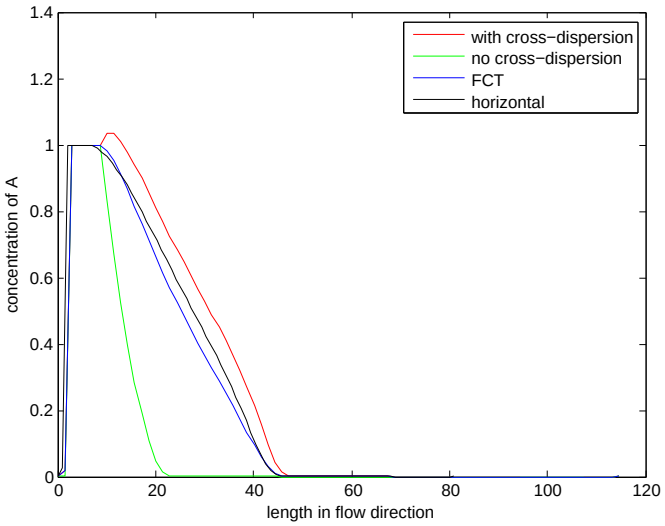

Figure 5.34: Comparison of concentration of A in flow direction,

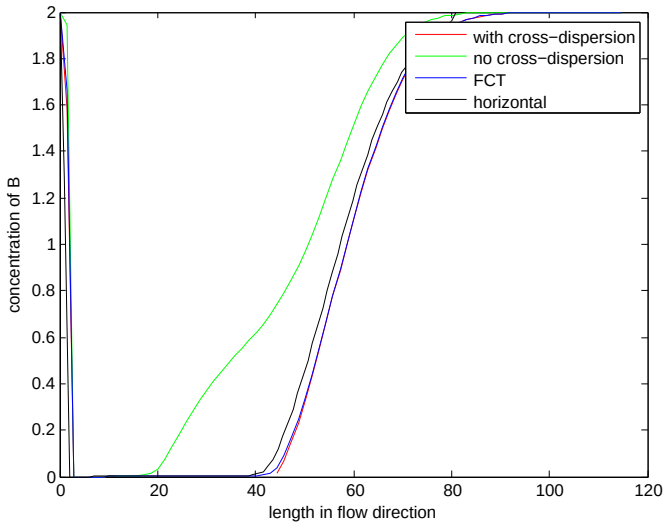

Figure 5.35: Comparison of concentration of B in flow direction

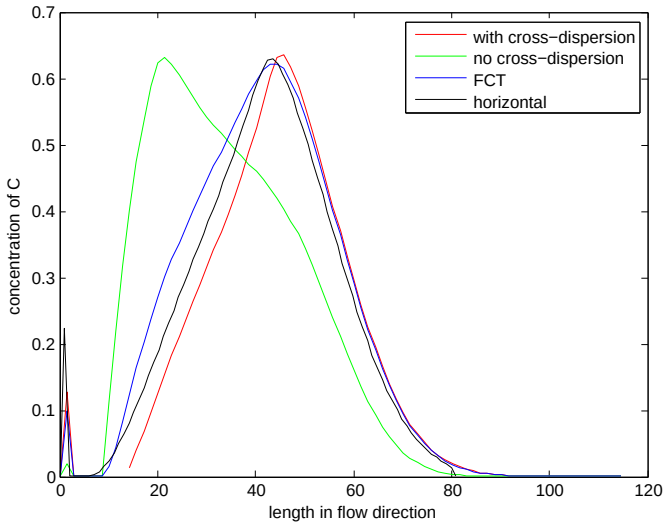

Figure 5.36: Comparison of concentration of C in flow direction

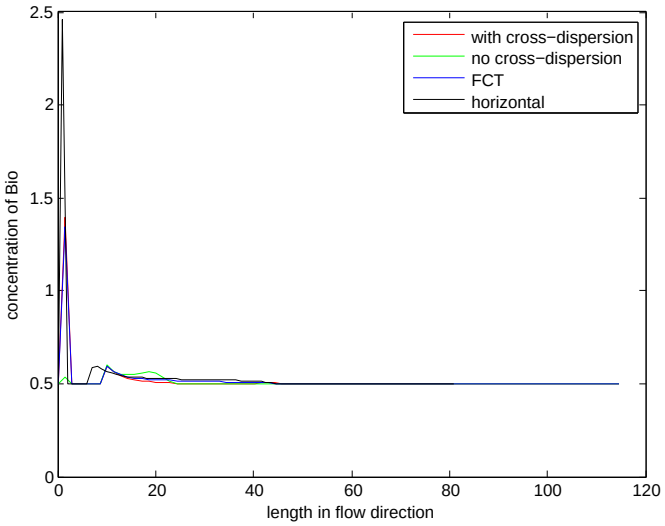

Figure 5.37: Comparison of concentration of biomass in flow direction

the distribution of the concentration of reactants A,B, product C and biomass along the flow direction in the four cases. The distributions of A,B,C are similar as the kinetic reactions but is less accurate than the kinetic reaction tests.

Table 5.18: Minimum and maximum concentration for case 1

	min	max
A	-8.89E-002	1.03E+000
B	-1.98E-002	2.09E+000
C	-2.83E-002	6.36E-001
Biomass	2.35E-002	3.19E+000

Table 5.19: Minimum and maximum concentration for case 2

	min	max
A	1.28E-045	1.00E+000
B	1.00E-046	3.00E+000
C	1.00E-015	6.32E-001
Biomass	5.00E-001	4.00E+000

Table 5.20: Minimum and maximum concentration for case 3

	min	max
A	5.51E-034	1.00E+000
B	1.00E-046	3.00E+000
C	1.00E-015	6.61E-001
Biomass	5.00E-001	3.87E+000

Table 5.18, Table 5.19, Table 5.20 and Table 5.21 show the minimum and maximum of the concentration of the reactants, product and biomass. Table 5.18 shows that for the biological reaction, the negative value problem for A is the greatest, even though the average reaction rate/ the amount of product C is similar. So it can be concluded that for the biological reaction in diagonal flow field, the negative concentration problem and the growth rate of biomass are hard to be solved accurately.

Table 5.21: Minimum and maximum concentration for case 4

	min	max
A	1.79E-046	1.00E+000
B	1.00E-046	2.00E+000
C	1.00E-015	6.30E-001
Biomass	5.00E-001	2.46E+000

5.2 Nonlinear Sorption

The tests in the mixing-controlled section shows that for bilinear or Monod reaction in the diagonal flow field, the reactive transport can have the negative value problems which is caused by the cross-dispersion term and amplified by the reaction. So for non-linear reactions, the negative value can be greatly influenced by the non-linear interactions. One of the common linear reactions in contaminant hydrology is nonlinear sorption. In the reactive transport model, the sorption can be either treated as equilibrium reaction or non-equilibrium reaction based on the time scale of the model. In this section, both equilibrium and non-equilibrium reaction are tested in the diagonal flow field considering the full-tensor dispersion by using the SIA method for the immobile phase.

5.2.1 Equilibrium sorption

The most common way to express the relationship between dissolved concentration c and sorbed concentration $\bar{c}$ is called the isotherm. In the test of this thesis, Freudlich isotherm is applied:

$$\bar{c} = K_f c^{\alpha} \tag{5.13}$$

where the constant K_f is the distribution coefficient and α is the nonlinear power. The Freudlich isotherm assumes the solid matrix has infinite sorption capacity. So the continuous input test may be suitable for this assumption, so in this part, "initial pulse" test is applied as shown in Figure 5.38.

The domain is square with width $L_x = L_y = 81$ and the source zone is also square with width $S_x = S_y = 9$. The grid space is $dx = dy = 9/5$. The time step for the simulation is 1000. The longitudinal dispersivity α_L

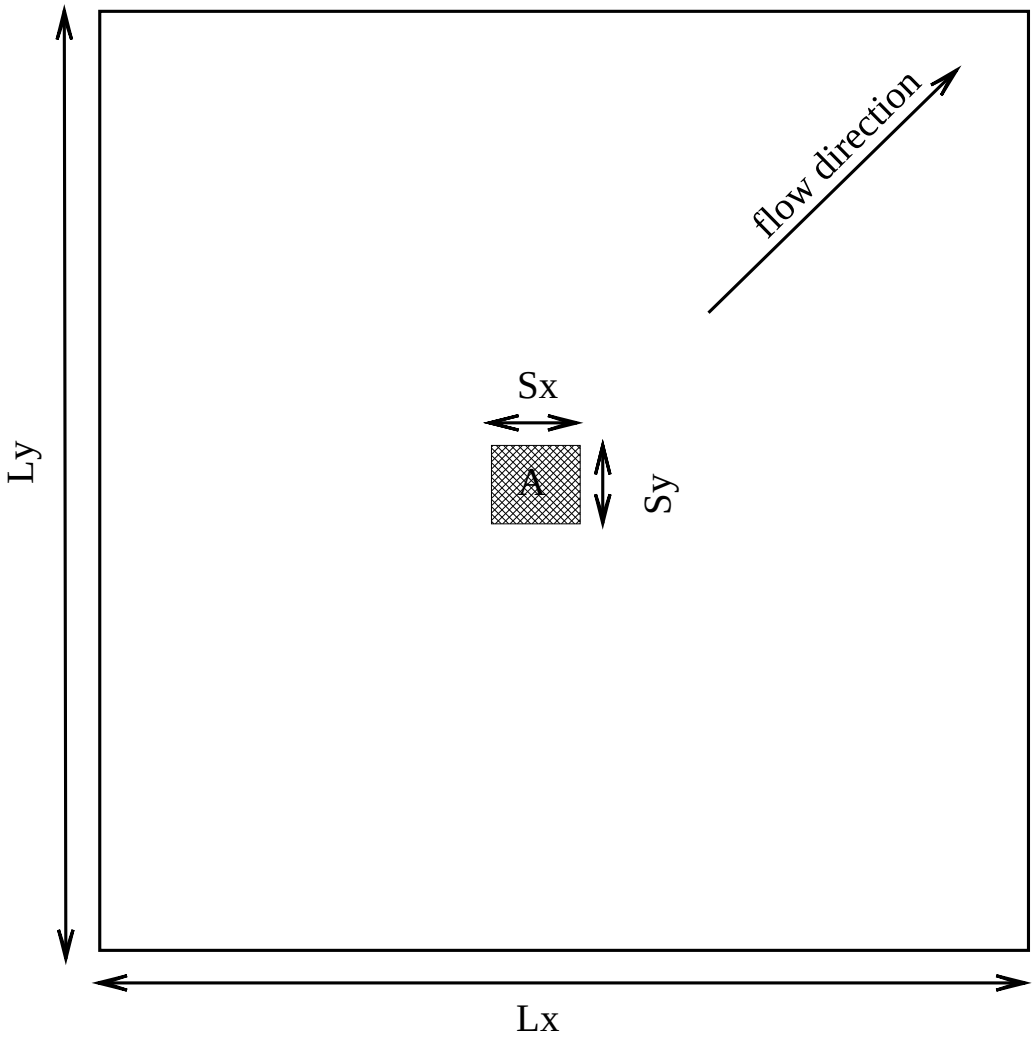

Figure 5.38: Initial pulse test condition, the square in the center of the domain is the initial pulse with high concentration of A with length $S_x \times S_y$.

is 1 and the transverse dispersivity α_T is 0.1. The velocity for diagonal flow field is $v_x = v_y = 10^{-2}/\sqrt{2}$ (so the total velocity is $v_{total} = 10^{-2}$ for the test). Under this condition, the longitudinal grid Peclet number and transverse grid Peclet number are smaller than 2, so the oscillation caused by the advection is ignored, the only possible reason to get non-physical value is dispersion [62]. The distribution coefficient $K_f = 0.88$ and the nonlinear-power $\alpha = 1.2$. The boundary condition is constant concentration condition (same as background concentration). The initial condition of concentration in the pulse is $C_A = 1$, in the background is $C_A = 10^{-5}$ and A is in the equilibrium of sorption.

Figure 5.39a and Figure 5.39b show the distribution of concentration of A for diagonal flow field and horizontal flow field. The negative value caused by cross-dispersion term can crash the model by calculating the sorption term C_A^α. So for nonlinear sorption situation, the usual method cannot guarantee the model to work and applying FCT method for the diagonal or heterogeneous flow field is necessary.

For the SIA approach, this kind of nonlinear sorption is hard to converge even without negative concentration. By ignoring the cross-dispersion term, the diagonal flow field test cannot converge. The reason for the convergence problem is not clear, but this result indicates that considering the cross-dispersion term and applying FCT method may also increase the stability of the problem.

5.2.2 Non-equilibrium sorption

It has been recognized that the local equilibrium assumption is not always appropriate when the sorption rate is not sufficient fast compared to the solute transport [2]. In these situation, it is more appropriate to describe the sorption as non-equilibrium process [66] [67]. So the reaction rate for $\bar{c_A}$ is:

$$\frac{\partial \bar{c}_A}{\partial t} = r_{max} \left(K_f c_A^\alpha - \bar{c}_A \right) \tag{5.14}$$

The parameters for the non-equilibrium test are: the initial background concentration is 10^{-2}, the time step is set shorter as 100, the total time step is 5, the distribution coefficient $K_f = 0.5$, and the nonlinear power $\alpha = 0.8$. All the other parameters are same as the equilibrium tests.

Figure 5.40 shows the distribution of concentration of A at time 500 and

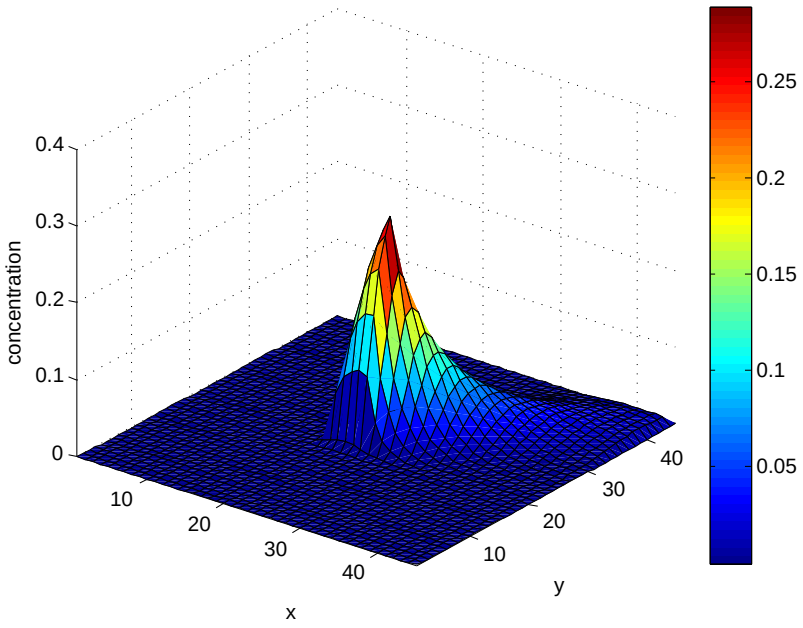

(a) Diagonal flow with full-tensor dispersion

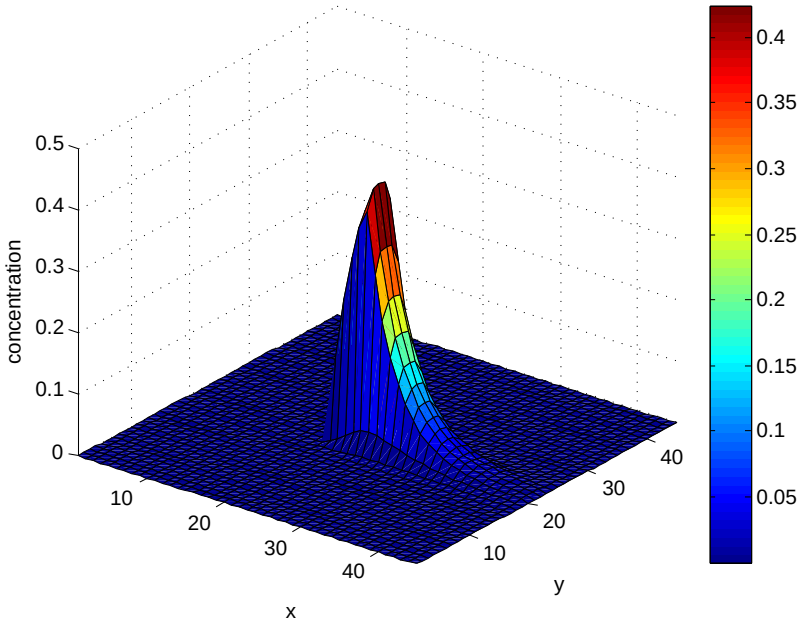

(b) Horizontal flow with full-tensor dispersion

Figure 5.39: Two-dimensional distribution of concentration of A for diagonal flow and horizontal flow cases

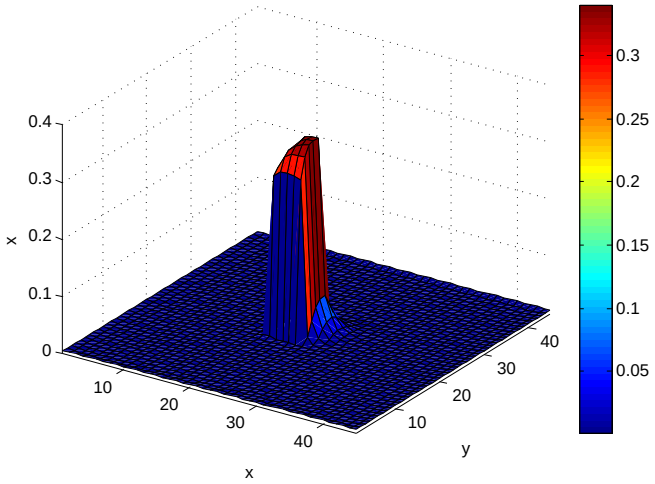

Figure 5.40: Distribution of concentration of A in kinetic sorption

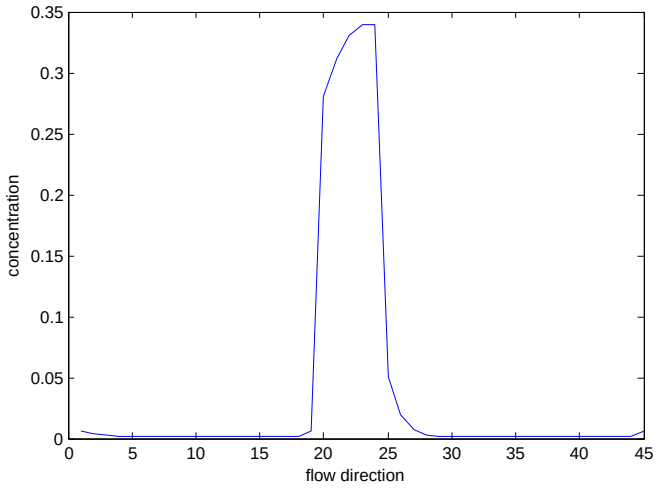

Figure 5.41: Concentration of A in the flow direction for non-equilibrium sorption

Figure 5.41 shows the concentration of A along the diagonal direction. It is clear that for the nonlinear power $\alpha < 1$, the plume is lagged in the front, which is the opposite of the equilibrium results with $\alpha > 1$. During the sorption test, the iteration steps to reach the convergence limit are much more than the mixing-controlled linear tests. So for the nonlinear reactions with immobile phase, the convergence speed of SIA approach is not quite convenient for this type of problem.

Just as for the equilibrium sorption test, the negative value problem can crash the model while calculating the reaction rate of the sorbed phase, so FCT method is still necessary to apply to the non-equilibrium sorption problems.

5.3 Summary

In this chapter, FCT method is applied with global implicit or sequential iteration approach for mixing-controlled reaction or initial pulse sorption problem. The test results show that ignoring cross-dispersion term can make the distribution of concentration quite inaccurate. By considering full-tensor dispersion in diagonal flow field or heterogeneous flow field, the negative value will be generated and amplified by the reactions. For nonlinear reactions, the negative value can crash the model. So FCT method is necessary to be applied to these kind of problems and it has been tested that FCT method can generate accurate solution for different type of problems.

CHAPTER 6

CONCLUSION AND SUMMARY

In this thesis, I have illustrated the approach to numerically solve the advection-dispersion-reaction equation, the procedure to apply FCT method to correct the solution to guarantee the non-negative concentration, the h-convergence test of FCT method and different reaction tests to confirm the accuracy of the FCT method.

The following conclusion can be made:

1. FCT method is tested, for full tensor dispersion transport problem in diagonal flow field, and is shown to have the convergence rate of second-oder. Although, FCT is based on a low-order solution, the test shows that FCT does not decrease the order of the high-order solution even though it may have "clipping" phenomenon.

2. Applying FCT method take longer CPU time to compute the fluxes between each nodes. This approach loop over all the nodes of the domain, so it takes a long time. But since the correction for the flux of each node is individually, this approach can be done in parallel and hence save the CPU time.

3. Cross-dispersion term in the reactive transport models is important and cannot be ignoring in diagonal or heterogeneous flow field. The cross-dispersion term can change the solution of the solute transport part and the chage of the solution will greatly change the reaction solutions especially for the mixing-controlled problems.

4. By considering-dispersion term in diagonal flow field, negative value can always be generated since the cross-dispersion term breaks the M-matrix property of the coefficient matrix. FCT method has been tested to be a good method to avoid the negative concentration problem in the reaction.

5. The approach to solve the ADR problems shows that global implicit is fast to converge and is most accurate. The procedure of applying FCT method into the global implicit approach has been illustrated. In this way, the correction of concentration can be applied simultaneous with the Newton approach. So the accuracy of correcting solute concentration is guaranteed.

REFERENCES

[1] D. Dunavant, "High degree efficient symmetrical gaussian quadrature rules for the triangle," *International journal for numerical methods in engineering*, vol. 21, no. 6, pp. 1129–1148, 1985.

[2] C. Zheng and G. D. Bennett, *Applied contaminant transport modeling: Theory and practice*. Van Nostrand Reinhold New York, 1995, vol. 1. [Online]. Available: http://www.getcited.org/pub/103276388

[3] J. Noye and C. Fletcher, "RECENT DEVELOPMENTS IN THE FINITE ELEMENT METHOD," in *Computational techniques and applications, CTAC-83: proceedings of the 1983 International Conference on Computational Techniques and Applications, held at the University of Sydney, Australia*, vol. 1, 1984, p. 2.

[4] A. E. M. Baptista, "Solution of advection-dominated transport by eulerian-lagrangian methods using the backwards method of characteristics," Ph.D. dissertation, Massachusetts Institute of Technology, 1987. [Online]. Available: http://dspace.mit.edu/handle/1721.1/14946

[5] S. P. Neuman, "Adaptive Eulerianagrangian finite element method for advectionispersion," *International journal for numerical methods in engineering*, vol. 20, no. 2, pp. 321–337, 1984. [Online]. Available: http://onlinelibrary.wiley.com/doi/10.1002/nme.1620200211/abstract

[6] P. Herrera and A. Valocchi, "Positive solution of two-dimensional solute transport in heterogeneous aquifers," *Ground water*, vol. 44, no. 6, pp. 803 – 813, 2006. [Online]. Available: http://onlinelibrary.wiley.com/doi/10.1111/j.1745-6584.2006.00154.x/full

[7] A. Harten, "High resolution schemes for hyperbolic conservation laws," *Journal of computational physics*, vol. 49, no. 3, pp. 357–393, 1983.

[8] P. Sweby, "High resolution schemes using flux limiters for hyperbolic conservation laws," *SIAM journal on numerical analysis*, vol. 21, no. 5, pp. 995–1011, 1984.

[9] S. Zalesak, "Fully multidimensional flux-corrected transport algorithms for fluids," *Journal of computational physics*, vol. 31, no. 3, pp. 335–362, 1979.

[10] K. Nakshatrala and A. Valocchi, "Non-negative mixed finite element formulations for a tensorial diffusion equation," *Journal of Computational Physics*, vol. 228, no. 18, pp. 6726 – 6752, 2009. [Online]. Available: http://www.sciencedirect.com/science/article/pii/S0021999109002897

[11] A. Jameson, "Positive schemes and shock modelling for compressible flows," *International Journal for Numerical Methods in Fluids*, vol. 20, no. 8-9, pp. 743–776, 1995.

[12] K. Lipnikov, D. Svyatskiy, and Y. Vassilevski, "Interpolation-free monotone finite volume method for diffusion equations on polygonal meshes," *Journal of Computational Physics*, vol. 228, no. 3, pp. 703–716, 2009.

[13] K. Nakshatrala, M. Mudunuru, and A. Valocchi, "A numerical framework for diffusion-controlled bimolecular-reactive systems to enforce maximum principles and non-negative constraint," *arXiv preprint arXiv:1210.5290*, 2012.

[14] D. Kuzmin, M. Moller, and S. Turek, "High-resolution fem–fct schemes for multidimensional conservation laws," *Computer Methods in Applied Mechanics and Engineering*, vol. 193, no. 45, pp. 4915–4946, 2004.

[15] G. Dietachmayer, "A comparison and evaluation of some positive definite advection schemes. computational techniques and applications: Ctac-85," 1986.

[16] D. Kuzmin, "Explicit and implicit fem-fct algorithms with flux linearization," *Journal of Computational Physics*, vol. 228, no. 7, pp. 2517–2534, 2009.

[17] D. Kuzmin, "On the design of algebraic flux correction schemes for quadratic finite elements," *Journal of Computational and Applied Mathematics*, vol. 218, no. 1, pp. 79–87, 2008.

[18] B. A. Robinson, H. S. Viswanathan, and A. J. Valocchi, "Efficient numerical techniques for modeling multicomponent ground-water transport based upon simultaneous solution of strongly coupled subsets of chemical components," *Advances in Water Resources*, vol. 23, no. 4, pp. 307–324, 2000.

[19] G.-T. Yeh and V. S. Tripathi, "A model for simulating transport of reactive multispecies components: Model development and demonstration," *Water Resources Research*, vol. 27, no. 12, pp. 3075–3094, 1991.

[20] C. W. Liu and T. Narasimhan, "Redox-controlled multiple-species reactive chemical transport: 1. model development," *Water Resources Research*, vol. 25, no. 5, pp. 869–882, 1989.

[21] S. Krautle and P. Knabner, "A reduction scheme for coupled multicomponent transport-reaction problems in porous media: Generalization to problems with heterogeneous equilibrium reactions," *Water resources research*, vol. 43, no. 3, 2007.

[22] C. I. Steefel and K. T. MacQuarrie, "Approaches to modeling of reactive transport in porous media," *Reviews in Mineralogy and Geochemistry*, vol. 34, no. 1, pp. 85–129, 1996.

[23] A. J. Valocchi and M. Malmstead, "Accuracy of operator splitting for advection-dispersion-reaction problems," *Water Resources Research*, vol. 28, no. 5, pp. 1471–1476, 1992.

[24] J. Bear, *Dynamics of fluids in porous media*. Dover publications, 1988.

[25] M. Edwards, "Cross flow tensors and finite volume approximation with by deferred correction," *Computer methods in applied mechanics and engineering*, vol. 151, no. 1, pp. 143–161, 1998.

[26] E. Wexler, *Analytical solutions for one-, two-, and three-dimensional solute transport in ground-water systems with uniform flow*. US Government Printing Office, 1992.

[27] R. J. Charbeneau and R. Charbeneau, *Groundwater hydraulics and pollutant transport*. Prentice Hall Upper Saddle Riveˆ eNJ NJ, 2000.

[28] M. Heath, *Scientific computing*. McGraw-Hill, 1997.

[29] O. Strack, "Groundwater mechanics," *National Water Well Association, Dublin, Ohio. 1989. 732*, 1989.

[30] R. Freeze, "Subsurface hydrology at waste disposal sites," *IBM Journal of Research and Development*, vol. 16, no. 2, pp. 117–129, 1972.

[31] M. Abramowitz and I. Stegun, *Handbook of mathematical functions: with formulas, graphs, and mathematical tables*. Dover publications, 1965, vol. 55.

[32] J. Lyness and D. Jespersen, "Moderate degree symmetric quadrature rules for the triangle," *IMA Journal of Applied Mathematics*, vol. 15, no. 1, pp. 19–32, 1975.

[33] P. Hammer, O. Marlowe, and A. Stroud, "Numerical integration over simplexes and cones," *Mathematical Tables and Other Aids to Computation*, pp. 130–137, 1956.

[34] P. Silvester, "Symmetric quadrature formulae for simplexes," *Mathematics of Computation*, vol. 24, no. 109, pp. 95–100, 1970.

[35] D. Kuzmin, R. Löhner, and S. Turek, *Flux-Corrected Transport: Principles, Algorithms, and Applications, Scientific Computation*. Springer, 2005.

[36] J. Boris and D. Book, "Flux-corrected transport," *Journal of computational physics*, vol. 135, no. 2, pp. 172–186, 1997.

[37] D. Kuzmin and S. Turek, "Flux correction tools for finite elements," *Journal of Computational Physics*, vol. 175, no. 2, pp. 525–558, 2002.

[38] O. Garcia-Cabrejo and A. Valocchi, "Application of flux corrected transport for multicomponent reactive transport modeling," 2012.

[39] D. Kuzmin, M. Möller, and S. Turek, "Multidimensional fem-fct schemes for arbitrary time stepping," *International journal for numerical methods in fluids*, vol. 42, no. 3, pp. 265–295, 2003.

[40] C. DeVore, "An improved limiter for multidimensional flux-corrected transport," DTIC Document, Tech. Rep., 1998.

[41] A. Jameson, "Computational algorithms for aerodynamic analysis and design," *Applied Numerical Mathematics*, vol. 13, no. 5, pp. 383–422, 1993.

[42] P. C. Lichtner, "Continuum formulation of multicomponent-multiphase reactive transport," *Reviews in Mineralogy and Geochemistry*, vol. 34, no. 1, pp. 1–81, 1996.

[43] F. Zhang, G.-T. Yeh, J. C. Parker, S. C. Brooks, M. N. Pace, Y.-J. Kim, P. M. Jardine, and D. B. Watson, "A reaction-based paradigm to model reactive chemical transport in groundwater with general kinetic and equilibrium reactions," *Journal of contaminant hydrology*, vol. 92, no. 1, pp. 10–32, 2007.

[44] D. Barry, H. Prommer, C. Miller, P. Engesgaard, A. Brun, and C. Zheng, "Modelling the fate of oxidisable organic contaminants in groundwater," *Advances in Water Resources*, vol. 25, no. 8, pp. 945–983, 2002.

[45] R. Hills, K. Fisher, M. Kirkland, and P. Wierenga, "Application of flux-corrected transport to the las cruces trench site," *Water resources research*, vol. 30, no. 8, pp. 2377–2385, 1994.

[46] A. D. Gupta, L. Lake, G. Pope, K. Sepehrnoori, and M. King, "High-resolution monotonic schemes for reservoir fluid flow simulation," *In Situ;(United States)*, vol. 15, no. 3, 1991.

[47] J. A. Christ and L. M. Abriola, "Modeling metabolic reductive dechlorination in dense non-aqueous phase liquid source-zones," *Advances in water resources*, vol. 30, no. 6, pp. 1547–1561, 2007.

[48] P. K. Kitanidis and P. L. McCarty, *Delivery and Mixing in the Subsurface: Processes and Design Principles for in Situ Remediation*. Springer, 2012, vol. 4.

[49] S. Molins, J. Carrera, C. Ayora, and M. W. Saaltink, "A formulation for decoupling components in reactive transport problems," *Water Resources Research*, vol. 40, no. 10, p. W10301, 2004.

[50] P. C. Lichtner, C. I. Steefel, E. H. Oelkers, U. P. Sabatier, D. Suarez, and J. Simdnek, "Reactive transport in porous media," 1996.

[51] P. Engesgaard and K. L. Kipp, "A geochemical transport model for redox-controlled movement of mineral fronts in groundwater flow systems: A case of nitrate removal by oxidation of pyrite," *Water Resources Research*, vol. 28, no. 10, pp. 2829–2843, 1992.

[52] A. Zysset, F. Stauffer, and T. Dracos, "Modeling of reactive groundwater transport governed by biodegradation," *Water Resources Research*, vol. 30, no. 8, pp. 2423–2434, 1994.

[53] C. Tebes-Stevens, A. J Valocchi, J. M. VanBriesen, and B. E. Rittmann, "Multicomponent transport with coupled geochemical and microbiological reactions: model description and example simulations," *Journal of Hydrology*, vol. 209, no. 1, pp. 8–26, 1998.

[54] B. Leonard, "The ultimate conservative difference scheme applied to unsteady one-dimensional advection," *Computer methods in applied mechanics and engineering*, vol. 88, no. 1, pp. 17–74, 1991.

[55] O. A. Cirpka and A. J. Valocchi, "Two-dimensional concentration distribution for mixing-controlled bioreactive transport in steady state," *Advances in water resources*, vol. 30, no. 6, pp. 1668–1679, 2007.

[56] O. A. Cirpka, E. O. Frind, and R. Helmig, "Numerical simulation of biodegradation controlled by transverse mixing," *Journal of Contaminant Hydrology*, vol. 40, no. 2, pp. 159–182, 1999.

[57] S. F. Thornton, S. Quigley, M. J. Spence, S. A. Banwart, S. Bottrell, and D. N. Lerner, "Processes controlling the distribution and natural attenuation of dissolved phenolic compounds in a deep sandstone aquifer," *Journal of Contaminant Hydrology*, vol. 53, no. 3, pp. 233–267, 2001.

[58] M. Thullner, L. Mauclaire, M. H. Schroth, W. Kinzelbach, and J. Zeyer, "Interaction between water flow and spatial distribution of microbial growth in a two-dimensional flow field in saturated porous media," *Journal of contaminant hydrology*, vol. 58, no. 3, pp. 169–189, 2002.

[59] W. E. Huang, S. E. Oswald, D. N. Lerner, C. C. Smith, and C. Zheng, "Dissolved oxygen imaging in a porous medium to investigate biodegradation in a plume with limited electron acceptor supply," *Environmental science & technology*, vol. 37, no. 9, pp. 1905–1911, 2003.

[60] P. A. Ham, R. J. Schotting, H. Prommer, and G. B. Davis, "Effects of hydrodynamic dispersion on plume lengths for instantaneous bimolecular reactions," *Advances in water resources*, vol. 27, no. 8, pp. 803–813, 2004.

[61] O. A. Cirpka and A. J. Valocchi, "Reply to comments on two-dimensional concentration distribution for mixing-controlled bioreactive transport in steady state by h. shao et al." *Advances in Water Resources*, vol. 32, no. 2, pp. 298–301, 2009.

[62] P. Huyakorn and G. Pinder, "Computational methods in subsurface flowacademic press," *New York*, p. 473, 1983.

[63] O. A. Cirpka and A. J. Valocchi, "Two-dimensional concentration distribution for mixing-controlled bioreactive transport in steady state," *Advances in Water Resources*, vol. 30, no. 67, pp. 1668 – 1679, 2007, ¡ce:title¿Biological processes in porous media: From the pore scale to the field¡/ce:title¿. [Online]. Available: http://www.sciencedirect.com/science/article/pii/S0309170806001424

[64] S. Zalesak, "A preliminary comparison of modern shock-capturing schemes: linear advection," *Advances in Computer Methods for PDEs. Publ. IMACS*, pp. 15–22, 1987.

[65] P. Baveye and A. Valocchi, "An evaluation of mathematical models of the transport of biologically reacting solutes in saturated soils and aquifers," *Water Resources Research*, vol. 25, no. 6, pp. 1413–1421, 1989.

[66] J. M. Bahr and J. Rubin, "Direct comparison of kinetic and local equilibrium formulations for solute transport affected by surface reactions," *Water Resources Research*, vol. 23, no. 3, pp. 438–452, 1987.

[67] A. J. Valocchi, "Spatial moment analysis of the transport of kinetically adsorbing solutes through stratified aquifers," *Water Resources Research*, vol. 25, no. 2, pp. 273–279, 1989.